MT1-MMP and integrin $\alpha_5\beta_1$ promote HT1080 cell migration on 2D, but not on 3D fibronectin environments

Silke Corall

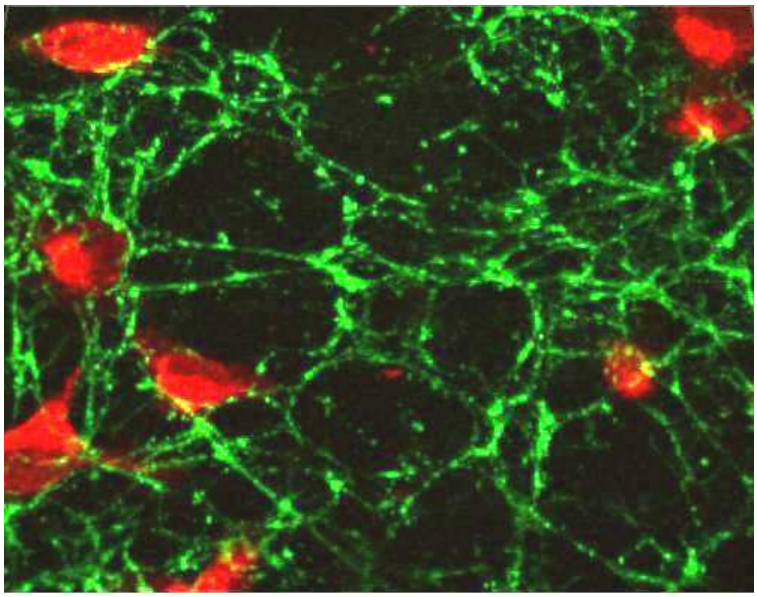

Dissertation
submitted to the
Combined Faculties for the Natural Sciences and for Mathematics
of the Ruperto-Carola University of Heidelberg, Germany
for the degree of
Doctor of Natural Sciences

presented by:

Dipl.-biol. Silke Melanie Corall
born in: Schweinfurt (Germany)
Oral-examination: 6th of November 2013

MT1-MMP and integrin $\alpha_5\beta_1$ promote HT1080 cell migration on 2D, but not on 3D fibronectin environments

Referees:
Prof. Dr. Peter Angel
Prof. Dr. Joachim Spatz

Table of Contents

1. Summary

Cell migration is not only crucial for a range of physiological processes, such as embryonic development or wound healing, but also a major determinant for pathological processes, including cancer dissemination and metastasis. Cancer cell migration relies on two coordinated and interdependent functions, adhesion and proteolysis. While cell adhesion receptors of the integrin family orchestrate interactions between cells and the extracellular matrix (ECM), matrix metalloproteinases (MMPs) degrade matrix barriers and subsequently create space for cell movement. Most studies on cancer cell migration are based on two model systems: collagen gels and reconstituted basement membrane extracts. The ECM however, is a highly complex structure that consists of several components whose function and contribution to cell migration in physiological and pathological conditions is still poorly understood. Hence, new model systems are required to gain a more profound understanding about the interactions between tumor cells and their microenvironment, which in turn drive malignancy. Accordingly, fibronectin (FN), an adhesive fibrillar ECM protein, came into focus, since its expression levels are upregulated in several tumors and it has been associated with the formation of premetastatic niches. In this thesis, cell migration of human fibrosarcoma cells was investigated in two-dimensional (2D) and three-dimensional (3D) FN environments. In 2D environments, FN molecules in their globular form were physisorbed onto surfaces to form a thin, homogenous layer. 3D environments were assembled via a cell-driven process leading to the formation of fibrillar FN networks. Cell migration behavior in these two types of FN environments was examined using integrin blocking approaches and FN cell-binding site mutation. Here, it was demonstrated that on 2D FN coatings, cell migration is strongly dependent on $\alpha_5\beta_1$ integrin, whereas within 3D FN matrices neither $\alpha_5\beta_1$ nor $\alpha_v\beta_3$ mediate cancer cell migration. Furthermore, the impact of proteolytic activity on cancer cell migration within both FN environments was investigated. The results of this thesis suggest that general inhibition of MMPs does not influence fibrosarcoma cell migration on FN, regardless of its topography. However, as demonstrated by RNA interference, silencing of a membrane-type MMP, namely MT1-MMP, had opposite effects on cancer cell migration behavior in both FN environments. Depletion of MT1-MMP on 2D FN resulted in reduced migration speed and loss of directionality through inactivation of cofilin activity, which is associated with reduced actin dynamics. On 3D FN matrices, migration speed and cofilin activity was increased upon MT1-MMP silencing.

Since cancer cells are able to switch between proteolysis-driven and actomyosin-based migration modes, the influence of the myosin II inhibitor blebbistatin on cancer cell locomotion was further investigated. In this thesis, fibrosarcoma cell migration in 3D fibrillar FN was highly dependent on myosin II contractility, whereas blebbistatin treatment did not influence the migratory behavior on 2D FN coatings. Therefore, cell migration on both substrates showed remarkable differences regarding adhesion, protease activity and myosin II mediated contractility.

These results highlight the importance of substrate topography for regulating cell migration and the need for more physiological model systems to investigate cancer cell migration. They further suggest that targeting of matrix molecules, rather than cellular receptors or proteolytic enzymes, is a promising approach to inhibit metastatic processes.

2. Zusammenfassung

Zellmigration ist nicht nur ein essentieller Vorgang für eine Vielzahl biologischer Prozesse, wie der Embryonalentwicklung oder der Wundheilung, sondern auch ein bestimmender Faktor pathologischer Prozesse, wie etwa der Ausbreitung von Krebs oder der Metastasierung. Krebszellmigration beruht auf zwei aufeinander abgestimmten, ineinandergreifenden Vorgängen, der Adhesion und der Proteolyse. Während Zelladhäsionsrezeptoren der Integrinfamilie die Interaktionen zwischen Zellen und der extrazellulären Matrix regulieren, bauen Matrixmetalloproteinasen Matrixbarrieren ab und schaffen somit den notwendigen Raum für die Zellmigration. Die meisten Studien, die sich mit Zellmigration beschäftigen, basieren auf zwei Modellsystemen: Kollagengelen oder Basalmembranextrakten. Die extrazelluläre Matrix ist jedoch eine hoch komplexe Struktur, die aus vielen unterschiedlichen Komponenten aufgebaut ist. Funktionen und Einfluss dieser Komponenten auf die Zellmigration unter physiologischen und pathologischen Bedingungen sind noch wenig verstanden. Aus diesem Grund werden neuartige Modellsysteme benötigt, mit deren Hilfe man ein tieferes Verständnis über diejenigen Interaktionen zwischen Tumorzellen und ihrem Mikromilieu gewinnt, welche die Malignität fördern. Hierbei rückte Fibronektin, ein adhesives fibrilliäres Protein der extrazellulären Matrix, in den Fokus, da dessen Expression in vielen Tumoren hochreguliert ist und es die Bildung von prämetastatischen Nischen induzieren kann. In dieser Doktorarbeit wurde das Migrationsverhalten von Fibrosarkomzellen sowohl in einer zweidimensionalen als auch in einer dreidimensionalen Fibronektinmikroumgebung untersucht. Die zweidimenionale Mikroumgebung wird durch Physisorption globulärer Fibronektinmolekülen auf geeigneten Oberflächen als homogener Film hergestellt. Die dreidimensionale Mikroumgebung hingegen, besteht aus einem fibrillären Fibronektinnetzwerk, welches durch zellgesteuerte Prozesse gebildet wird. Durch Blockieren von Integrinen und Mutation der Fibronektindomäne welche die Interaktion mit Zellen ermöglicht, wurde das Zellmigrationsverhalten auf beiden Mikroumgebungen untersucht. Dabei konnte gezeigt werden, dass Zellmigration auf Fibronektinfilmen stark von Integrin $\alpha_5\beta_1$ abhängig ist, während Zellen zur Migration innerhalb des Fibronektinnetzwerkes weder Intergin $\alpha_5\beta_1$ noch Integrin $\alpha_v\beta_3$ benötigen. Darüber hinaus wurde der Einfluss von proteolytischer Aktivität auf die Krebszellmigration untersucht.

Die Ergebnisse dieser Arbeit legen nahe, dass eine generelle Inhibition von Matrixmetalloproteinasen das Migrationsverhalten von Fibrosarkomzellen nicht beeinflusst und zwar unhabhängig von der Beschaffenheit der angebotenen Fibronektinmikroumgebung. Interessanterweise konnte durch RNA Interferenz gezeigt werden, dass eine Membran-assoziierte Metalloproteinase, nämlich MT1-MMP, einen entgegengesetzten Einfluss auf die Zellmigration innerhalb beider Mikroumgebungen ausübt. Auf den Fibronektinfilmen führte die Herunterregulierung der MT1-MMP Expression zu einer Verminderung der Migrationsgeschwindigkeit und dem Verlust von gerichteter Zellmigration. Diesem Phänomen liegt eine Inaktivierung von Cofilin zugrunde, die wiederum eine reduzierte Aktindynamik zur Folge hat. Auf den fibrillären Fibronektinnetzwerken erhöhte sich die Migrationsgeschwindigkeit durch entsprechende Steigerung der Cofilinaktivität, infolge der MT1-MMP Stilllegung.
Da Krebszellen zwischen proteolytisch-gesteuerter und aktinmyosin-basierter Zellmigration umschalten können, wurde der Einfluss des Myosin II Inhibitors Blebbistatin auf die Krebszellmigration untersucht. Es konnte gezeigt werden, dass die Migration von Fibrosarkomzellen auf dreidimensionalen Fibronektinnetzwerken stark von Myosin II abhängig ist. Im Gegensatz dazu, wurde das Zellmigrationsverhalten auf zweidimensionalen Fibronektinfilmen durch die Behandlung mit Blebbistatin nicht beeinflusste. Demnach konnte hier gezeigt werden, dass die Zellmigration auf den beiden Fibronektinmikroumgebungen bemerkenswerte Unterschiede hinsichtlich Zelladhesion, proteolytischer Aktivität und Myosin II vermittelter Kontraktilität aufweist.

Die Ergebnisse dieser Arbeit verdeutlichen, welche Bedeutung die Substrattopographie für Regulierung von Zellmigration hat und dass neue physiologischere Modellsysteme zur Erfoschung von Krebszellmigration benötigt werden. Sie legen weiterhin nahe, dass die direkte Manipulation von Matrixmolekülen und weniger von proteolytischen Enzymen oder zellulären Rezeptoren, ein vielversprechender Ansatz ist Metastasierung erfolgreich zu inhibieren.

3. Introduction

After cardiovascular diseases, cancer is the second most common cause of human deaths in industrial nations [1, 2]. In fact, every third person falls victim to this disease [3]. In the EU, it accounted for 166.9 deaths per 100,000 inhabitants in the years between 2000 and 2010[1]. Since there is a strong correlation between age and cancer risk, aging of the European population will lead to a strong increase in cancer incidences and death rates [4]. Accordingly, almost every second person will be diagnosed with cancer during their life-time [1]. Despite many discoveries made in cell and molecular biology so far, the development of potent anti-cancer drugs shows one of the poorest clinical success rates [5, 6]. These difficulties in anti-cancer drug development originate from the complexity and heterogeneity of this disease. In the following chapter, the current state of cancer research and current challenges for basic research are discussed.

3.1 Cancer – a complex disease

The human body consists of billions of cells forming multiple tissues with diverse functions. Under physiological conditions, tissues are in homeostasis whereby cells proliferate only when necessary and undergo apoptosis when they are either not needed anymore or show signs of genomic damage beyond repair. These processes are controlled by complex cellular mechanisms. Over time, cells may acquire mutations that overcome regulatory control processes resulting in the transformation of normal cells into tumor cells. Usually, transformed cells first form benign tumors which may later progress into malignant neoplasm through additional genomic alterations. Depending on their genotype and origin, cancers can be classified into more than 100 distinct types and tumor subtypes [7, 8]. In fact, even within a single carcinoma, genetic alterations and phenotypes may vary from cell to cell [8], suggesting that there might be no two tumors alike. This heterogeneity impedes not only diagnosis but also the development of generalized potent anti-cancer therapies.

Hanahan and Weinberg suggest that genomic instability and mutations enable cancer cells to acquire a specific set of capabilities which are essential for tumor growth and cancer progression [7, 9]. These so-called hallmarks of cancer (figure 1) help categorizing the vast amount of tumor promoting genomic alterations and provide a common framework for tumor

[1] http://epp.eurostat.ec.europa.eu/statistics_explained/index.php/Causes_of_death_statistics

biology. According to this, cancer cells not only need to sustain proliferative signals and inhibit growth suppression, but also have to evade cell death and gain a limitless replicative potential to survive. In addition, cancer cells have to be able to induce angiogenesis to sustain the supply of oxygen and nutrients within the tumor. Furthermore, malignant cancer cells acquire the ability of invasion and formation of metastases at distant sites. Beside these six well established capabilities characterizing cancer cells, two new hallmarks have emerged in the past few years [9]. First, cancer cells often adjust their metabolism to provide enough energy for sustained cell proliferation. Second, cancer cells develop mechanisms to evade eradication by immune cells. The immune system does not only fight cancer cells, on the contrary, especially cells of the innate immune response show tumor-promoting abilities. While inducing inflammation in the tumor tissue, immune cells excrete a variety of molecules including growth factors, survival factors, proangiogenic factors as well as proteolytic enzymes, such as matrix metalloproteinases (MMPs), that remodel the tumor microenvironment enabling angiogenesis, invasion and metastasis [10]. In doing so, immune cells contribute to the acquisition of hallmark capabilities [9].

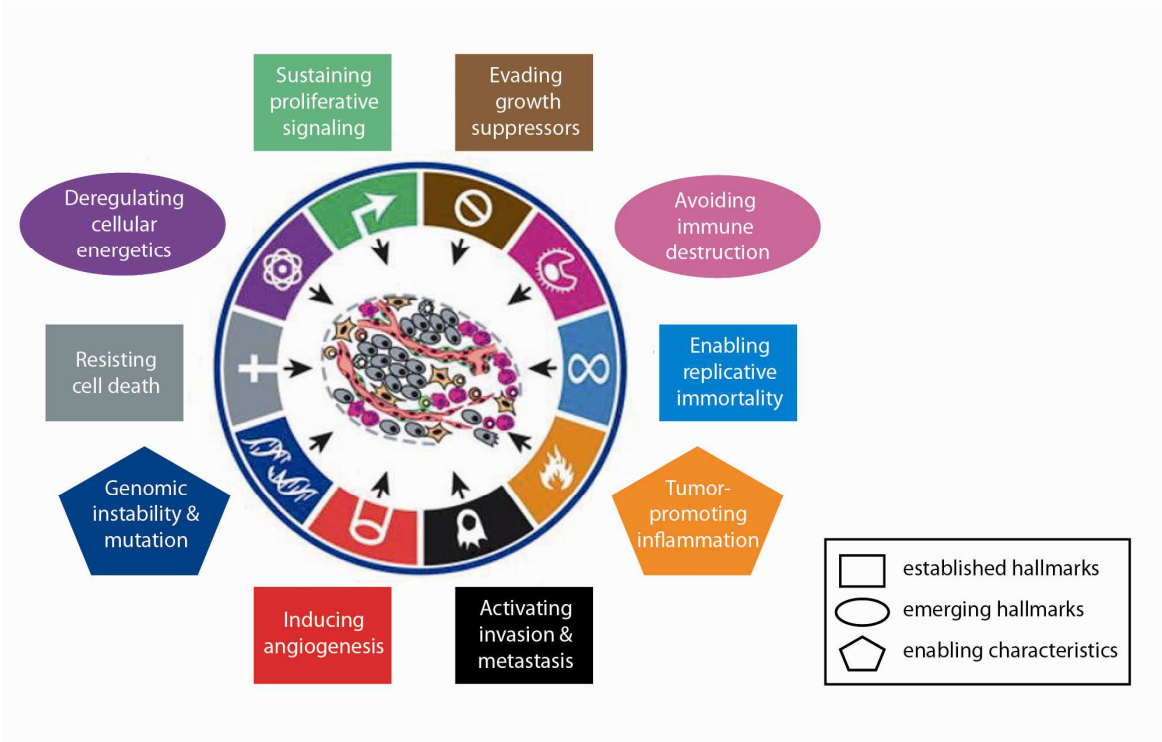

Figure 1: Hallmarks of cancer (adapted from [9])

Enabling characteristics (indicated as pentagons) allow cancer cells to acquire a specific set of abilities, the so-called “hallmarks” of cancer, which are crucial for malignancy. Each hallmark can be obtained through various mechanisms and thus represents a mean to categorize the vast amount of cellular alterations present in cancer. Established hallmarks (indicated as rectangles) describe validated abilities that can be attributed to each carcinosis, whereas emerging hallmarks (indicated as ellipses) are not yet generalized and need to be further evaluated.

3.2 Metastasis

The actual death of cancer patients is mainly caused by metastases [8, 11]. Accordingly, inhibition of metastasis is a promising strategy for reducing cancer-associated deaths. Metastasis is a multistep process through which cancer cells disseminate from the primary tumor to some distal tissue [9, 11] (figure 2).

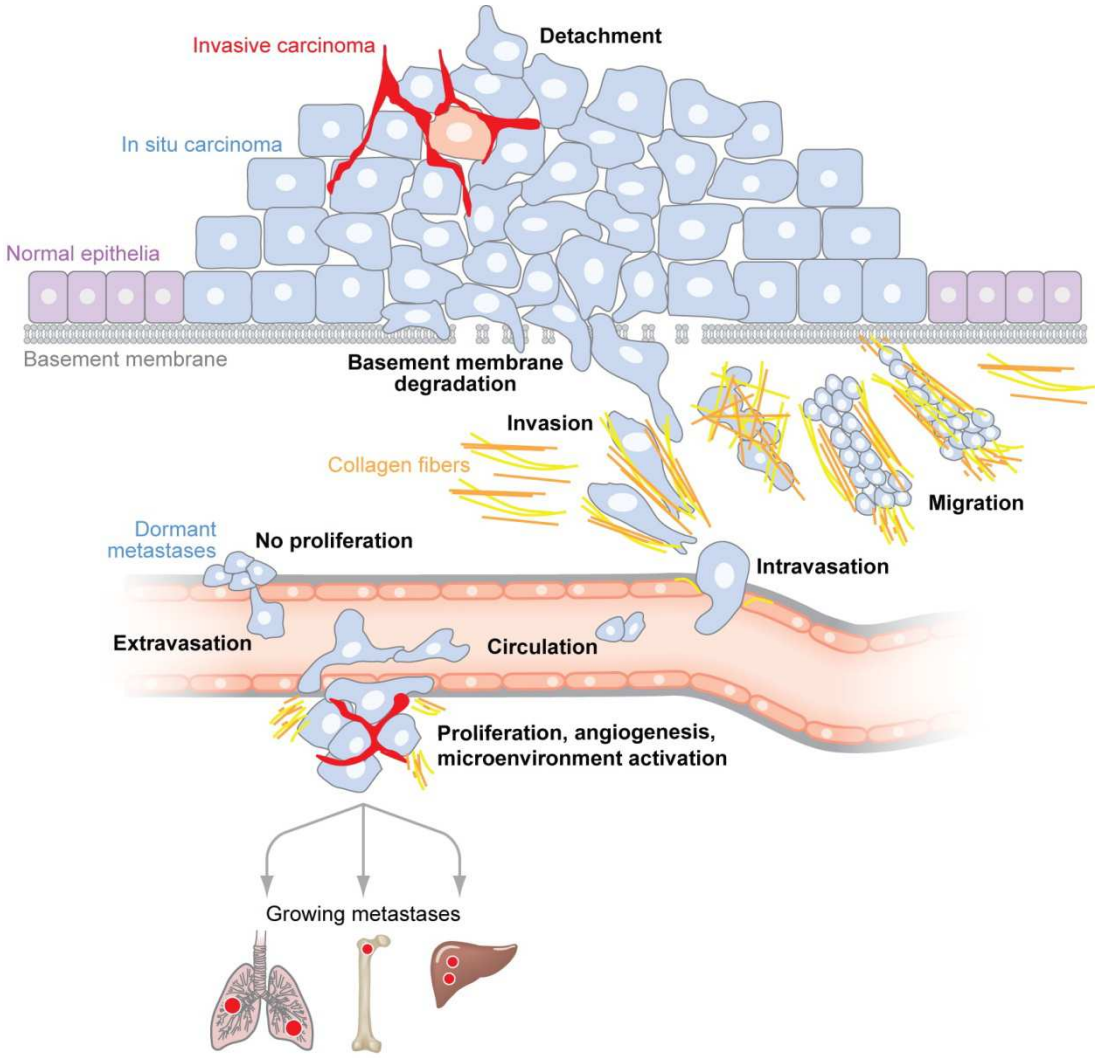

Figure 2: Scheme of the metastatic process [12]

Transformation of epithelial cells is characterized through detachment of cells from the epithelium and the formation of a carcinoma *in situ.* After breaching the basement membrane, tumor cells invade the local stroma, enter the blood or the lymph system and circulate until arrest in small capillaries of distant tissues occurs. Here, they extravasate into the local stroma and eventually colonize.

More than 80 % of human cancers originate within the epithelium [13]. In this case, tumor cells first need to breach the basement membrane to be able to invade the surrounding tissue [9, 11, 12]. Subsequently, they enter the blood circulatory system directly via blood vessels or indirectly through the lymphatic system, a process called “intravasation”. The blood flow carries cancer cells to nearby organs where they are arrested in small capillaries by size restriction and subsequent extravasate in the local parenchyma. These steps are performed with high efficiency, as most of the invading cancer cells successfully reach secondary sites [11].

However, only a small percentage of these cells is able to form micrometastases and even fewer persist to progress into vascularized macrometastases [14, 15], a process termed “colonization”. The inefficient formation of solid tumors at secondary sites is based on the different microenvironments cancers cells are exposed to. Different tissues show specific extracellular as well as cellular compositions with distinct proteomic expression patterns. Hence, the mechanisms cancer cells acquired for surviving at primary sites might be ineffective at their new location. As such, metastases formation only occurs if the cancer cell obtains hallmark abilities that ensure its survival at the new site [16] and if the microenvironment favors tumor cell proliferation [11].

3.3 The tumor microenvironment

The metastatic process depends on more than genetic alterations in malignant tumor cells [17]. In fact, cancer can be referred to as a complex tissue which contains, in addition to neoplastic cells, various non-malignant cell types, secreted molecules (such as MMPs) and non-cellular structures (such as fibrillar ECM proteins). These components form the so-called "tumor microenvironment". In the following paragraphs, the contribution of non-neoplastic cells and of the ECM to malignant progression, are discussed.

3.3.1 Non-neoplastic cells

Normal cells in the body are recruited by cancer cells to participate in tumorigenesis [7, 9]. As mentioned in paragraph 3.1, some immune cells are involved in cancer progression, causing tumor promoting inflammation. In addition, endothelial cells are stimulated to form new blood vessels to supply the growing tumor mass with oxygen and nutrients and recycle metabolic waste products [18]. In contrast to normal blood vessels, which are formed by a monolayer of tightly connected endothelial cells, tumor vasculature shows a defective endothelial monolayer with intercellular openings and transcellular holes [19]. This leakiness of tumor vasculature facilitates cancer cell intravasation as well as immune cell infiltration and subsequent cancer progression. Another cell type found in multiple carcinomas is the fibroblastic cell type [9]. By secreting diverse components of the ECM as well as MMPs, cancer-associated fibroblasts (CAFs) form the stroma of many malignant tumors and thus promote tumorigenesis.

3.3.2 The ECM in cancer

The ECM is a crucial regulator of organ homeostasis and function [20]. Hence, its production, degradation and remodeling is tightly regulated [21]. In cancer patients, ECM dynamics are disturbed, promoting tumor growth and dissemination [13]. As mentioned above, MMPs are key players in matrix remodeling (for more information on MMPs see 3.7). Their expression is highly upregulated in almost every tumor [22, 23], leading to destruction of the healthy ECM and its subsequent replacement by a microenvironment that favors tumor cell proliferation and promotes malignancy [13]. Accordingly, deposition of the ECM components collagen and fibronectin (FN) by CAFs is increased in malignant tissue [24]. Another common ECM alteration is the enhanced stiffness of the tumor stroma in comparison to healthy tissue, which can be elevated up to ten-fold in the case of breast cancer [25-27]. It has

been shown recently, that these changes in the physical properties of the ECM are already present in pre-malignant tissue and drive malignancy [27]. The increased stiffness is mainly caused by enhanced crosslinking of collagen through lysyl oxidases and subsequent linearization of collagen fibers [27]. This increase in tissue stiffness leads to clustering of cell adhesion receptors of the integrin family [28] (introduced in 3.6). Integrin clustering accompanied by increased mechanotransduction enables cell migration, (discussed in 3.9) which is crucial for metastasis.

Moreover, the ECM surrounding tumor blood vessels, the so-called basement membrane, is more porous and fragmentary than in healthy vasculature [29], contributing to leakiness of tumor blood vessels. Interestingly, remodeling of the ECM is not only a local phenomenon. In fact it has been observed recently, that yet unidentified growth factors excreted by different tumor cell lines (LLC and B16 cells) implanted in mice led to enhanced deposition of FN at distant sites, initiating the formation of pre-metastatic niches [30, 31]. The location of these pre-metastatic niches shows a tumor-specific distribution pattern, suggesting that each tumor synthesizes its own set of soluble factors that acts only in specific tissues. Hence, tumors actively create sites for future formation of metastases.

In contrast, there is some evidence that cancer cells might be restored to a normal phenotype if their surrounding ECM is manipulated accordingly [32].

For the development of new anti-cancer drugs, it will be important to gain a better understanding on how the tumor microenvironment, in particular the ECM, influences cancer progression and tumor invasion during metastasis.

3.4 Composition and function of the ECM

Since the ECM is a crucial determinant of tumorigenesis, more information on its function and composition within healthy tissue is presented in the following paragraphs.

Within tissues, cells are surrounded by a complex, insoluble network of various macromolecules that form the ECM [33, 34]. The ECM provides the structural support for tissues and plays a pivotal role for mediating signals that regulate cell fate [20, 33, 34] (figure 3). Such signals are transmitted through different mechanisms. First, cells can interact with ECM components via specific receptors such as integrins that induce cell adhesion and signal transduction. Depending on the tissue type, the ECM is composed of a different set of molecules with distinct physical, biochemical and mechanical properties. In fact, even within tissues the ECM is constantly remodeled to ensure organ function [35]. Cell adhesion receptors mediate ECM characteristics inside the cell and induce the appropriate molecular responses. A second mechanism is based on the interaction of cells with soluble growth factors. Their distribution, activity and availability are regulated by ECM components which bind these factors and enzymes such as MMPs that release these molecules. Hydrolyzed ECM fragments generated by proteases provide further signaling cues.

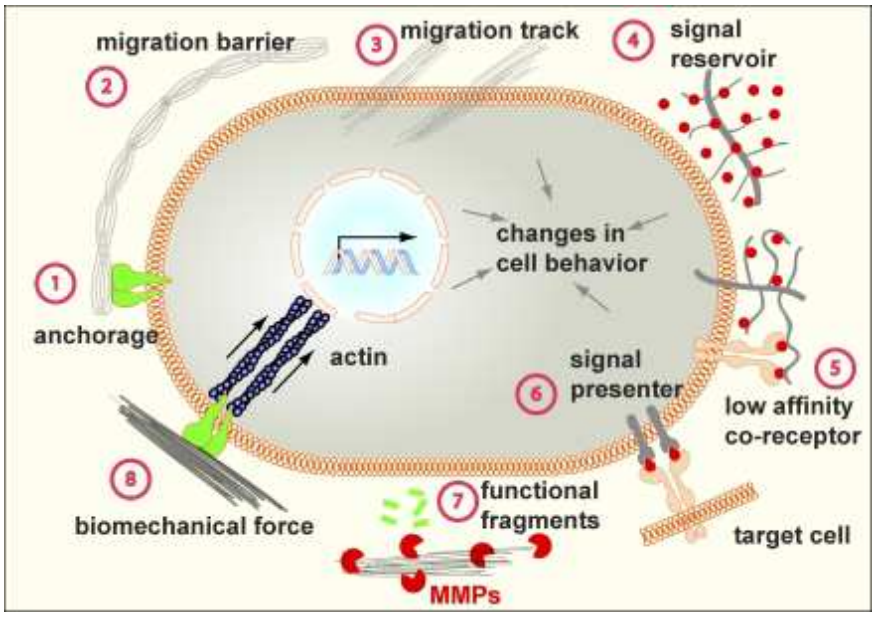

Figure 3: ECM functions [18]

This scheme provides an overview of the diverse ECM functions which are based on its physical, biochemical and mechanical properties. Accordingly, it provides an anchorage site for epithelial cells (1). Depending on the context, the ECM functions either as migration barrier (2) or migration track (3). By binding to diverse soluble molecules, it acts as a signal reservoir and contributes to create diffusion gradients (4). While binding soluble factors, some ECM components function as co-receptors (5) or signal presenters (6). After processing through MMPs, ECM fragments provide further signaling cues (7). Mechanical properties such as ECM stiffness regulate cell behavior (8).

There are two main structural types of ECM [33, 34]: the ECM present in the connective tissue and a specialized ECM sheet that organizes and regulates epithelial tissues, the basal lamina or basal membrane. Both types of ECMs are altered during tumorigenesis to promote cancer progression [18]. In the following paragraphs their composition and functions are discussed.

3.4.1 Composition and function of the basal membrane

The basal lamina is a 2D sheet-like meshwork with a thickness of only 40-120 nm [33, 34]. It surrounds not only individual cells (e. g. muscle or fat cells), but also entire tissues, such as endothelia and epithelia. Within epithelia, the basal membrane constitutes a cellular anchorage site and thus separates the epithelium from the connective tissue and concomitant connects both structures. Furthermore, it provides cues for the establishment of basal cell polarity and cell differentiation [13] and acts as migration pathway during development or tissue regeneration [33, 34].

The basal membrane is mainly formed by the fibrillar glycoproteins laminin and collagen IV as well as the proteoglycan perlecan. While laminin and collagen IV form branched networks, perlecan functions as their cross-linker. Depending on the tissue type, a variety of additional ECM components are intertwined in this meshwork, including FN.

3.4.2 Composition and function of the ECM in the connective tissue

In the human body, the connective tissue has the highest variety of ECM components [33, 34]. Depending on its composition, the ECM can become solid, as in the case of calcified bone or teeth, it can form hydrogel structures, such as the *corpus vitreum* of the eye or structures such as the tendons that have to withstand extremely high tensile strengths. The main components of these different structures are glycosaminoglycans (GAGs) and fibrillar proteins.

GAGs are unbranched polysaccharide chains that are usually covalently bound to proteins as proteoglycans. They form porous hydrated gels, allowing the ECM to resist compressive forces. The fibrillar components of the ECM are embedded in these GAG gels. Collagen I is the most abundantly expressed fibrillar protein within the connective tissue that assembles into large polymers called “collagen fibers”, which bestow upon the matrix the ability to withstand stretching forces. Another type of fibers present in the ECM is elastin fibers that provide resilience. The final class of fibrillar ECM components consists of adhesive

molecules that allow cells to attach to the matrix and are crucial for cell migration. The key member of this group is FN. Structure and function of FN is discussed below.

3.4.3 Fibronectin and its assembly into a fibrillar matrix

FN is a multi-adhesive fibrillar protein of the ECM that is not only able to bind other FN molecules, but also provides binding sites for GAGs, other extracellular proteins as well as cellular receptors [36]. There are two major classes of FN molecules, namely plasma FN and cellular FN [34]. Plasma FN is excreted by hepatocytes into the blood in a soluble, compact, inactive form [37]. It has an important function during early stages of wound healing by being incorporated into the fibrin clot that closes the open wound. Cellular FN is expressed by many cell types, in particular fibroblasts, and assembled into a complex fibrillar network which constitutes a part of the ECM [33, 34].

FN forms a 440 kDa large dimer through a pair of antiparallel c-terminal disulfide bonds [38]. Each subunit shows a modular multidomain structure (figure 4) [36]. In humans, there are 20 isoforms that are generated by alternative splicing at three domains (EIIIA/EDA, EIIIB/EDB and the variable region V). The molecular weight of these subtypes ranges between 230-270 kDa. All FN subtypes consist of three types of modules: the type I, II and III repeats. Cells can interact with FN via the cell binding domain consisting of two type III repeats, the III_9 synergy site and the III_{10} RGD site. The RGD site contains the tripeptide sequence *Arg-Gly-Asp* and can induce integrin binding even if the synergy site is lacking [36]. There are at least nine integrin receptors that are able to interact with FN, namely $\alpha_3\beta_1$, $\alpha_4\beta_1$, $\alpha_5\beta_1$, $\alpha_8\beta_1$, $\alpha_9\beta_1$, $\alpha_v\beta_1$, $\alpha_v\beta_3$, $\alpha_v\beta_6$, and $\alpha_{IIb}\beta_3$ [39, 40]. Except for integrin $\alpha_3\beta_1$, $\alpha_4\beta_1$ and $\alpha_9\beta_1$ all integrins bind to the RGD sequence of FN [40, 41]. Of all FN-binding integrins, $\alpha_5\beta_1$ integrin has the highest affinity to bind FN and the highest FN binding strength [36]. A single point mutation exchanging the amino acid aspartic acid (D) to glutamate (E) results in the formation of an inactive RGE site which does no longer support integrin binding [42]. *In vivo*, mice embryos with a homozygous FN-RGE mutation develop severe vasculature defects and die before birth [43].

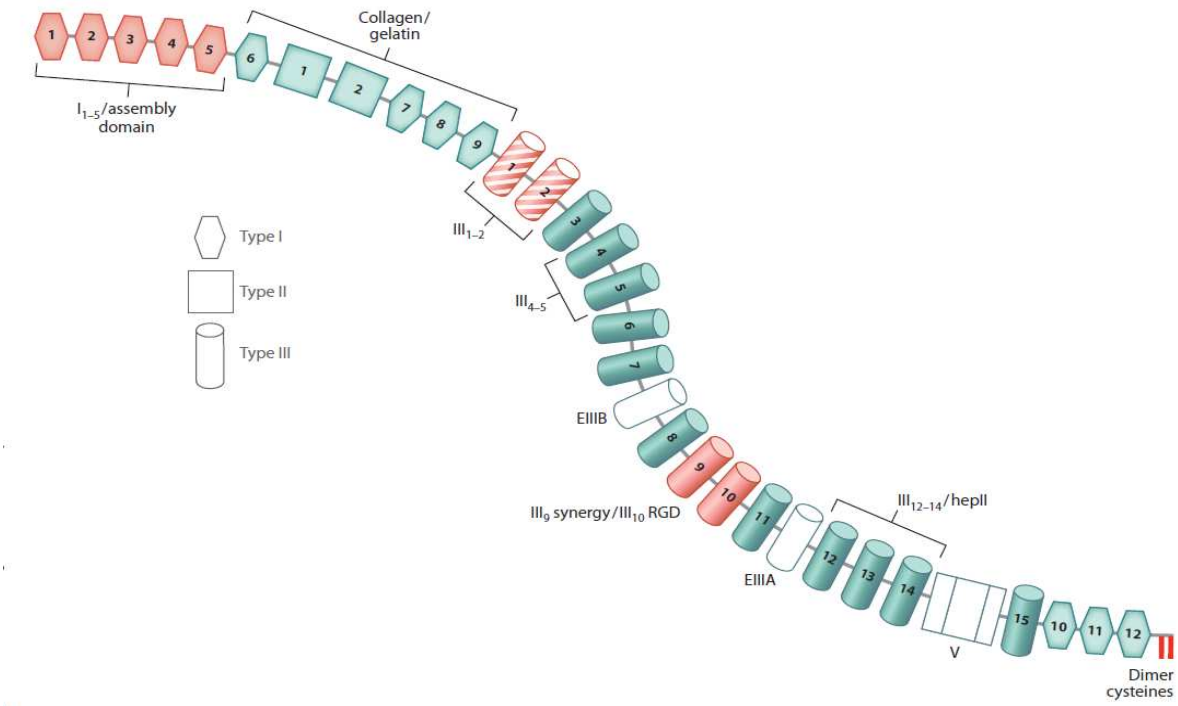

Figure 4: Schemata of FN with its different domains and binding sites [36]

FN is depicted as multi-domain protein consisting of three different types of modules, namely type I (hexagonal), type II (quadratic) and type III (cylindric) repeats. Domains that are necessary for FN matrix assembly are highlighted in red. Alternative splicing sites are indicated in white. All other domains are shown in green. Important domains and binding sites are indicated by name.

FN in solution has a compact conformation and shows no self-assembly ability, even at high concentrations [36]. For the formation of insoluble FN matrices *in vivo*, cellular participation is crucial. In figure 5, the process of FN matrix formation is depicted schematically [36]. FN dimers bind to integrins (mainly $\alpha_5\beta_1$ integrin) via their RGD and synergy sites. Interestingly, cells are also able to assemble FN matrices containing an RGE sequence through binding of $\alpha_v\beta_3$ integrin to an isoDGR motif present in the FN module I_5 [43]. FN binding induces local clustering of integrins that triggers the recruitment of multiple cellular molecules to the integrin cytoplasmatic domains and connect the integrins with the actin cytoskeleton [44]. This connection allows the transmission of forces generated by actin-myosin II contractility to the FN dimers resulting in unfolding of FN molecules. These stretch-induced conformational changes render cryptic FN-binding sites accessible. As a consequence, multiple FN-FN interactions via the N-terminal assembly domain $I_{1\text{-}5}$ and other FN binding sites ($III_{1\text{-}2}$, $III_{4\text{-}5}$ and $III_{12\text{-}14}$) are induced, resulting in the formation of extended insoluble FN fibers.

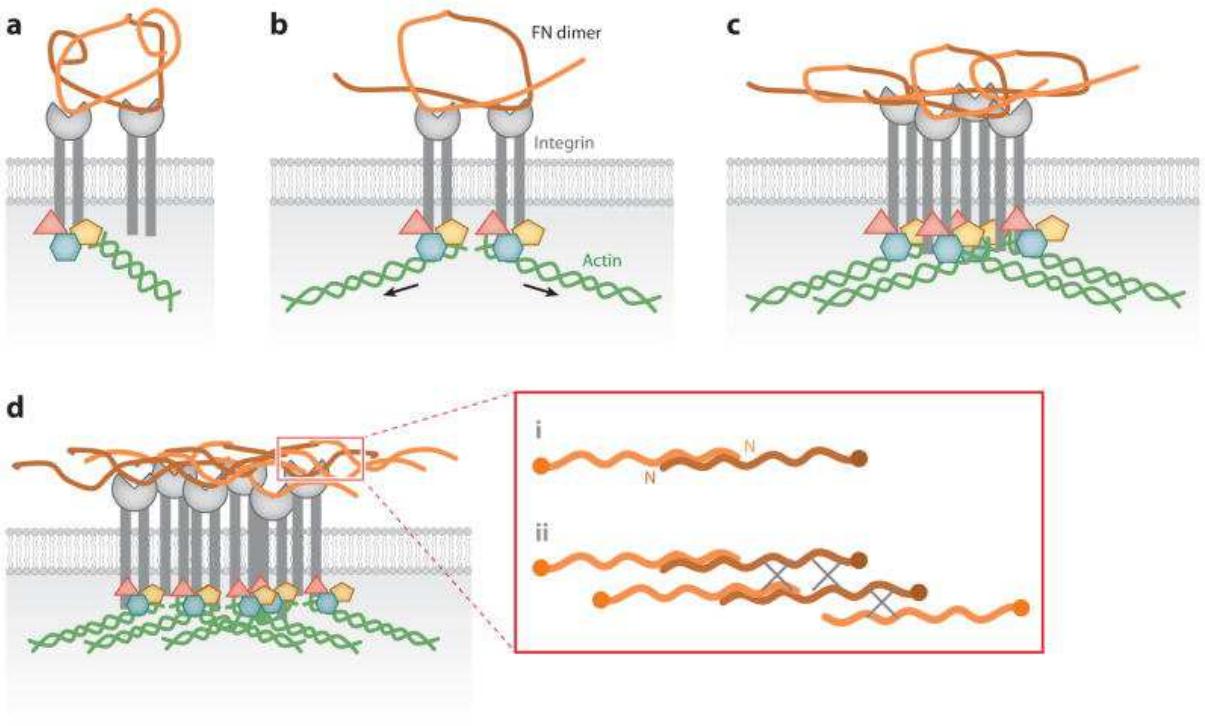

Figure 5: Scheme of FN matrix assembly [36]

The four main steps in FN matrix assembly are depicted. **a**) First, FN dimers (dark and light orange) bind to integrin receptors (gray) recruiting varies cellular molecules (pink, blue, yellow) which connect the cytoplasmatic tail of integrins with the actin cytoskeleton. **b**) Second, the FN dimers are unfolded through contractile forces transmitted via the integrin-actin connection. **c**) Unfolding of the FN molecules and integrin clustering induce FN-FN interactions and further conformational changes in FN resulting in the assembly of an insoluble fibrillar FN network (**d**). The red box indicates FN-FN interactions that lead to FN fiber formation. **i**) FN dimers associated via their n-terminal regions. **ii**) Lateral interactions between FN fibers are marked with X.

3.5 Cell-matrix adhesions

Cell–matrix adhesions are crucial for cell migration, differentiation as well as tissue organization and subsequently regulate embryonic development and tissue homeostasis [45]. In addition, adhesion-mediated signaling is a fundamental requirement for physiological processes such cell survival or cell proliferation and pathological indications, such as wound healing or tumorigenesis [45]. The molecular composition, stability and shape define several different types of cell-matrix adhesions. Most of these structures have been identified *in vitro* on 2D surfaces. Their existence within 3D environments has also been demonstrated, though with varying molecular composition and morphology [45].

3.5.1 Nascent adhesions and focal complexes

The first adhesive structures that can be observed in migrating cells on 2D environments are nascent adhesions and focal complexes [46]. Nascent adhesions are small structures that either continue to mature into focal adhesions (FAs) or disassemble fast. They are formed within the lamellipodium and are dependent on actin. Due to their transient nature and small size, it is challenging to observe them. Focal complexes are found at the lamella-lamellipodium boundary and are associated with myosin [46]. This type of adhesion is larger than nascent adhesions, but shares their transient nature.

3.5.2 Focal adhesions

Mature 2D adhesion structures, so-called FAs, form slowly over time [47] and are usually linked to prominent actomyosin stress fibers [48]. FAs are complex structures that contain more than 150 molecules [49]. By using 3D super-resolution fluorescence microscopy, the organization of some key molecules within FAs has recently been revealed [50]. As shown in figure 6, the cell binds to the ECM with multiple integrins. Integrin clustering induces talin binding and the recruitment of other molecules like focal adhesion kinase (FAK) and paxillin to the cytoplasmic tail of integrins forming the integrin signaling layer. Recently, an alternative mechanism has been published, according to which talin is recruited to adhesive structures by FAK [51]. FAK is a key regulator in integrin signaling and modulates FA formation and turnover, processes that are crucial for cell migration and invasion [52]. Upon activation through autophosphorylation at tyrosin residue 397 (Tyr397), FAK can interact with diverse adaptor proteins and subsequently trigger different signaling pathways including the mitogen-activated protein kinase (MAPK) / extracellular-signal-regulated kinase-2

(ERK2) cascade [12]. ERK2 activation is important for cell proliferation and survival. In addition, it can influence adhesion dynamics in migrating cells. Due to its vertical orientation, talin further functions as a direct linker between the cytoplasmic tails of integrins and actin filaments [50]. Together with vinculin it forms an intermediate force transduction layer. Zyxin and vasodilator-stimulated phosphoprotein (VASP) coordinate the assembly of actin filaments at FAs and are hence located in close proximity to actin. Other proteins like α-actinin help to organize actin-filaments.

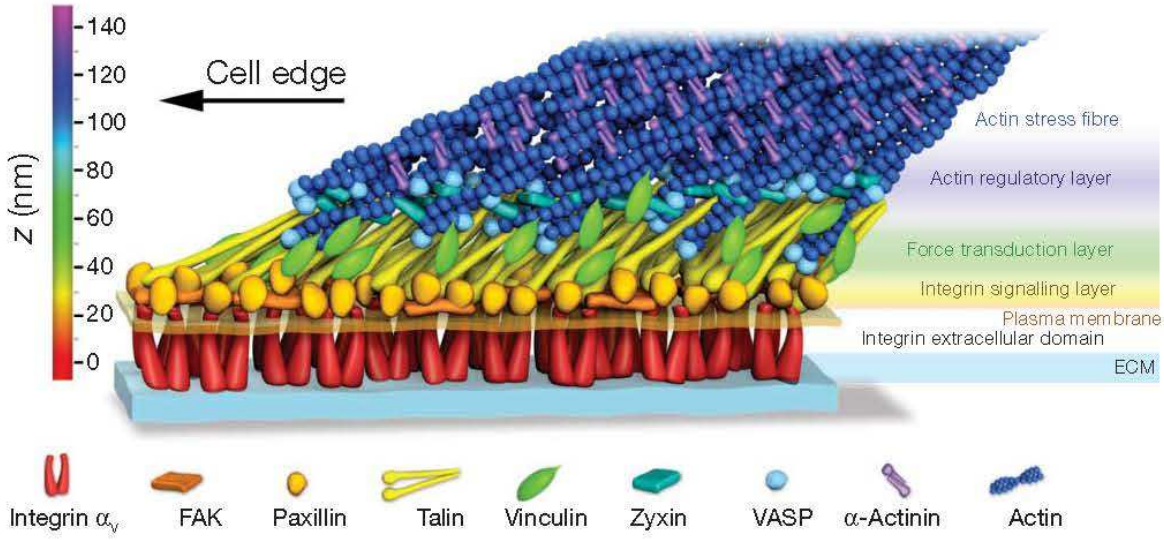

Figure 6: Schematic model of focal adhesion architecture [50]

The organization of some important molecules within FAs is depicted as a non-stoichometric model.

3.5.3 Invadopodia

Malignant tumor cells often form adhesive membrane protrusions termed “invadopodia” [53, 54]. These structures have no defined adhesive borders and display an invasive potential, since they are associated with proteases such as MMPs. Co-localization of ECM degradation and actin polymerization is a main characteristic of these structures. Although it has been demonstrated that integrin $\alpha_5\beta_1$ and $\alpha_v\beta_3$ are important components of invadopodia in different cancer cells [55, 56], no major integrin clusters are detectable. Accordingly, the mechanism how these protrusions interact with the ECM remains to be determined [54].

Non-neoplastic cells can form similar structures, so-called podosomes, that also show matrix degrading abilities [54].

3.6 Cell adhesion receptors of the integrin family

In vertebrates, integrins constitute the major class of cell adhesion receptors. They are not only major determinants in many physiological processes such as embryonic development, immune response and homeostasis, but are also involved in pathological events including cancer [41]. Intergin receptors are heterodimeric molecules consisting of an α- and a β-chain that are non-covalently linked. In mammals, 18 α and 8 β subunits have been identified that can form 24 different receptors. Both integrin subunits are transmembrane proteins with a large N-terminal extracellular domain and a small C-terminal intracellular tail [33, 34]. The extracellular part of an integrin binds to its respective ligands and the cytoplasmic tail interacts with numerous proteins that eventually connect the integrins to the cytoskeleton, enabling cell migration. Ligand specificity is determined by the combination of α and β subunits. An overview of integrins and their respective ligands is given in figure 7. Integrins can be activated through either ligand binding (outside-in activation) or via intracellular regulatory molecules that induce talin binding to cytoplasmatic domains of integrin β-subunits (inside-out activation) [33, 34]. Although some integrins share the same ligands, various knockout experiments in mice demonstrated that each integrin has specific, non-redundant functions [41].

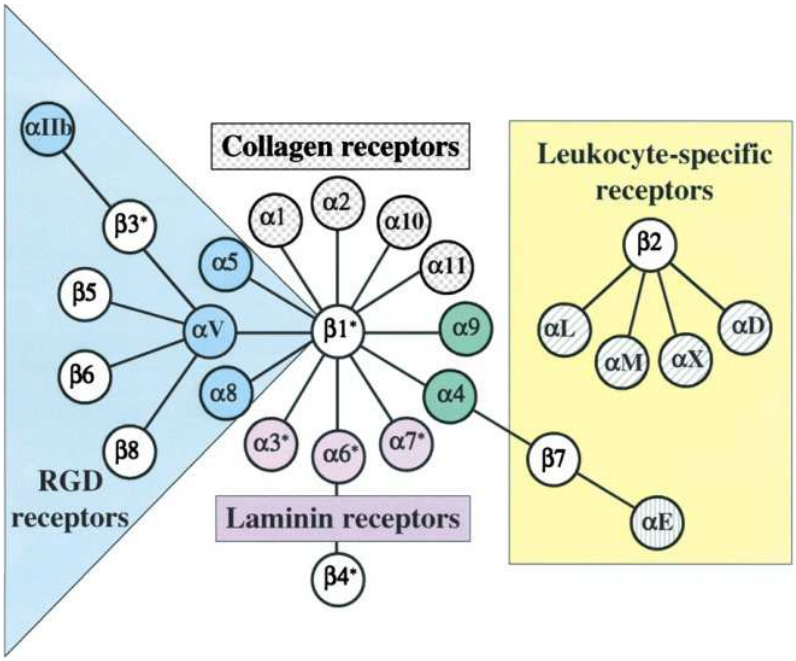

Figure 7: Integrin receptors and their ligands [41]

The associations of the 18 α and 8 β integrin subunits into 24 distinct receptors are depicted. They are further classified into subfamily according to evolutionary relations (indicated by colored α subunits), ligand specificity or exclusive expression on leukocytes.

3.6.1 Integrins in cancer

As discussed above, integrins regulate adhesion to ECM components and subsequently transduce various signals inside the cell that regulate cell fate. In doing so, integrins also modulate cancer cell proliferation, survival, invasion, migration as well as angiogenesis [57].

One common characteristic of cancer cells is their ability to upregulate the expression of integrins, such as $\alpha_v\beta_3$, $\alpha_5\beta_1$ and $\alpha_v\beta_{6,}$ which positively regulate proliferation, survival and migration. In contrast, the expression of integrins that context-dependently suppress tumor progression, such as $\alpha_2\beta_1$ and $\alpha_3\beta_{1,}$ is usually lost [57, 58]. Integrin mediated FAK signaling which is associated with tumor growth, metastasis and cancer cell migration, is activated in many tumors [59, 60]. Furthermore, integrins are involved in ECM remodelling during tumorigenesis, since they recruit and activate proteases, including MMPs. Accordingly, $\alpha_v\beta_3$ integrin localizes pro-MMP2 to the plasma membrane, where it forms a complex with tissue inhibitor of matrix metalloproteinases 2 (TIMP2) and MT1-MMP, thus resulting in its activation [61, 62].

3.7 Matrix metalloproteinases (MMPs)

Remodeling of the ECM by production and degradation of its components is important for organ development and for maintaining organ function. As such, these processes are tightly regulated [21]. In cancer, ECM dynamics are abnormal, thus resulting in defective organ homeostasis and function [18]. During the last decades, a family of proteolytic enzymes, the matrix metalloproteinases (MMPs), have become of major interest due to their role in tissue remodeling under physiological and pathological conditions [21, 22, 61]. The expression of many MMPs is upregulated in various cancer types and their involvement in almost every step of tumorigenesis has been demonstrated [22, 23]. For efficient ECM degradation during tumor cell invasion, MMP activity is confined and concentrated to the pericellular microenvironment [63].

MMPs are multidomain calcium-dependent zinc-containing endopeptidases. In 1962, the first member of this family was discovered as an enzyme present in different tissues of a tad pol, being able to degrade fibrillar collagen [64]. Up-to-date, at least 26 different MMPs have been identified in human [65].These enzymes can be separated into two major groups, soluble enzymes that are excreted into the extracellular microenvironment and so-called membrane type MMP (MT-MMPs) that are present at the cell surface. Almost all MMPs contain at least three domains (figure 8), namely the aminoterminal signal sequence (Pre), important for transport in the endoplasmatic reticulum (ER), the pro-peptide (Pro), usually containing a furin-cleavage site, and a catalytic domain [23]. In addition, many MMPs have a hemopexin-like domain which is usually connected with the catalytic domain through a flexible hinge region. MT-MMPs are inserted in the plasma membrane either via a transmembrane region which is linked to a cytoplasmatic tail, or through a glycosylphosphatidylinositol (GPI) anchor.

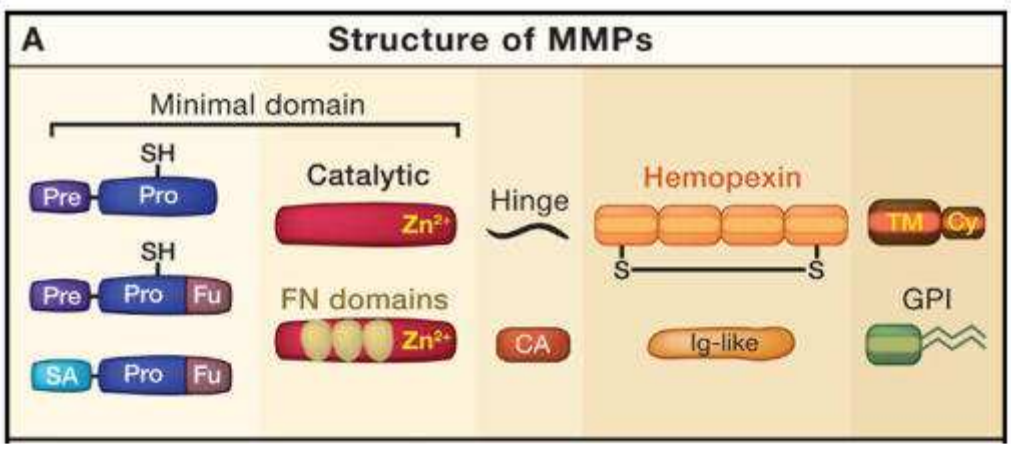

Figure 8: Domain composition of MMPs (adapted from [23])

This scheme provides an overview on the domains present in MMPs. **Pre**: aminoterminal signal sequence, **Pro**: pro-domain containing a thiol-group and an optional furin-cleavage site, **Catalytic**: catalytic domain including a zinc-binding site and optional FN domains, **Hinge**: hinge region, **Hemopexin**: hemopexin-like domain, **TM**: transmembrane domain, **Cy**: cytoplasmatic tail and **GPI**: a GPI-anchor. MMP23 has a unique structure including **SA**: an amino-terminal signal anchor, **CA**: a cysteine array and **Ig-like:** an immunoglobulin (Ig)-like domain.

MMPs are synthesized as inactive zymogens. A cysteine residue within in the pro-domain blocks the catalytic center of the enzyme through interaction with the zinc ion present in the catalytic site. Activation occurs through pro-domain cleavage or chemical alteration of the cysteine residue, a process called “cysteine-switch” [23]. The main physiological mechanisms to regulate the activity of MMPs are the conversion of the zymogen to the active protease as well as the expression of physiological MMP inhibitors, in particular tissue inhibitors of metalloproteinases (TIMPs). For membrane type 1 matrix metalloproteinase (MT1-MMP) an additional activity control mechanism has been reported. Its catalytic active domain can be shed through autocatalytic or MMP-2 mediated cleavage, resulting in the generation of a 44 kDa metabolite [66, 67].

Each MMP is able to degrade a specific set of ECM components with partially overlapping substrate specificities to other members of its family. Hence, the variety of MMPs not only enables the degradation of nearly every component of the ECM, but also the compensation for the loss of one member. This has been demonstrated in MMP-knockout experiments in mice, where the loss of a single MMP did not strongly affect the development of the animals, with the exception of MT1-MMP [68-70]. MT1-MMP deficient mice showed severe defects in organization of the connective tissue due to inefficient collagen turnover resulting in dwarfism, osteopenia and arthritis [68].

3.8 Membrane type 1 – matrix metalloproteinase (MT1-MMP)

MT1-MMP, a 66 kDa protease, was the first MT-MMP to be discovered in 1994 [71]. Its expression levels are highly upregulated in invasive and metastatic cancer [72] as well as during angiogenesis [69] and tumor progression in general [73]. Therefore, it is a potentially important target for the development of therapeutic interventions. Up to date, only general MMP inhibitors against the catalytic activity of MMPs were developed. However, clinical trials did not yield the desired benefits for patients [74, 75].

The proteolytic function of MT1-MMP is well understood. MT1-MMP is able to activate pro-MMP2 [71] as well as pro-MMP13 thereby acting as a pacemaker of proteolytic cascades [76]. Moreover, it cleaves different extracellular matrix (ECM) components, for instance collagen or fibronectin as well as various cell surface associated molecules including integrins [77, 78]. By doing so, MT1-MMP alters the pericellular microenvironment and influences cellular fate. It is known that MT1-MMP proteolytical activity is necessary for degrading the basement membrane during cancer invasion [79]. Pericellular matrix degradation at FAs, an important process during cell invasion, is mediated through a complex between MT1-MMP and FAK-p130Cas [80]. In addition, MT1-MMP degrades the ECM surrounding blood vessels during angiogenesis [81, 82].Beyond its function in degrading ECM components to create space for cell migration, MT1-MMP directly interacts with integrins and subsequently regulates locomotion of cancer cells in a more defined way. In fact, MT1-MMP acts as an integrin convertase by processing different pro-forms of integrins including α_v and α_5 subunits [83]. MT1-MMP processed $\alpha_v\beta_3$ integrins are more efficient in promoting FAK phosphorylation and cancer cell migration [84]. It was further demonstrated that MT1-MMP co-localizes with $\alpha_v\beta_3$-integrin at motility-associated structures where it degrades ECM components and promotes endothelial cell migration [85]. In 3D collagen matrices, β_1 integrins localize with MT1-MMP at the leading edge of cancer cells, promoting matrix degradation and cancer cell migration [86].During the last decade, non-proteolytic functions of MT1-MMP came into focus. As a membrane-bound enzyme, MT1-MMP possesses a cytosolic domain that is important for its trafficking and intracellular signaling processes [87]. Thus, it has been demonstrated that MT1-MMP is able to enhance ERK and reduce FAK autophosphorylation, promoting FA turnover and consequent cell migration in a 2D FN environment [88].Despite the information on single aspects of MT1-MMP function, it is still not completely understood which changes within the complex interplay of MT1-MMP and the ECM drive cancer cell migration within 3D environments, especially concerning FN.

3.9 Tumor cell migration

Adhesion and proteolysis represent the main mechanisms that govern the metastatic process and are essential for cancer cell invasion and migration [12]. According to Friedl and Wolf [89, 90], cancer cells move either as a collective or as individuals assuming an amoeboid or mesenchymal migration mode. Here, only single cell migration types are introduced, since fibrosarcoma cells – the cell type studied in this thesis - disseminate as single cells [90].

3.9.1 Mesenchymal migration

Mesenchymal migration is observed in 2D as well as in 3D environments [45]. It is maybe the best characterized migration mode and can be divided into multiple steps [33, 34, 90]. First, membrane protrusions extend at the leading edge of the cell by actin polymerization. The cell binds to a component of the ECM via cell adhesion receptors (mainly integrins). These interactions induce integrin clustering and the formation of focal contacts that may evolve into FAs. Actin filament contraction mediated by the motor protein myosin II results in forward movement of the cell body [91, 92]. Therefore, MMP-dependent, pericellular proteolysis of the surrounding substrate creates the required space [90]. Finally, FAK mediates the disassembly of FAs and subsequent recycling of their components at the trailing edge [90]. This process is further enhanced by MMP-dependent degradation of the substrate.

Migration speed is dependent on the turnover rate of FAs [93, 94]. On the one hand, cells have to form FAs to be able to exert forces required for their forward movement. On the other hand, FAs that are not disassembled fast enough hinder migration. As such, an intermediate level of adhesion is favorable for fast cell migration [93, 94]. Beside the importance of FA turnover, dynamic modulation of the actin cytoskeleton is crucial for fast cell migration. A main regulator of actin dynamics during cell migration in cancer is cofilin [95-99]. Depolymerisation of actin filaments by cofilin creates a pool of free actin monomers for new actin polymerization and subsequently enhances actin filament dynamics [100]. In addition, it leads to the formation of free barbed ends that are needed for the initiation of actin polymerization [101]. Activity of cofilin is inhibited by phosphorylation of serin at residue 3 (Ser3) [102].

3.9.2 Amoeboid migration

Besides the mesenchymal migration type, cells also exhibit a less adhesive amoeboid movement in 3D environments [90, 103, 104]. Characteristics of amoeboid migration are weak and transient interactions between cells and their substrate as well as the lack of FAs and actin stress fibres. In fact, cell movement is driven by cortical filamentous actin and myosin activity. Instead of using proteolytic activity to degrade migration barriers, amoeboid cells are highly deformable and squeeze their body through holes in the ECM meshwork. The absence of FAs enables these cells to move 10-30 times faster than cells showing mesenchymal migration [104].

4. Motivation

During metastasis, cell migration is driven by interaction of cancer cells with the tumor microenvironment, including the ECM. In order to study such interactions *in vitro*, two main model systems, namely 3D fibrillar collagen gels or Matrigel (reconstituted basement membrane) have been used [79]. The study of other ECM proteins, in particular FN, has not received much attention in the context of 3D matrices. FN is usually studied in a non-physiological state, where globular FN molecules are physisorbed onto 2D plastic or glass surfaces. Experiments with fibroblasts demonstrated that cells show differences in morphology, adhesion, proliferation and cell signaling between 2D and 3D FN environments [105]. These findings highlight the need for more physiological systems to study the influence of 3D FN environments on cancer cell migration. In this thesis, a more physiological approach, using cell derived 3D fibrillar FN matrices, is proposed.

The aim of this work was to compare HT1080 cell migration behavior on 2D FN coatings and 3D FN fibrillar matrices. Using time-lapse microscopy HT1080 cell migration was monitored on both substrates. While cell morphology and the interaction between cells and FN fibers were studied qualitatively, average velocity and directionality of cell migration were analyzed in a quantitative manner. The involvement of some key molecules in ECM remodeling and cancer cell migration, namely $\alpha_5\beta_1$ and $\alpha_v\beta_3$ integrins as well as MT1-MMP, were investigated.

In this thesis, the following questions were addressed:

1) Do HT1080 cells show the same phenotype and migration mode on 2D and 3D FN environments?
2) Are there any differences concerning average velocity and directionality of cell migration between both FN environments?
3) Which impact do $\alpha_5\beta_1$ and $\alpha_v\beta_3$ integrins have on cancer cell migration on 2D and 3D FN environments?
4) How do MMPs, and in particular MT1-MMP, influence cancer cell migration on both FN environments?

5. Materials and Methods

5.1 Cell Culture

All experiments in this section were performed under a sterile bench (# 51022515, Herasafe KS12, Thermo Fisher Scientific, Kendro Laboratory Products GmbH, Germany) with sterile equipment from Greiner Bio-One GmbH, (Germany) and BD Biosciences (Falcon™, Germany) to prevent contamination of samples and cells.

5.1.1 Cell lines and culture conditions

Different cell lines (see table 1) were cultured in the respective medium supplemented with 10 % (v/v) fetal bovine serum (FBS; # F7524, Sigma-Aldrich Chemie GmbH, Germany) or newborn calf serum (NCS; # 16010, Life Technologies GmbH, Gibco®, Germany), 1 % (v/v) L-Glutamine (# 25030, Gibco®) and 1 % (v/v) Penicillin/Streptomycin (# 15140-122, Gibco®) (see table 1).

Table 1: Information on cell lines and culture media

Cell line	Origin	Culture medium
HT1080 [106]	*Homo sapiens* connective tissue; fibrosarcoma	DMEM (# 10938, Gibco®) + 10 % FBS + 1 % L-Glutamine + 1 % Penicillin/Streptomycin
MCF7 [107]	*Homo sapiens* mammary gland (breast); adenocarcinoma	RPMI (# 31870, Gibco®) + 10 % FBS + 1 % L-Glutamine + 1 % Penicillin/Streptomycin
MV3 [108]	*Homo sapiens* epithelial cell line; melanoma	RPMI + 10 % FBS + 1 % L-Glutamine + 1 % Penicillin/Streptomycin
COS [109, 110]	*Cercopithecus aethiops* fibroblast cell line from kidney; SV40 transformed	αMEM (# P04-21250, Pan Biotech GmbH, Germany) + 10 % FBS + 1 % L-Glutamine + 1 % Penicillin/Streptomycin
NIH3T3 FN-YPet[2] [111]	*Mus musculus* embryonic fibroblast stably expressing YPet-fibronectin	DMEM + 10 % NCS + 1 % L-Glutamine + 1 % Penicillin/Streptomycin
$FN^{RGE/RGE}$ [3] [43]	*Mus musculus* embryonic fibroblast stably expressing fibronectin with mutated cell binding domain	DMEM + 10 % FBS + 1 % L-Glutamine + 1 % Penicillin/Streptomycin

[2] Kindly provided by T. Ohashi and HP Erickson, Duke University, USA
[3] Kindly provided by R. Fässler, Max Planck Institute for Biochemistry, Martinsried, Germany

Cells were kept in an incubator at 37 °C under 5 % CO_2 atmosphere. After reaching 90-100 % confluence, culture medium was removed and the cell monolayer was washed once with warm Dulbecco´s phosphate buffered saline (DPBS; # H15-002, GE Healthcare, PAA laboratories GmbH, Germany) to remove residual medium. Cells were detached by using 0.05 % Trypsin-EDTA (# 25300, Gibco®). The enzymatic reaction was neutralized by adding culture medium and cells were passaged in a 1:10 dilution.

5.1.2 Preparation of fibronectin (FN) and vitronectin (VTN) coatings

Human cellular fibronectin (# F2518, Sigma-Aldrich) and human plasma vitronectin (VTN; # V8379 Sigma-Aldrich) were shipped as lyophilized powder. The FN stock solution [1 mg / ml] was prepared by adding 0.5 ml sterile MilliQ-water to 0.5 mg FN. For optimal solubilization, the FN solution was incubated for 30 min at room temperature (RT) without agitation. In contrast, 50 µg VTN was resuspended in 1 ml sterile MilliQ-water. The VTN stock solution [50 µg / ml] was filtered through a 0.2 µm sterile cellulose mixed esters syringe filter (# KH54.1, Carl Roth GmbH & Co. KG, Germany). Both solutions were aliquoted and stored at -20 °C.

The FN working solution [10 µg/ml] was obtained by diluting the FN stock solution with sterile DPBS. For coating of 35 mm high µ-dishes (# 1156, ibidi GmbH, Germany), 300 µl of FN working solution was pipetted in the inner circle of the dish (area: 3.5 cm^2) and incubated for at least 45 min at RT. For coating of 8-well µ-slides (# 80826, ibidi), 200 µl of FN working solution was pipetted in each well (area: 1 cm^2) and incubated for at least 45 min at RT.

The VTN working solution [0.5 µg/ml] was obtained by diluting the stock solution with sterile MilliQ-water. 200 µl/cm^2 working solution was pipetted in the inner circle of a 35 mm dish. The surfaces were incubated at 37°C for 1-2 h. Before cell seeding, excess solution was removed and surfaces were gently rinsed with DPBS.

5.1.3 Preparation of fibrillar fibronectin matrices

An overview of the preparation of fibrillar FN matrices is shown in figure 9. Either 35 mm high µ-dishes or 8-well µ-slides were used. All solutions/liquids were applied at a volume of 1 ml per 35 mm dish and 250 µl per well of an 8-well µ-slides respectively. Dishes/slides were coated with a silane solution containing 5.4 ml 100 % ethanol (EtOH; # A3678, AppliChem GmbH, Germany), 400 µl MilliQ-water and 120 µl 3-aminopropyl triethoxysilane

(# A3648, Sigma-Aldrich) for 1 h at RT. The used dishes/slides were plasma-treated by the manufacturer to render them hydrophilic (ibiTreat). Hence, the silane reacted with available OH-groups and bound covalently to the surfaces. Then, the dishes/slides were washed twice with 100 % EtOH as well as MilliQ-water, followed by a 30 min incubation in a 2 % (v/v) glutaraldehyde solution (# G7651, Sigma-Aldrich) diluted in MilliQ-water. After rinsing with MilliQ-water the dishes/slides were incubated in plasma FN solution [10 µg / ml] (# F1141, Sigma-Aldrich) for 15-30 min. The cross-linking agent glutaraldehyde reacted with amino groups of the silane and immobilized FN on the surfaces. This procedure helped to increase adhesiveness of cells and their produced FN matrix on the culture dishes/slides. Before plating NIH3T3 FN-YPet or $FN^{RGE/RGE}$ cells (3.5 x 10^5 cells per 35 mm µ-dish, 0.5 x 10^5 cells per well of the 8-well µ-slides), the dishes were rinsed with MilliQ-water. Cells were cultured for four days until reaching confluence. During this time the fibroblasts expressed cellular FN and preassembled it into FN matrices. To obtain cell-free FN matrices, cells were washed once with warm DPBS and then lysed according to an adapted protocol published in [112]. In brief, cells were washed once with buffer 1 (100 mM Na_2HPO_4, 2 mM $MgCl_2$, 2 mM EGTA; pH: 9.6). Cell lysis buffer (8 mM Na_2HPO_4, 1 % NP-40; pH: 9.6) was added and the samples were incubated for 10 min at 37 °C, followed by an additional 20 min incubation at 37 °C with fresh lysis buffer. The FN matrix was washed once with buffer 2 (300 mM KCl, 10 mM Na_2HPO_4; pH: 7.5) and subsequently rinsed with MilliQ-water as well as DPBS. Although FN matrices can be stored for several days at 4 °C, they were freshly prepared for each experiment.

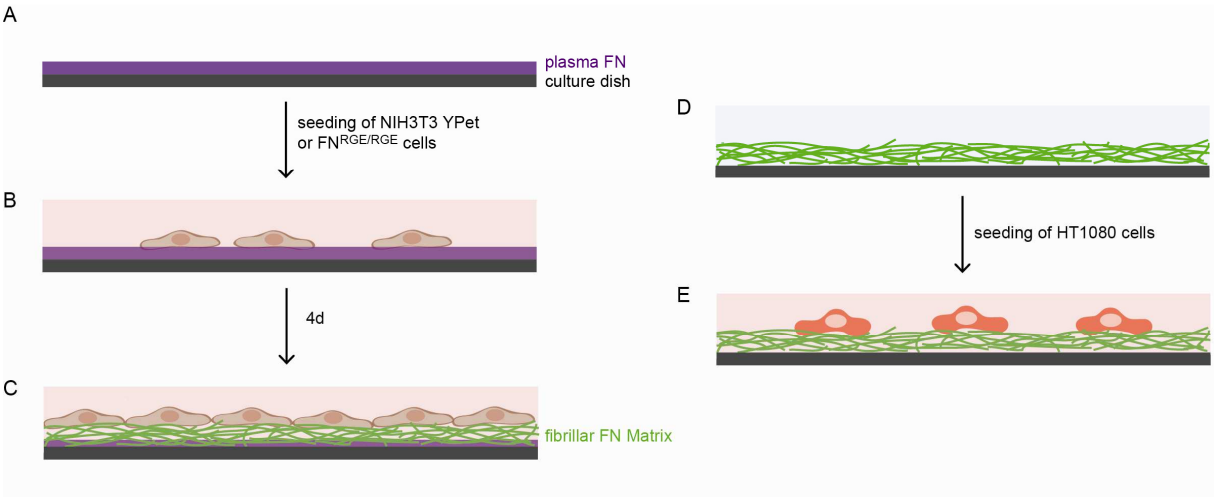

Figure 9: Preparation of fibrillar FN matrices
Here, an overview of the preparation of fibrillar FN matrices is shown. **a)** Surfaces were crosslinked with plasma FN by silane and glutharaldehyde. **b)** NIH3T3 FN-YPet or $FN^{RGE/RGE}$ cells were seeded on the substrates and **c)** cultured until reaching confluence. During this time the cells expressed cellular FN and preassembled it into FN matrices. **d)** Fibroblasts were lysed and **e)** HT1080 cells were seeded on the FN matrices for further analysis.

5.1.4 MT1-MMP silencing via small interfering ribonucleic acids (siRNAs)

RNA interference (RNAi) is a widely-used method for effective and selective inhibition of protein expression. Cells are transfected with synthesized single stranded RNA molecules that are designed to bind selected mRNA transcripts. The formation of double stranded RNA molecules activates the ribonuclease Dicer, which degrades these complexes and hence prevents their transcription. The reduction in protein expression is further dependent on the stability/half-life of the respective protein.

For silencing MT1-MMP protein transcription, the ON-TARGET*plus* Human MMP14 siRNA SMARTpool (# L-004145-00-0005, Thermo Fisher Scientific, Abgene Ltd, Dharmacon®, UK) was chosen. In the text, it is named "siMT1-MMP" or "siM". As non-targeting control siRNA#1 was selected (# D-001210-01-05, Dharmacon®) indicated with "siControl" or "siC". A 100 µM siRNA stock solution was prepared by resuspending 5 nM siRNA with 50 µl of siRNA buffer (5x) (# B-002000-UB-100, Dharmacon®) diluted in RNase-free water (# B-002000-WB-100, Dharmacon®). For optimal solubilization, the siRNA solution was incubated on an orbital shaker for 30 min at RT. The siRNA was aliquoted and stored at -20 °C.

The optimal conditions for MT1-MMP silencing in HT1080 cells were determined. One day before siRNA-transfection, HT1080 cells were seeded in a 24-well plate at different cell densities: 0.6×10^5, 1.2×10^5 and 1.8×10^5 cells per well (area: 2 cm^2). The siRNA-transfection was performed with the DharmaFECT transfection reagent number 4 (# T-2004-01, Dharmacon®) according to manufacturers' instructions. A 5 µM siRNA working solution was prepared by diluting the 100 µM stock solution with siRNA buffer. For each well 2.5 µl of this siRNA solution was mixed with 47.5 µl Opti-MEM® (# 31985, Gibco®). Meanwhile, DharmaFECT transfection reagent 4 (recommended for transfecting HT1080 cells) was mixed with Opti-MEM® to a final volume of 50 µl. Different volumes of transfection reagent (0.5 µl, 1 µl, 1.5 µl or 2 µl) were used to find the optimal conditions for MT1-MMP silencing. The siRNA and the transfection reagent solutions were incubated for 5 min at RT. Then, both solutions were combined, gently mixed and further incubated for 20 min at RT. Culture medium was removed and HT1080 cells were washed once with warm DPBS. Finally, 400 µl antibiotic-free complete medium was added, followed by dropwise pipetting of 100 µl transfection mix per well. The next day, the medium was replaced by standard culture medium. Subsequent steps (e. g. FACS-staining, RNA-extraction, western blot) were performed 48 h and/or 72 h after siRNA-transfection if not indicated otherwise.

5.1.5 Integrin blocking approach

To study the influence of $\alpha_5\beta_1$ and $\alpha_v\beta_3$ integrin binding to FN matrices, the blocking effect of antibodies directed against these integrins was investigated. FN and VTN coatings were prepared according to recommendation of the manufacturer (see 5.1.2). Bovine serum albumin [10 µg/µl in DPBS] (BSA; # B4287-5G, Sigma-Aldrich) coated surfaces were used as a negative control.

After removing culture medium and washing HT1080 cells with DPBS, cell were incubated with cell dissociation buffer (# 13150-016, Gibco®) for 5 min at 37 °C. After adding standard culture medium, the cell number was determined with a Neubauer counting chamber (# 718605; Brand GmbH & Co. KG, BlauBrand®, Germany). Then, 1.5×10^5 cells were centrifuged at 500 x g for 5 min in a microcentrifuge (5417R, Eppendorf Vertrieb Deutschland GmbH, Germany). Cell pellets were resuspended in 50 µl serum-free DMEM containing 2 mg/ml BSA and a 1:20 dilution of primary antibodies against $\alpha_v\beta_3$ (# MAB1976, Millipore, Merck KGaA, Germany), $\alpha_5\beta_1$ (# MAB1969, Millipore, Merck) or mouse IgG (# I5381, Sigma-Aldrich). Cells were incubated on ice for 30 min, centrifuged at 500 x g for 5 min at 4 °C, resuspended in culture medium and plated on coated surfaces. After 1 h, non-adherent cells were removed by DPBS rinsing. Images from five different fields were acquired per sample with a brightfield microscope Axiovert 40C and an A-PLAN 10 x Ph1 phase contrast objective (both Carl Zeiss AG, Germany). The experiment was performed in three biological replicates. Cell number was determined with the cell counter plugin of Image J [113]. For data analysis and statistical testing see paragraph 5.7.1.

5.2 Analysis of integrin mRNA expression in different cell lines

5.2.1 Phenol-chloroform based RNA extraction

To determine integrin mRNA expression in different cell lines, 2.4 x 10^6 cells of each cell line were seeded in 100 mm plates and cultured until complete confluence was reached. RNA was extracted using peqGOLD RNAPure (# 30-1010, Peqlab Biotechnologie GmbH, Germany) according to the manufacturers' instructions. All centrifugation steps were performed at 12,000 x g in a precooled centrifuge at 4 °C. Cells were lysed by mixing with 6 ml peqGOLD RNAPure reagent. Samples were kept at RT for 5 min to ensure dissociation of nucleotide complexes. After adding 1.2 ml chloroform, samples were shaken vigorously for 15 s, followed by an incubation on ice for 3-10 min. Subsequent centrifugation for 5 min leads to separation of the solution in three different phases: a lower yellow phenol-chloroform phase, an interphase and an upper aqueous phase containing the RNA. The watery phase was transferred into a fresh 1.5 ml tube. Precipitation of the RNA was achieved by adding equal volumes of isopropanol. After 15 min incubation on ice, RNA-lysates were centrifuged for 10 min. The supernatant was removed and the RNA precipitate was washed with 1 ml 75 % EtOH followed by another centrifugation for 10 min. The RNA pellet was air dried and then resuspended in RNAse-free water. Heating the RNA solution to 55-60 °C facilitated the solubility. Quality and quantity of the RNA were determined using the spectrophotometer ND-1000 (Peqlab).

5.2.2 CopyDNA (cDNA) synthesis

For cDNA synthesis with the RevertAid™ first strand cDNA synthesis kit (# K1622, Thermo Fisher Scientific Inc., Fermentas GmbH, Germany), 1 µg total RNA was used. Oligo(dT) primer (1 µl) were mixed with the RNA solution and diethylpyrocarbonate (DEPC) treated water to a final volume of 13 µl. After incubation of the RNA-oligo(dT) mix for 5 min at 70 °C, 7 µl of a mastermix containing 4 µl reaction buffer (5 x), 1 µl inhibitor and 2 µl dNTP mix [10 mM] were added. The reaction mixture was incubated for 5 min at 37°C. Finally, 1 µl of reverse transcriptase was added and the reaction mix was placed in a PCR machine (Bio-Rad Laboratories GmbH, DNAEngine®, Germany). The samples were first incubated for 60 min at 42 °C, followed by an incubation at 70 °C for 10 min. Quality and quantity of cDNA samples were determined using the spectrophotometer ND-1000. The cDNAs were stored at -20 °C until usage.

5.2.3 Polymerase chain reaction (PCR) of integrin transcripts

PCR-products of different integrin transcripts were amplified with sequence specific primers (Table 2) using the HotSTARTaq Master Mix Kit (# 203443, Qiagen GmbH, Germany). Therefore, 1 µl of cDNA [500 ng/µl] was mixed with 0.625 µl forward and 0.625 µl reverse primer (final concentration 0.25 µM each), 12 µl of a master mix (2 x) (containing Taq polymerase, dNTPs PCR-buffer and $MgCl_2$) and 10.75 µl PCR water. In table 3 the applied PCR program is shown.

Table 2: Primers used for integrin PCR
Primers were purchased from Life Technologies. Upon arrival, nuclease-free water (# C7112985, US Biological, Biomol GmbH, Germany) was added to each vial to obtain a primer stock concentration of 100 µM.

Name	Sequence (5' to 3')	Fragment size	Reference
α_v for	AGAATCATTCCTATTCTCTG	260 bp	[114] DNA-sequence: NM_002210.3 *homo sapiens* integrin, alpha v
α_v rev	TTCTTCTTGAGGTGGCCGGA		
α5 for	CCTCACTTACGGCTATGTCA	347 bp	designed with NCBI Primer-BLAST Primer designing tool, DNA-sequence: NM_002205.2 *homo sapiens* integrin, alpha 5
α5 rev	CGATGGCCACATCATTTAG		
β_1 for	CAAGGTAGAAAGTCGGGACA	308 bp	designed with NCBI Primer-BLAST Primer designing tool, DNA-sequence: NM_033667.2 *homo sapiens* integrin, beta 1
β_1 rev	TGGCATTCATTTTCTCCTTTTCA		
β_3 for	CCTACATGACGAAAATACCT	516 bp	[114] DNA-sequence: NM_000212 *homo sapiens* integrin, beta 3
β_3 rev	AATCCCTCCCCACAAATACTG		
GAPDH for	GCATCCTGGGCTACACTG	305 bp	[114] DNA-sequence: NM_002046.3 *homo sapiens* GAPDH
GAPDH rev	GTGAGGAGGGGAGATTCAG		

Table 3: PCR program for the amplification of integrin transcripts

Time	Temperature	Number of cycles	Description
15 min	95 °C	1	activation step for Taq polymerase
30 s	95 °C	35 cycles	denaturation of double stranded cDNA
30 s	51 °C		annealing of sequence specific primer
1 min	72 °C		amplification of target sequences
10 min	72 °C	1	final extension
∞	4 °C	1	storage

5.2.4 Agarose gel electrophoresis of integrin amplicons

2 % (w/v) agarose (#11404.05, Serva Electrophoresis GmbH, Germany) was dissolved in Tris-acetate-EDTA (TAE) buffer (40 mM Tris, 1 mM EDTA, 40 mM acetic acid) by heating it until obtaining a viscous solution. After a brief cooling, the solution was poured into a gel chamber, where 0.5 µg/ml ethidium bromide solution (# E1510-10ML, Sigma-Aldrich) was added and evenly distributed with a pipette tip. For the formation of wells in the agarose gel, a comb was mounted. The polymerized agarose gel was placed in an electrophoresis chamber filled with TAE buffer. The amplicons generated via PCR (see 5.2.3) were mixed with loading dye solution (6 x) (# R0611, Fermentas) and loaded together with GeneRuler™ 100 bp DNA ladder (# SM0243, Fermentas) as a marker. Separation of PCR fragments was achieved by applying 150 V for 1-2 h. The amplicons were detected in a transilluminator (Peqlab).

5.3 Analysis of gene expression with RT^2 Profiler™ PCR Arrays

By means of the PCR Array Human Cell Motility (# 330231 PAHS-128G, Qiagen GmbH, SABiosciences, Germany), it was investigated if MT1-MMP silencing has an effect on the expression of genes that are involved in cell migration. This array is provided in a 384-well plate format (4 x 96), where four different samples can be analyzed at once. In total, the mRNA expression of 84 genes involved in cell migration can be investigated. Here, cells were either transfected with siMT1-MMP or left untreated. 32 h after siRNA transfection, 1.5 x 10^5 cells were plated on 35 mm ibiTreat dishes or on freshly prepared FN matrices. Samples were incubated at 37° C for 16 h before extraction of RNA.

5.3.1 RNA extraction

RNA extraction was done with the RNeasy® Mini Kit (# 74104, Qiagen) as described in the RNeasy® Mini Handbook. Cells were lysed directly by adding 350 µl Buffer RLT. Cell lysates were collected with a cell scraper, transferred to a microcentrifuge tube and mixed thoroughly to avoid the formation of cell clumps. Samples were pipetted into a QIAshredder spin column (# 79656, Qiagen) and centrifuged at 20,000 x g for 2 min. Cell lysates were mixed with 350 µl of 70 % EtOH for homogenization. The mixture was transferred to an RNeasy spin column. After centrifugation at 8,000 x g for 15 s, the spin column membrane was washed by adding 350 µl of Buffer RW1, followed by another brief centrifugation. Then, an on-column DNA digestion was performed with the RNAse-free DNAse set (# 79254, Qiagen). 10 µl of DNAse I stock solution was mixed with 70 µl Buffer RDD and then carefully applied on the spin column membrane. After 15 min incubation at RT, 350 µl of Buffer RW1 was added and the samples were centrifuged at 8,000 x g for 15 s. The spin column membrane was washed with 500 µl Buffer RPE and centrifuged at 8,000 x g for 2 min. To avoid carryover of EtOH that may affect downstream reactions, the spin columns were centrifuged at 20,000 x g for an additional 1 min. The RNA was eluted by adding 30 µl of RNase-free water and by centrifuging the samples at 8,000 x g for 1 min. Quality of RNA was measured with the spectrophotometer ND-1000. The RNA was only used for cDNA synthesis if it matched the following criteria (see RT^2 Profiler™ PCR Array System Handbook):

- A_{260} : A_{230} greater than 1.7
- A_{260} : A_{280} ratio 1.8 to 2.0
- Concentration by A_{260} > 40 µg / ml total RNA

5.3.2 cDNA synthesis for RT^2 Profiler™ PCR Arrays

The cDNA synthesis was performed as described in the RT^2 Profiler™ PCR Array System Handbook with the RT^2 First Strand Kit (# C-03/330401, SABiosciences). Thereby, 400 ng total RNA was used. The genomic DNA (gDNA) elimination mixture was prepared by pipetting 2 µl of gDNA Elimination Buffer (5 x) to the RNA. Water was added to a final volume of 10 µl. The solution was mixed by gentle pipetting, followed by a brief centrifugation. After 5 min incubation at 42 °C, the samples were directly placed on ice for at least 1 min. Meanwhile, the RT-PCR cocktail was prepared. Therefore, 16 µl of RT Buffer (5 x), 4 µl of Primer and External Control Mix, 8 µl of RT Enzyme Mix 3 and 12 µl of water were combined. The first strand cDNA synthesis reaction was prepared by adding 10 µl of the RT-PCR cocktail to each 10 µl gDNA elimination mixture. The solution was gently mixed and incubated at 42 °C for exactly 15 min. The cDNA synthesis was immediately stopped by heating the samples to 95 °C for 5 min. To each cDNA reaction mix 91 µl water was added. The solution was mixed and then placed on ice until preparation of the RT^2-PCR.

5.3.3 RT^2-PCR with RT^2 Profiler™ PCR Arrays

The reaction mixes were prepared by combining 550 µl of RT^2 SYBR®Green qPCR Mastermix (2 x) (# 330509, Qiagen) with 102 µl of the respective cDNA and 448 µl of water. The experimental cocktails were dispensed in a RT^2 PCR Array Loading Reservoir (# 338162, SABiosciences). With help of a multichannel pipette and the provided 384 EZLoad™ Covers 10 µl of the experimental cocktails were loaded per well. The 384-well plate was analyzed with a LightCycler® 480 System (Roche Diagnostics Deutschland GmbH, Germany) kindly provided by the Genomics and Proteomics Core Facilities (Microarray Unit) at the DKFZ. The programs for RT^2-PCR and for melting curve analysis respectively are shown in table 4 and 5.[4]

Table 4: Two-step cycling program for the RT^2-PCR Array

Time	Temperature	Number of cycles	Description
10 min	95 °C	1	activation step for HotStart DNA polymerase
15 s	95 °C	45 cycles	denaturation of double stranded cDNA
1 min	60 °C		annealing of sequence specific primer and amplification of targeted sequences

[4] More detailed information about the instrument settings can be found in the Instrument Setup guide available on the Sabioscience Hompage: http://sabioscience.com/pcrarrayprotocolfiles.php

Table 5: Program for melting curve analysis

Temperature	Hold	Acquisition mode	Ramp rate	Description
60 °C	15s	none	4.8 °C/s	all cDNAs are double stranded
95 °C	-	continuous	0.3 °C/s	denaturation of double stranded cDNA; denaturation temperature depends on length of the transcripts and their GC content

The data was analyzed with an online tool from SABioscience that was further used for the generation of graphs.[5]

[5] See http://sabiociences.com/pcrarraydataanalysis.php

5.4 Protein expression analysis

5.4.1 Preparation of protein lysates

Culture medium was removed and cells were washed once with ice cold DPBS. The 12-well plates were placed on ice, 150 µl of cell lysis buffer (1 % NP-40, 0.25 % DOC, 50 mM Tris-HCl, 5 M NaCl, 0.67 M EDTA, 100 mM PMSF, 200 mM Na_3VO_4) supplemented with protease inhibitor (# 11836170001, Roche) was added per well. Cells were detached from the culture dish/well with a cell scraper and incubated on ice for 45 min while shaking. Lysates were transferred into tubes and centrifuged in a precooled centrifuge at 20,000 x g for 15 min at 4 °C. After centrifugation, protein extracts were transferred into new tubes and the pellet containing cell debris was discarded. Protein lysates were stored at -20 °C.

5.4.2 Determination of protein concentration with BCA Protein Analysis Kit (Pierce)

To load equal amounts of cell lysates, the protein concentration of each sample was determined with the BCA Protein Analysis Kit (# 23227, Pierce®, Thermo Fisher Scientific, p/a Perbio Science, Germany) according to manufacturers' instructions. The assay was performed in a 96-well plate format. First, BSA standards with the following concentrations were prepared by dissolving BSA in cell lysis buffer: 2 mg/ml, 1.5 mg/ml, 1 mg/ml, 0.75 mg/ml, 0.5 mg/ml, 0.25 mg/ml, 0.125 mg/ml, 0.025 mg/ml and a blank sample (lysis buffer only). Then, 25 µl of the BSA standards and samples were pipetted in each well. After adding 200 µl of the working reagent (50:1 mixture of solutions A and B), the 96-well plate was shaken for 30 s followed by an incubation at 37 °C for 30 min. The 96-well plate was equilibrated to RT and absorption of the solutions was measured at 562 nm with the microplate reader Infinite® M200 (Tecan Deutschland GmbH, Germany). Data was analyzed with the provided Magellan™ data analysis software (Tecan Software Competence Center GmbH, Germany) calculating standard curve and protein concentration of each sample.

5.4.3 Sodium dodecylsulfate polyacrylamide gel electrophoresis (SDS-PAGE)

The SDS-PAGE was performed with Life Technologies equipment. Equal amounts of total protein lysates were mixed with LDS sample buffer (4x) (# NP0007), sample reducing agent (10x) (# NP0009) as well as MilliQ-water and heated for 10 min at 70 °C. Samples were loaded either on 4-12 % Bis-Tris gels (# NP0321BOX) in MOPS SDS running buffer (20x) (# NP0001) or on 3-8 % Tris-Acetate gels (# EA0375BOX) in Tris-Acetate SDS running

buffer (20x) (# LA0041) according to the molecular weight of the protein of interest. Precision Plus Protein™ Standard Dual Color (# 161-037, Bio-Rad Laboratories GmbH, Germany) was used as a molecular weight marker. Separation of proteins was achieved by applying 150 V for 1.5 h.

5.4.4 Western blot

Transfer of proteins from the polyacrylamide gel to a polyvinylidene fluoride (PVDF) membrane was achieved with the iBlot® Gel Transfer Device, a dry blotting system (Life Technologies). After protein transfer, the membrane was blocked with 5 % (w/v) milkpowder (# T145.2, Carl Roth GmbH und Co. KG, Germany) in DPBS including 0.1 % (v/v) Tween® 20 (# 9127.1, Carl Roth) while incubating on a shaker for 1 h. Then, the membrane was incubated in 5 % (w/v) milk powder/DPBS-T containing the primary antibody while shaking (see table 6) either for 1 h at RT or overnight (ON) at 4 °C. The membrane was washed three times for 10 min with DPBS-T, followed by an incubation at RT in 5 % (w/v) milk powder in DPBS-T containing the secondary antibody on a shaker (see table 7) for 45 min. After washing the membrane as described above, the protein bands were detected with the luminescent imaging analyzer LAS-3000 (Fujifilm Europe GmbH, Germany) using the ECL Plus Western Blotting detection Kit (# RPN2132, GE Healthcare Europe GmbH, Amersham, Germany).

5.4.5 Dot Blot

The purity of FN matrices and presence of collagen I were tested with a dot blot. NIH3T3 FN-YPet and $FN^{RGE/RGE}$ cells were seeded and cultured as described in 5.1.3 in 35 mm dishes. Protein cell lysates were obtained as described in 5.4.1.

5 µg of each lysate was pipetted on a nitrocellulose transfer membrane (Protran® BA 79, # 10402096, Schleicher und Schuell BioScience GmbH, Germany). As positive control for FN, human FN was used. Rat tail collagen I (# 354249, BD Biosciences) was taken as control for collagen I detection. BSA was chosen as negative control. Per control 5 µg protein solution was applied on the nitrocellulose membrane.

To ensure the complete binding of proteins to the membrane, the membrane was incubated for 1 h at RT until it was completely dried. Empty binding sites were blocked with 5 % (w/v) milk powder in DPBS-T for 1 h at RT. Then, the membrane was incubated in 5 % (w/v) milk powder/DPBS-T containing the primary antibody (see table 6) while shaking ON at 4 °C. The

membrane was washed three times for 10 min with DPBS-T, followed by an incubation in 5 % (w/v) milk powder in DPBS-T containing the secondary antibody (see table 7) on a shaker for 45 min at RT. After washing the membrane as described above, samples were analyzed with the ECL Plus Western Blotting detection Kit in the luminescent imaging analyzer LAS-3000.

Table 6: Information on primary antibodies for blotting techniques

Antigene / Clone	**Host / Isotype**	**Manufacturer / Order number**	**Concentration → Dilution**
α-Tubulin / B-5-1-2	mouse / IgG_1	Sigma-Aldrich / T6074	2 mg/ml → 1:1000
β-Actin / AC-15	mouse / IgG_1	Sigma-Aldrich / A1978	~2 mg/ml → 1:4000
Cofilin	rabbit / polyclonal	Cell Signaling / 3312S	NA → 1:500
Collagen I / COL-1	mouse / IgG_1	Sigma-Aldrich / C2456	NA → 1:1000
ERK / 16/ERK (pan ERK)	mouse / IgG_{2a}	BD Biosciences / 610123	250 µg/ml → 1:1000
FAK / 77/FAK	mouse / IgG_1	BD Biosciences / 610087	250 µg/ml → 1:1000
FAK (pY397) / 14/FAK(Y397)	mouse / IgG_1	BD Biosciences / 611722	250 µg/ml → 1:1000
Fibronectin	rabbit / polyclonal	Sigma-Aldrich / F3648	0.5 - 0.7 mg/ml 1:1000
Integrin α_5 / 1/CD49e	mouse / IgG_{2a}	BD Biosciences / 610633	250 µg/ml → 1:1000
Integrin β_1 / 18/CD29	mouse / IgG_1	BD Biosciences / 610467	250 µg/ml → 1:1000
MMP14 / EP1264Y	rabbit / IgG	Epitomics / 2010-1	NA → 1:1000
p44/42 MAPK (Erk1/2) / 137F5	rabbit / IgG	Cell Signaling / 4695S	NA → 1:1000
Phospho-Cofilin (Ser3) / 77G2	rabbit / IgG	Cell Signaling / 3313S	NA → 1:500

Table 7: Information on secondary antibodies for blotting techniques

Reactivity / Conjugate	**Host / Isotype**	**Manufacturer / Order Number**	**Concentration / Dilution**
α-mouse / HRP conjugated	goat / IgG	Santa Cruz / sc-2005	400 µg/ml → 1:4000
α-rabbit / HRP conjugated	goat / IgG	Santa Cruz / sc-2004	400 µg/ml → 1:4000

5.5 Fluorescence staining techniques

5.5.1 Indirect immunofluorescence staining (IIF) of cells

Medium was removed and cells were washed with DPBS. All following steps were performed at RT. First, cells were fixed with 3.7 % (w/v) paraformaldehyde (PFA) in DPBS for 30 min. Then, cells were permeabilized by incubation in 0.2 % (v/v) Triton-X 100 diluted in 3.7 % PFA/DPBS for 1 min. After rinsing three times with DPBS, samples were kept in 1 % (w/v) BSA/DPBS for 30 min to reduce background signal. Afterwards, cells were incubated with the primary antibody (see table 8) diluted in 1 % (w/v) BSA/DPBS for 1 h. Samples were then rinsed three times with DPBS and incubated with the secondary antibody (see table 9) diluted in 1 % (w/v) BSA/DPBS for 45 min. After rinsing three times with DPBS, samples were mounted with ibidi mounting medium (# 50001, ibidi).

5.5.2 IIF staining of FN matrices

FN matrices were incubated in 1 % (w/v) BSA/DPBS for 30 min. Then, cells were incubated with the primary antibody (see table 8) diluted in 0.1 % w/v BSA/DPBS for 1 h. Samples were rinsed three times with DPBS and incubated with the secondary antibody (see table 9) diluted in 0.1 % (w/v) BSA/DPBS for 45 min. After rinsing three times with DPBS, samples were stored in DPBS.

Table 8: Information on primary antibodies for IIF stainings

Antigene / Clone	**Host / Isotype**	**Manufacturer / Order number**	**Concentration / Dilution**
MMP14 / EP1264Y	rabbit / IgG	Epitomics / 2010-1	NA 1:200
Fibronectin	rabbit / polyclonal	Millipore / AB2033	1 mg/ml 1:80
Vinculin	mouse / IgG_1	Sigma-Aldrich / V9131	NA 1:400

Table 9: Information on secondary antibodies for IIF stainings

Reactivity / Conjugate	**Host / Isotype**	**Manufacturer / Order number**	**Concentration / Dilution**
α-rabbit / Alexa Fluor® 488	goat / IgG	Life Technologies / A-11034	2 mg/ml 1:200
α-mouse / Alexa Fluor® 647	goat / IgG	Life Technologies / A-21236	2 mg/ml 1:200

Table 10: Information on additional fluorescence markers

Name	Target structure	Manufacturer / Order number	Concentration / Dilution
Phalloidin-TRITC	F actin	Sigma-Aldrich / P1951	0.5 mg/ml / 1:200

5.5.3 Fluorescence activated cell sorting (FACS) analysis

For analysis of integrin surface expression 2.5 x 10^5 HT1080 and 3.5 x 10^5 MCF7 cells were seeded per well of a 12-well plate (area of one well: 3.8 cm^2) and cultured until they reached 100 % confluence. In contrast, for MT1-MMP silencing, cells were seeded in a 24-well plate at different cell densities: 0.6 x 10^5, 1.2 x 10^5 and 1.8 x 10^5 cells per well. FACS-staining was performed 48 h and 72 h after siRNA-transfection (see 5.1.4).

Culture medium was removed and cells were washed once with DPBS. Cells were gently detached with 100 µl cell dissociation buffer while incubating for 5 min at 37 °C. The reaction was stopped by adding 500 µl of culture medium. For each sample two aliquots of 200 µl were prepared. Cells were centrifuged at 500 x g in a pre-cooled centrifuge for 5 min at 4 °C. The medium was removed and the cell pellet resuspended in 50 µl FACS-buffer (DPBS, 5 % (v/v) heat inactivated NCS, 0.5 % (w/v) BSA, 0.5 % (w/v) N_3) containing the corresponding primary antibody (see table 11). The second sample was resuspended in 50 µl FACS-buffer without antibody (non-antibody control). After 20 min incubation on ice, cells were washed with 500 µl FACS-buffer and centrifuged as described above. The FACS-buffer was discarded and the cell pellet resuspended in 50 µl FACS-buffer containing the secondary antibody (see table 12). After a 20 min incubation period on ice, cells were washed with 500 µl FACS-buffer and centrifuged as described above. FACS-buffer was removed and the cell pellet was resuspended in 150 µl FACS-buffer containing 2 % (w/v) PFA dissolved in DPBS. Cells were stored at 4 °C until measurement with a FACS machine (FACScan, Becton Dickinson GmbH, Germany) at the Institute of Immunology (University Heidelberg). Fluorescence intensity of 10^4 cells was measured for each sample. The generated data was analyzed with the flow cytometry data analysis software FlowJo (Tree Star, Inc., USA). For information on statistical testing, see paragraph 5.7.1.

Table 11: Information on primary antibodies for FACS

Antigene / Clone	**Host / Iso type**	**Manufacturer / Order number**	**Concentration / Dilution**
Integrin α_5 / SAM-1	mouse / IgG	GeneTex / GTX26131	2 mg/ml → 1:100
Integrin α_v / AV1	mouse / IgG_1	Millipore / MAB2021Z	~110 µg/ml → 1:10
Integrin $\alpha_v\beta_3$ / LM609	mouse / IgG_1	Millipore / MAB1976	1 mg/ml → 1:50
Integrin β_1 / LM534	mouse / IgG	Millipore / MAB1981	NA → 1:10
Integrin β_3 / B3A	mouse / IgG	Millipore / MAB2023Z	1 mg/ml → 1:25
MMP14 / EP1264Y	rabbit / IgG	Epitomics / EP1264Y	NA → 1:50

Table 12: Information on secondary antibodies for FACS

Antigene / Conjugate	**Host / Iso type**	**Manufacturer / Order number**	**Concentration / Dilution**
α-mouse / PE	goat / F(ab´)2 fragment	Dianova / 115-116-146	NA → 1:200
α-rabbit / PE	donkey / F(ab´)2 fragment	Dianova / 711-116-152	NA → 1:200

5.6 Imaging techniques

5.6.1 Fluorescence microscopy

Fluorescence images were acquired with an inverted fluorescence microscope (Olympus IX, Olympus Europa Holding GmbH, Germany) and a Delta Vision system (Applied Precision Inc., Canada). Three different objectives were used: a 20 x UPlan FL PHI (Olympus), a 40 x Plan NEOFLUAR (Zeiss) and a 60 x PlanApo Oil (Olympus).

5.6.2 Confocal laser scanning microscopy

Confocal images or image stacks were acquired with a confocal laser scanning system (C1-CLEM) on a fully automated, inverted Nikon microscope (Eclipse Ti) equipped with three lasers (405 nm, 488 nm and 561 nm) at the Nikon Imaging Center Core Facility (University Heidelberg, Germany). The following Nikon objectives were used: a 40 x Plan Fluor Oil DIC objective and a 60 x Plan Apo VC Water PFS objective.

5.6.3 Live cell imaging of HT1080 cells on different FN surfaces

HT1080 cells were seeded on freshly prepared FN matrices or on FN coatings (for preparation of surfaces see 3.1.2 and 3.1.3) for migration studies.

Cells were detached from the culture dishes with an EDTA-based cell dissociation buffer for 5 min at 37°C. For each condition 1.5×10^5 cells were resuspended in 1 ml Opti-MEM® containing a final concentration of 10 µM of an unspecific cytoplasma labeling dye, CellTracker™ Red CMTPX (# C34552, Life Technologies, Molecular Probes®). Cells in suspension were first incubated for 30 min at 37°C and then centrifuged at 500 x g for 5 min. The labeling solution was removed by aspirating and the cell pellet was resuspended in 1.2 ml culture medium. For general MMP inhibition, the broad-spectrum hydroxamic acid inhibitor of matrix metalloproteinases GM6001 (# 364205, Merck, Calbiochem®) and GM6001 control (# 364210, Calbiochem) respectively were added to the culture media to a final concentration of 10 µM each. SiRNA transfected cells were used 48 h after transfection (see 3.1.4 for transfection protocol). Integrin receptor blocking was performed as described under 3.1.5. Cells were seeded on FN matrices or on FN coatings at a density of 2.5×10^4 per well. For myosin II inhibition, blebbistatin (#B0560-1MG, Sigma-Aldrich) was added to a final concentration of 50 µM or 25 µM, directly before imaging. Table 13 gives an overview of the different conditions. Live cell imaging was performed at a constant temperature of 37 °C

under 5 % CO_2 atmosphere. The migration behavior was monitored using an Olympus IX inverted fluorescence microscope and a 20x objective (see 5.6.1).

For a quantitative analysis of FN dependent cell migration, images of at least three different areas were acquired every 10 min for an observation period of 15 h per condition. Experiments were repeated at least three times. Cells that left the observation field (i), underwent apoptosis (ii), did not move at all (iii), were affected in their movement by neighboring cells (iv), migrated in areas where the FN matrix was either lacking or very sparse (v), or mitotic cells (vi) were not considered for further analysis. All other cells were tracked by a manual tracking plugin of Image J software [113]. The distance the cells moved during each time step was used for calculating migration speed values. The average velocities were determined by dividing the complete trajectory length by the duration of the observation period.

Table 13: Information on different conditions for cell migration experiments

Presentation of fibronectin	Blocked integrin receptor	SiRNA treatment	Inhibitor
fibrillar FN matrix	-	-	-
	$a_5ß_1$	-	-
	$a_vß_3$	-	-
	$a_5ß_1$ and $a_vß_3$	-	-
	$a_5ß_1$	siMT1-MMP [5 µM]	-
	-	siMT1-MMP [5 µM]	-
	-	sicontrol [5 µM]	-
	-	-	GM6001 [10 µM]
	-	-	GM6001 control [10 µM]
	-	-	blebbistatin [50 µM]
	-	-	blebbistatin [25 µM]
fibrillar FN-RGE matrix	-	-	-
FN coating	-	-	-
	$a_5ß_1$	-	-
	$a_vß_3$	-	-
	$a_5ß_1$ and $a_vß_3$	-	-
	$a_5ß_1$	siMT1-MMP [5 µM]	-
	-	siMT1-MMP [5 µM]	-
	-	sicontrol [5 µM]	-
	-	-	GM6001 [10 µM]
	-	-	GM6001 control [10 µM]
	-	-	blebbistatin [50 µM]
	-	-	blebbistatin [25 µM]

In order to determine the directionality of cell migration another variable was analyzed, namely the persistence. The persistence is defined as the ratio between the linear distance of start and end point of the trajectory and the complete length of the trajectory. This ratio gives a factor of 1 if cells migrate in a perfectly straight line and is smaller otherwise [115]. Time dependent migration behavior was estimated by grouping the trajectories into 2 h-long segments for both average velocity and persistence data.

5.7 Statistical analysis

5.7.1 Statistical analysis of integrin blocking and MT1-MMP silencing experiments

Considering the integrin blocking experiments (see 5.1.5), average number of cells counted on all five images was calculated for each experimental run. Accordingly, average fluorescence intensity levels were calculated for each treatment group in the MT1-MMP silencing experiment (see 5.1.4). Next, the mean of the average numbers and fluorescence intensities of all biological replicates were determined. The statistical analysis was conducted using the software Sigma Stat 3.0 (SSPS Inc. USA). In order to similarities between the mean values, the data was analyzed by a one way analysis of variance (ANOVA) adjusted by Holm-Sidak. The Null-hypothesis was that the mean values are equal and it was rejected at $\alpha = 0.05$. The alternative hypothesis was that the mean values differ from each other. Significant differences between the mean values are differentiated with highly significant ($P < 0.005$) and extremely significant ($P < 0.001$). The respective bar chart were generated in OriginPro 9.0 (OriginLab Corporation, USA) and indicate mean values with standard error of the mean (SEM).

5.7.2 Statistical analysis of cancer cell migration experiments

For each treatment group approximately 100 cells from three to five experimental runs were evaluated. The statistical analysis and the generation of graphs were kindly performed by Dr. Tamás Haraszti (University Heidelberg, Germany). The programming language R was used for all statistical testing as well as for generation of box-and-whisker plots. Gnuplot was used for plotting polar histograms of angular persistence angles, the histograms of average velocities or migration persistence. Considering the box-and-whisker plots, each box is defined by the 1st and 3rd quartile of the data with the median marked by a line. The whiskers either extend to the extreme of the data, or to maximum 1.5 times the interquartile range. Data values that exceed the whiskers, the so-called outliers, are indicated by black squares.

The polar plot show persistence migration as normalized histogram of the angles between consecutive steps, generated for 10 degree broad pockets (with 36 values between $-\pi - \pi$), The direction of the bars indicate the middle value of the histogram pockets, whereas the bar length is proportional to the probability density at a certain angle. The velocity histograms were generated based on the calculation of 50 pockets between the minimum and maximum of the data set. They were plotted as scatter plots including a line calculated by a cubic spline interpolation.

In order to test similarities between the mean values of data sets (for velocities or persistence angles), the Wilcoxon rank sum test was used. The null hypothesis was that the difference of the means is zero. Hence, the alternative hypothesis was that the means are not equal. For data sets with more than 50 elements, p-values were calculated according to a normal approximation. Similarities of sample distributions were evaluated using the two-sided Kolmogorov-Smirnov test. The null hypothesis was that both tested data sets show the same distribution. Since all samples have data with ties for which exact p-values cannot be calculated, asymptotic distributions were used.

6. Results and Discussion

FN is an important mediator of cell adhesion and migration [33, 34]. In cancer, FN is often overexpressed by CAFs and can initiate pre-metastatic niche formation [30]. So far, FN-dependent cancer cell migration was mainly investigated on 2D environments. Studies on fibroblasts highlighted the importance of more physiological FN model systems, since the conformation of FN (e.g. 2D FN: globular; 3D FN: fibrillar) strongly influences cell behavior [105]. The aim of this thesis was to characterize cancer cell migration on 2D FN coatings and 3D fibrillar FN matrices. Here, the main emphasis was placed on the interaction of FN with $\alpha_5\beta_1$ and $\alpha_v\beta_3$ integrins as well as MT1-MMP, proteins that have been reported as important regulators of cancer cell migration on 2D FN environments [88, 116].

6.1 Analysis of integrin and MT1-MMP expression in different cell lines

Since one aim was to create a more physiological *in vitro* model system for FN-dependent cancer cell migration, a tumor cell line was selected that endogenously expressed the FN-binding integrins $\alpha_5\beta_1$ and $\alpha_v\beta_3$ as well as MT1-MMP. Accordingly, no molecules had to be introduced artificially.

6.1.1 Evaluation of integrin mRNA expression via PCR analysis

First, three human cancer cell lines (MV3, MCF7 and HT1080 cells) and a transformed cell line originated from a green monkey (COS), each of them being widely used for studying cancer cell migration [84, 88, 104, 117], were screened for expression of the relevant FN-binding integrins at the mRNA level. PCR analysis revealed a distinct mRNA expression pattern of the tested integrin subunits α_5, α_v, β_1 and β_3 for each cell line (figure 10). HT1080 cells were the only ones that expressed all relevant integrin transcripts and were thus chosen for all further experiments. This cell line originates from a fibrosarcoma biopsy and is characterized by a highly invasive phenotype and a high potential to form metastasis [106]. This qualifies HT1080 cells as an optimal cell line to study FN-dependent cancer cell migration.

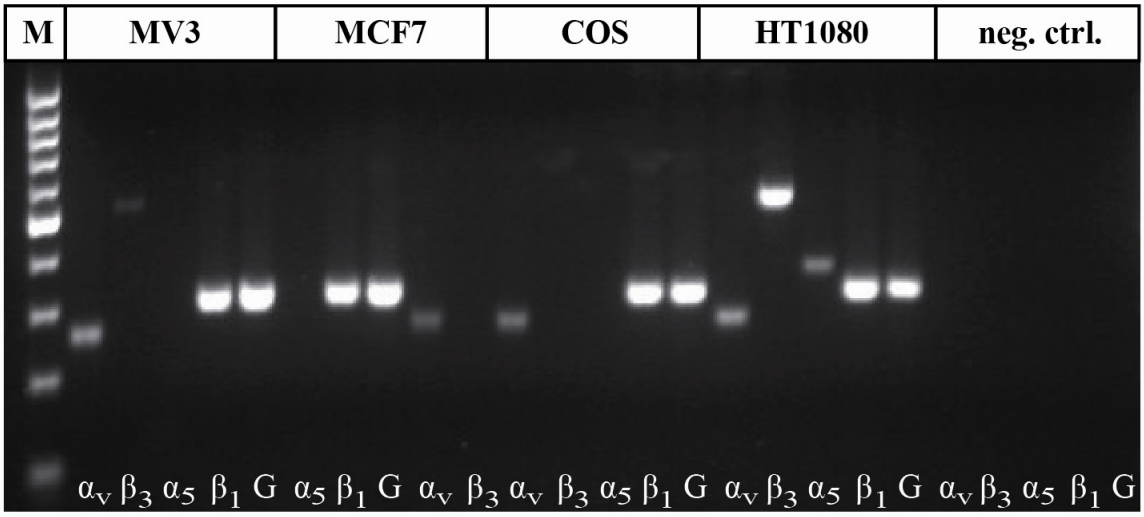

	MV3	MCF7	COS	HT1080
integrin α_5	-	-	-	+
integrin α_v	+	+	+	+
integrin β_1	+	+	+	+
integrin β_3	+	-	-	+

Figure 10: Agarose gel electrophoresis of integrin transcripts
mRNA expression of the integrin subunits **α_5**, **α_v**, **β_1** and **β_3** was analyzed in different cell lines (MV3, MCF7, COS and HT1080) via PCR and agarose gel electrophoresis. GAPDH (**G**) was chosen as an external positive PCR control. As DNA standard (**M)** 8 µl GeneRuler™ 100 bp DNA ladder was loaded on the agarose gel. To verify that the PCR components (e. g. water, primer and Taq polymerase) were not contaminated with gDNA, a negative control (**neg. ctrl.**) containing no template was used for each primer pair.
The results are summarized in a table indicating either no expression (-) or expression (+) of the respective integrin subunits, independent on the fluorescence intensity of the detected bands.

6.1.2 Evaluation of integrin and MT1-MMP protein expression via flow cytometry

In order to confirm that the studied integrins subunits α_5, α_v, β_1, and β_3 were expressed also at the protein level and presented at the plasma membrane, protein surface localization was investigated by flow cytometry. All four integrin subunits were detected at the plasma membrane of HT1080 cells (figure 11 A). These results are congruent with former studies on integrin expression in HT1080 cells [118, 119].
In addition, MT1-MMP protein expression in HT1080 cells was validated by flow cytometry analysis (figure 11 B) in agreement with previous reports [120].

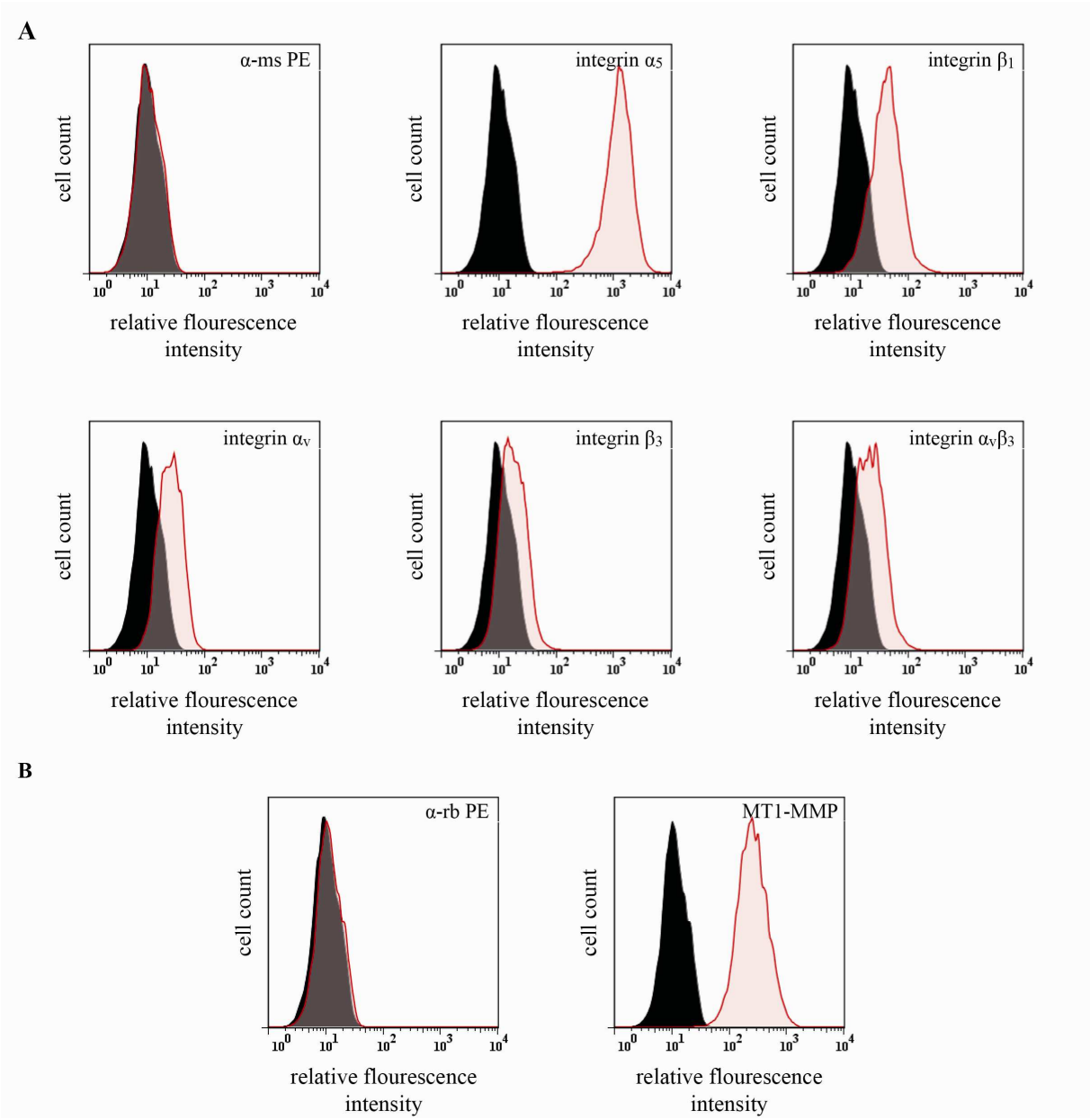

Figure 11: Flow cytometry histograms of integrin and MT1-MMP IIF stainings in HT1080 cells
Cell surface expression of the integrin subunits α_v, β_3, α_5, β_1, the whole $\alpha_v\beta_3$ receptor and MT1-MMP was analyzed via flow cytometry as described in paragraph 5.5.3. The histograms reflect the relative fluorescence intensities of differentially stained cell populations. Here, relative fluorescence intensity is plotted in a logarithmic scale on the x-axis and cell count is plotted on the y-axis. The black histograms marked with α-ms PE and α-rb PE, represent the autofluorescence intensities of unstained cells. As control for unspecific binding of the secondary antibody, cells were stained with the indicated PE-labeled secondary antibodies (red tainted histograms). In all other figures, black histograms refer to the fluorescence intensities of cells stained with these corresponding secondary antibodies. The red tainted histograms in those figures mark the cell population stained for the indicated molecules. Three biological replicates of this experiment were performed. For each tested protein a representative measurement was chosen.

6.1.3 Evaluation of MT1-MMP protein localization via IIF stainings

Further information on the intracellular localization of MT1-MMP molecules is provided through IIF images (figure 12). MT1-MMP was detected at cellular protrusions associated with migration where it co-localizes with filamentous actin. In addition, strong fluorescence signals were observed in the middle of the cells. This area is interpreted to be the ER, where MT1-MMP is synthesized. Moreover, fluorescent puncta localized between the ER and membrane protrusions were visible. Similar localization of MT1-MMP has already been demonstrated in other cell lines [85, 121, 122]. During cell migration, MT1-MMP is targeted to lamellipodia for local degradation of FA and the ECM barrier [121, 123, 124]. Accordingly, the observed fluorescent puncta are likely MT1-MMP-rich vesicles transported from the trans-Golgi network to membrane protrusions to sustain the amount of enzymes at the cell surface [125].There, MT1-MMP co-localized with actin filament, which is important for remodeling of the ECM in invading tumor cells [126].

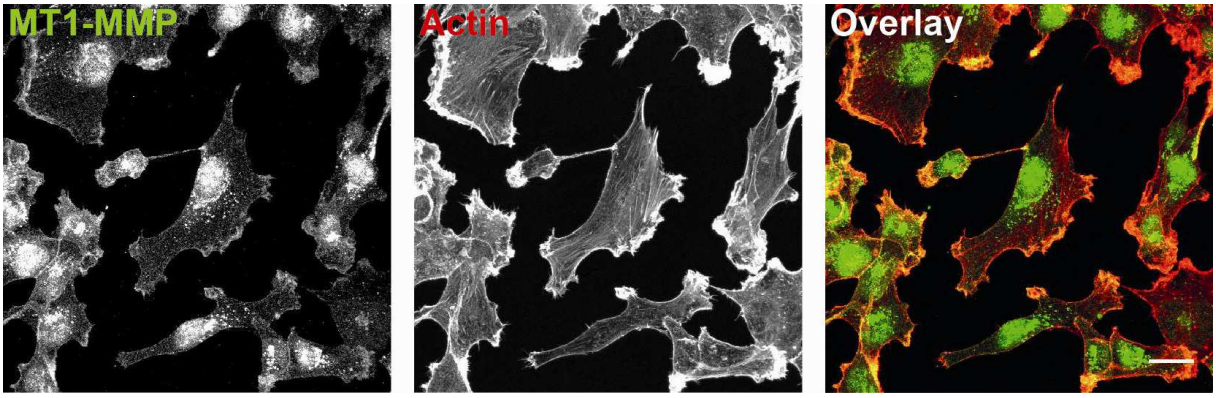

Figure 12: IIF staining of MT1-MMP in HT1080 cells
Cells are seeded at a density of 6×10^5 cells per 35 mm dish and kept ON at 37°C and under 5 % CO_2 atmosphere. IIF staining of MT1-MMP (green) is performed as described in paragraph 5.5.1. Actin filaments are stained with TRITC-Phalloidin (red). Each confocal image represents a maximum projection of 48 z-stacks with a step size of 0.3 µm. Scale bar, 25 µm.

6.2 Quality assessment of fibrillar FN matrices

In contrast to fibrillar collagens that spontaneously form 3D matrices *in vitro*, FN does not form fibers by self-assembly [34]. FN fibrillogenesis is a cell-mediated process which is dependent on the interaction of dimeric FN molecules with integrins, in particular $\alpha_5\beta_1$ integrin, and requires contractile forces [36].

Here, FN matrices were prepared using a modified procedure published previously [112]. For improved adhesion of the cell-derived FN matrices, fibroblasts were seeded on ibiTreat dishes with immobilized plasma FN as described in 3.1.3. This procedure improved matrix integrity and organization of the cell-free FN matrices. Apart from FN matrices assembled by NIH3T3-YPet cells, $FN^{RGE/RGE}$ cells were used for the generation of FN-RGE networks. FN-RGE contains a point-mutation in the RGD site, whereby aspartic acid (D) is replaced through glutamic acid (E). This alteration impairs binding of integrin to the RGD motif [42].

6.2.1 Evaluation of FN matrix quality by fluorescence microscopy

First, the structure of cell-derived FN matrices was examined by fluorescence microscopy. NIH3T3-YPet cells express YPet-labeled FN which enables direct analysis of fibrillar FN networks (figure 13 A). For imaging FN-RGE matrices assembled by $FN^{RGE/RGE}$ cells, FN fibrils were immunostained (figure 13 B). Although the antibody staining shows a higher background which complicates the identification of FN structures, the fibrillar organization and pore size of both types of FN matrices is considered as comparable.

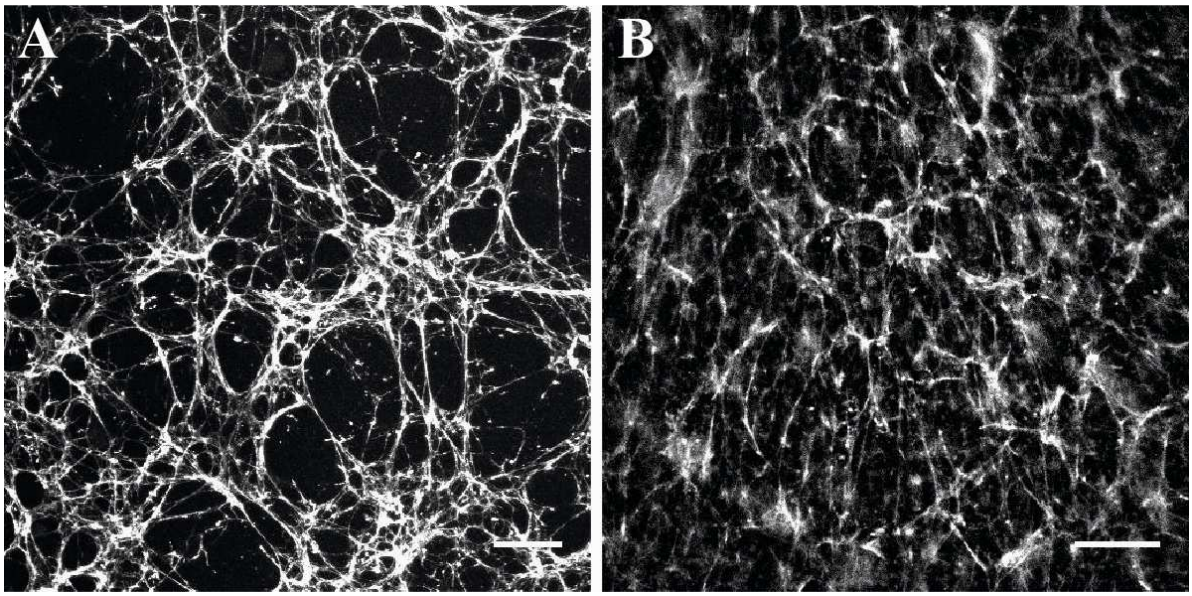

Figure 13: Fluorescence images of preassembled FN matrices

A) The FN matrix was preassembled by NIH3T3-YPet cells. Confocal iImages were acquired after lysis of fibroblasts with an inverted microscope and a 60 x objective. Image represents a maximum projection of 23 z-stacks with a step size of 0.3 µm. Scale bar, 25 µm **B)** The FN-RGE matrix was preassembled by $FN^{RGE/RGE}$ cells. After cell lysis the matrix was stained by IIF as described in paragraph 5.5.2. Image was acquired with an inverted microscope and a 40 x objective. Scale bar, 50 µm.

To evaluate how lysis of fibroblasts influenced matrix integrity, images of the same matrix area were acquired before and after cell lysis (figure 14). No matching structures could be identified between both images. Since the pore size was not altered by the cell lysis procedure, the observed differences in FN fiber arrangement might be caused by superficial FN lysis resulting in a reduced matrix thickness. Indeed, measurements of matrix thickness in z-direction showed that prior to cell lysis FN matrices had a thickness of 10-15 µm, whereas after treatment with the lysis buffer the final matrix thickness was approximately 5-10 µm. These findings are in agreement with previous publications [112]

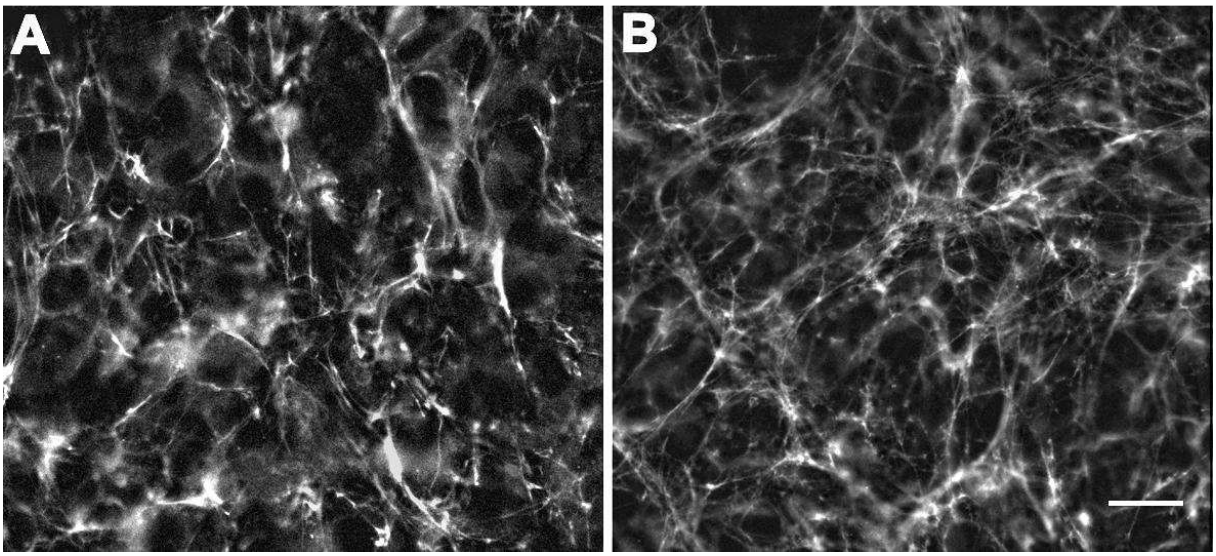

Figure 14: Fluorescence images of preassembled FN matrices

FN matrix was prepared as described in paragraph 5.1.3. Images were acquired before (A) and after (B) lysis of fibroblasts with an inverted microscope and a 40 x objective. Scale bar, 20 µm.

Although cell-derived FN matrices are more physiological than 2D FN coatings, one limitation of this system remains their modest thickness. As shown in figure 15, HT1080 cells are not completely embedded in FN (figure 15). The fibrillar FN organization is nonetheless referred to as 3D as it is commonly done in the literature [112].

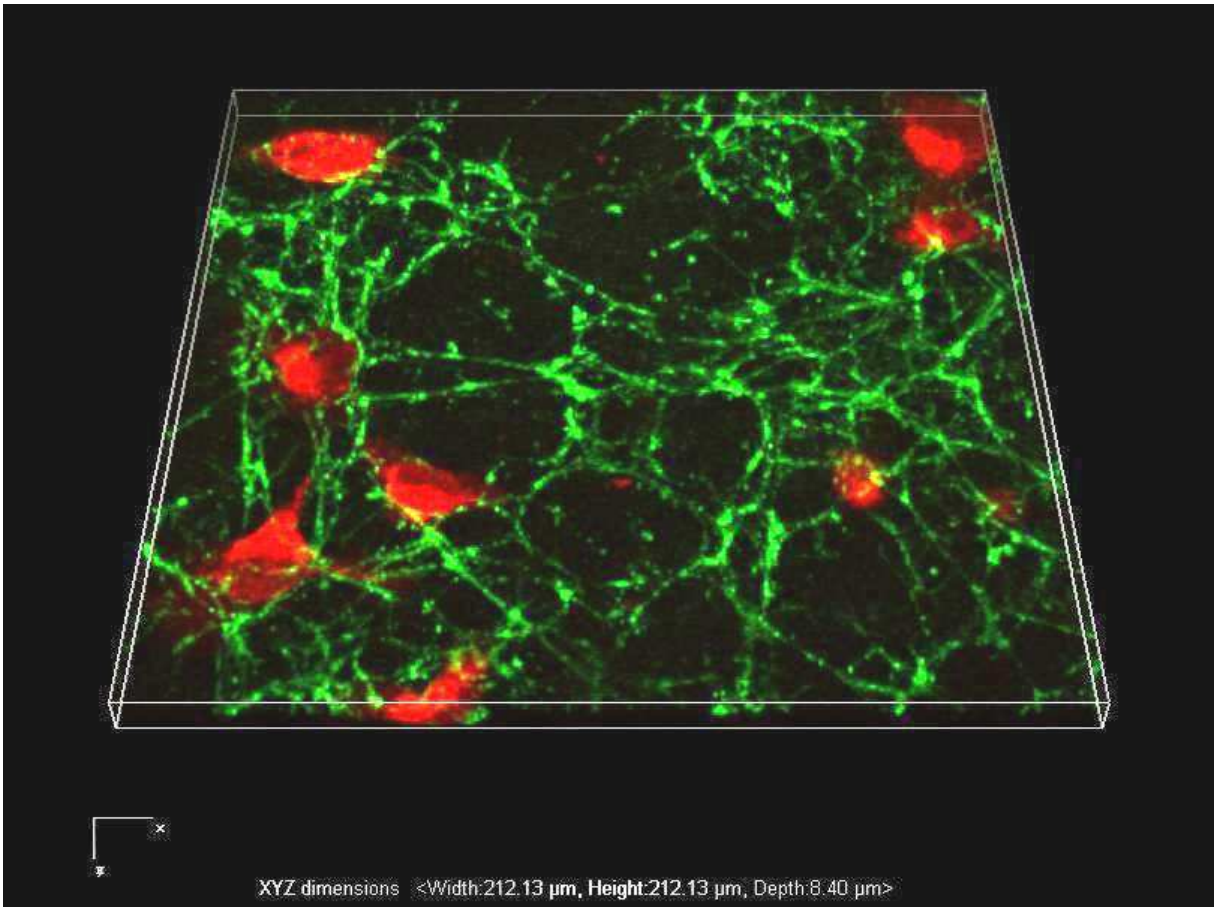

Figure 15: 3D projection of fluorescence images from HT1080 cells on FN matrix

HT1080 cells (red) were stained with a cytoplasmatic labeling dye and seeded on a freshly prepared FN matrix (green). The confocal image represents a 3D-projection of 20 z-stacks with a step size of 0.5 µm.

6.2.2 Evaluation of FN matrix purity by dot blot analysis

The ECM in the human body consists of different components with collagen I being the most abundantly expressed protein [33, 34]. Since the fibrillar FN matrices were produced by cells, it is possible that they also expressed collagen I and thereby "contaminate" the FN matrices. The presence of collagen I in this system would definitely complicate the conclusion of cell migration experiments. In order to clarify, whether the generated matrices contain FN only, a dot blot with cell/matrix lysates was performed. According to figure 16, NIH3T3-YPet cells do not produce collagen I and $FN^{RGE/RGE}$ cells excrete only minor amounts of collagen I. This is an important finding because cells can interact with collagen I through their $\alpha_2\beta_1$ integrin receptors [127]. The absence of this protein from fibrillar FN matrices guarantees an unbiased experimental set-up. For interpreting results on FN-RGE matrices, the presence of collagen I, albeit expressed only in low levels, should be kept in mind.

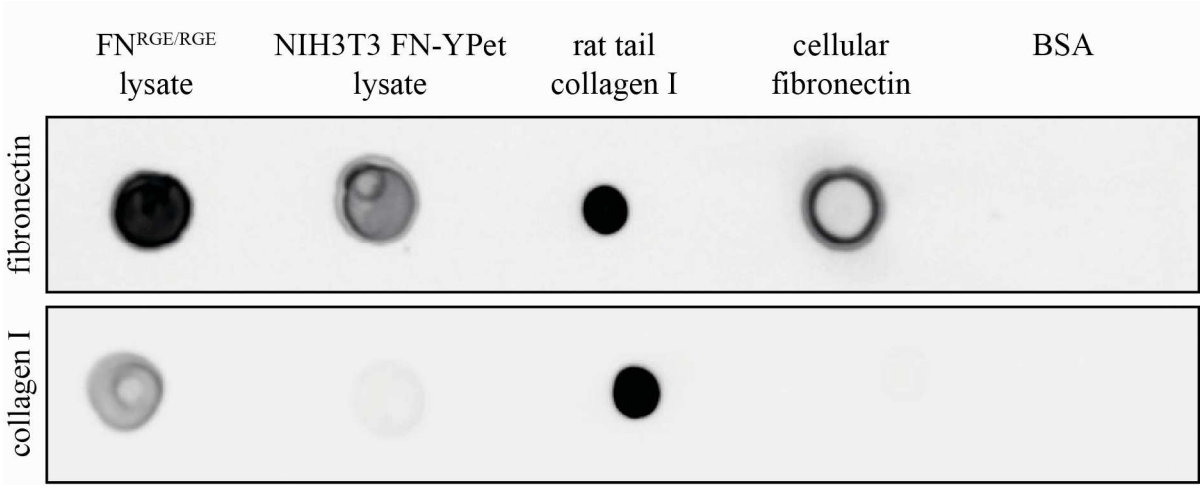

Figure 16: Dot blot for collagen I and FN of fibrillar FN matrices
Purity of the fibrillar FN matrices produces by NIH3T3 FN-YPet and $FN^{RGE/RGE}$ cells was determined with a dot blot. Here, 5 µg of total cell/matrices lysates are dropwise applied on a nitrocellulose membrane. As positive control 5 µg of the relevant proteins (rat tail collagen I or FN) was used. 5 µg of BSA serves as a control for unspecific binding of antibodies.

6.3 Cancer cell migration on different FN environments

Most of the research concerning FN dependent cancer cell migration has been performed on 2D rigid surfaces coated with globular FN. Within the connective tissue, however, FN is mainly presented to cells in a 3D fibrillar network structure. The aim of cell migration experiments presented in this section was to characterize and compare the migratory behavior of cells on 2D FN coatings and on 3D fibrillar FN matrices. First, cell morphology and interaction of HT1080 cells with fibrillar matrices was investigated in a qualitative manner. Next, quantitative analysis of both average velocity and directionality of cell migration, referred to as persistence, was performed.

6.3.1 The topography of presented FN molecules influences HT1080 cell morphology

It is known that the morphology of fibroblasts is affected by the conformation of presented FN molecules [105]. On 2D FN coatings, where FN shows a globular conformation; fibroblasts possessed fan-shaped lamellipodia while on 3D fibrillar FN matrices they assumed elongated spindle-like shapes. Here, similar changes were observed using HT1080 cells (figure 17). Cells seeded on FN coatings were flat and more round in shaped with large lamellipodia. In contrast, cells on FN matrices were elongated and formed long protrusions. On FN matrices containing a mutated RGE site, HT1080 cells were spindle-shaped, but did not spread as much as on FN matrices with a functional RGD motif. In addition, there were an increased number of round cells present.

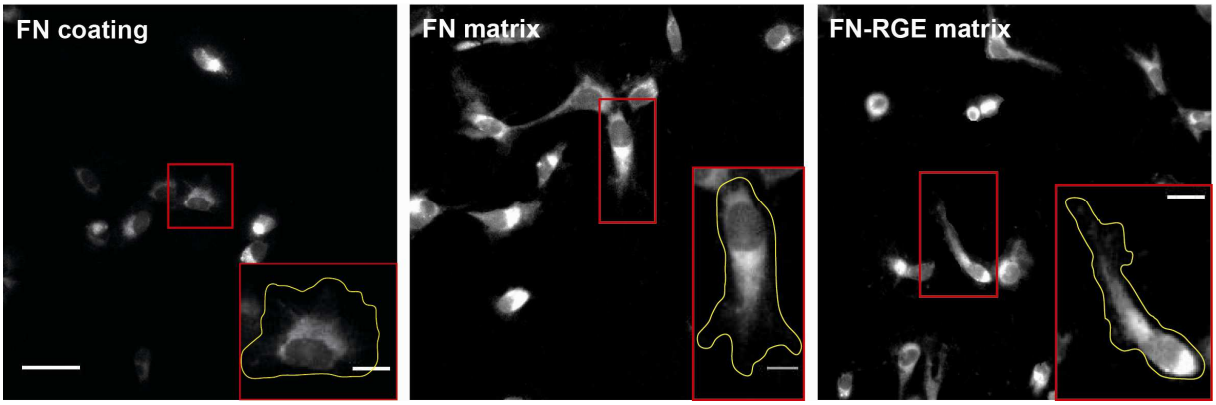

Figure 17: Fluorescence images of HT1080 cells on different FN surfaces

Fluorescence images show HT1080 cells on different FN environments (FN coating, FN matrix or FN-RGE matrix). Images were acquired 2 h after cell seeding with an inverted fluorescence microscope and a 20 x objective. Scale bar, 50 µm. The insets (red boxes) indicate zoom-ins of selected cells. The outline of the cell body is marked with a yellow line in order to discriminate cell morphology. Scale bar of insets, 15 µm.

These findings imply that interactions of cells with the RGD site in FN are important for spreading of HT1080 cells on fibrillar FN matrices. Cell morphology in general seems to be governed by FN topography.

6.3.2 HT1080 cells modulate FN matrices through FN fiber breakage

Single cell migration was observed via time-lapse live cell microscopy over a period of 15 h. Since FN matrices were completely destroyed by HT1080 cells over time, a closer look was taken at interactions between HT1080 cells and FN fibers. As shown in figure 18, the cancer cells wrap themselves with or move along FN fibers. Furthermore, cells preferentially migrate at places where FN matrix is still present and avoid FN-free areas. This leads to cell clustering, especially at later time points when only few FN fibers remain. Since these factors could influence cell migration behavior, only trajectories for the time period of 8 h were considered for further analysis, where FN matrices were still intact.

HT1080 cells seeded on FN-RGE matrices still interacted with the mutated FN to some extent. In fact, fluorescence intensity levels around cells increased over time, suggesting a rearrangement of FN fibers at these locations. There are two possible explanations for this observation. First, HT1080 cells do not interact with FN directly, but either through binding to the antibodies used to stain FN molecules or through binding to collagen I, which is present in minor amounts within FN-RGE matrices (figure 16). In order to avoid that FN binding antibodies interfere with cell migration behavior, FN-RGE matrices were not stained during cell migration experiments. Second, HT1080 cells could interact with FN via binding sites apart from RGD. It has been shown previously, that $\alpha_9\beta_1$ and $\alpha_4\beta_1$ can bind to FN via its EIIIA domain [40] and subsequently mediate adhesion to fibrillar FN independent of the RGD-motif. In addition, integrin $\alpha_v\beta_3$ can interact with an isoDGR motif present in the FN module I_5 [43].

Apart from that, HT1080 cells are not able to disrupt the fibrillar FN-RGE network as in case of FN matrices, at least not during the observed time period of 15 h. These results suggest that the disintegration of FN matrices is mainly mechanical in nature and might depend on cellular interaction with the RGD site in FN. It has previously been shown that detachment of HT1080 cells from FN matrices under shear is mediated through FN fiber breakage, while the detachment from FN coatings occurs through release of interactions between $\alpha_5\beta_1$ integrin and FN [128]. Accordingly, it can be assumed that HT1080 cells bind to FN fibers and pull them along their migration track until tearing of fibers.

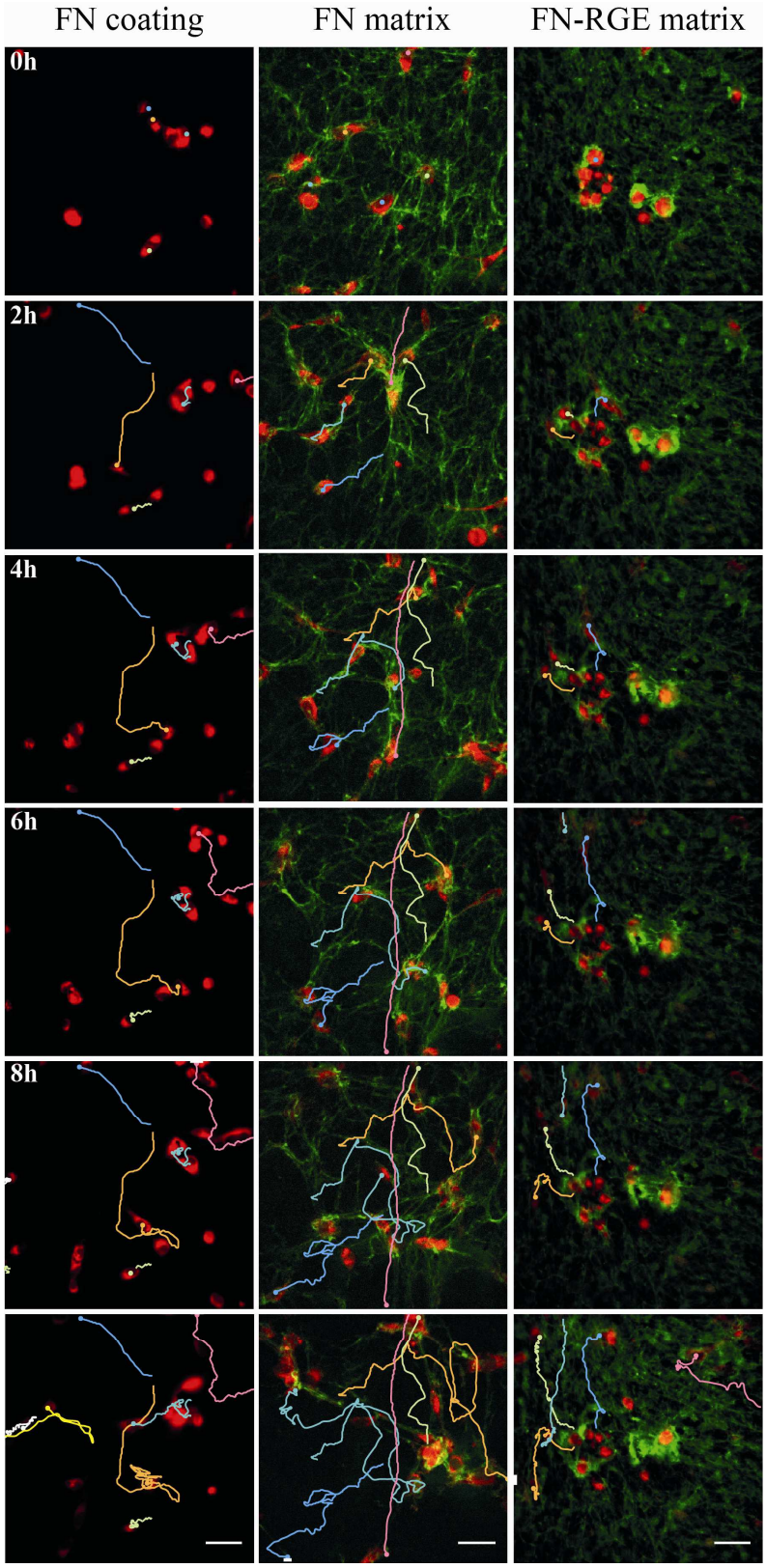

Figure 18: Fluorescence image time series of HT1080 cells on different FN environments

HT1080 cells (red) stained with a cytoplasmatic labeling dye were plated either on FN coating, FN matrix (green) or FN-RGE matrix (green) and were imaged over a period of 15 h. Here, representative time series for 0 h, 2 h, 4 h, 6 h 8 h and 15 h, are depicted. The colored lines indicate individual cell tracks. Scale bar, 50 µm.

6.3.3 3D FN matrices allow fast migration of HT1080 cells, which depends on the RGD-motif

Next, average velocity was calculated for cell migrating on FN coatings, FN matrices and FN-RGE matrices. As shown in figure 19 A and 19 B, HT1080 cells migrated faster on FN matrices (green) than on FN coatings (red) or FN-RGE matrices (cyan). According to the probability distribution plots (figure 19 C), the observed variations in cell migration speed between cells migrating on FN matrix and FN coatings or FN-RGE matrices are significantly different. The reduced migration speed of cells plated on FN matrices with a mutated RGE motif suggests that in a fibrillar FN environment migration is regulated by interactions of cells with the RGD site of FN. The results on the differences in migration speed between cells plated on FN coatings and FN matrices are in agreement with previous studies on NIH3T3 fibroblast and on human keratinocytes migration [129]. Both cell lines migrated significantly faster on fibrillar FN than on FN coatings. Hence, the observed changes in HT1080 cell migration on fibrillar FN cannot be attributed to cancer cells only but appear to be based on a general mechanism. Interactions between cells and their environment are regulated by variation of matrix stiffness [130]. In comparison to 2D FN coatings, 3D fibrillar matrices have a reduced matrix stiffness, resulting in low adhesion structures that enable fast cell migration [131]. The mechanical properties of the matrix are sensed through integrins and transduced inside the cell, where appropriate responses are triggered [20], suggesting that differenr integrin receptors could be involved in cell migration on FN coatings and on FN matrices.

One criterion for calculating the average velocity was that only cells that did not leave the observation field during the entire observation period were considered for analysis. It is more likely for a cell to stay within the observation field during shorter periods (4 h) than longer periods (8 h). Consequently, if the observation period is shortened (4 h), the number of analyzed trajectories increases, making the statistical evaluation more reliable. On the other hand, information on changes occurring over time might be lost. In order to evaluate which time period provides enough data for reliable statistical analysis but does not neglect time dependent effects, box-and-whisker plots for 4 h and 8 h observation periods were generated (figure 19 A and B). As shown in both box-and-whisker plots, on each FN substrate HT1080 cells migrate with constant speed over time. Hence, the 4 h period was chosen for all further calculations and statistical analysis.

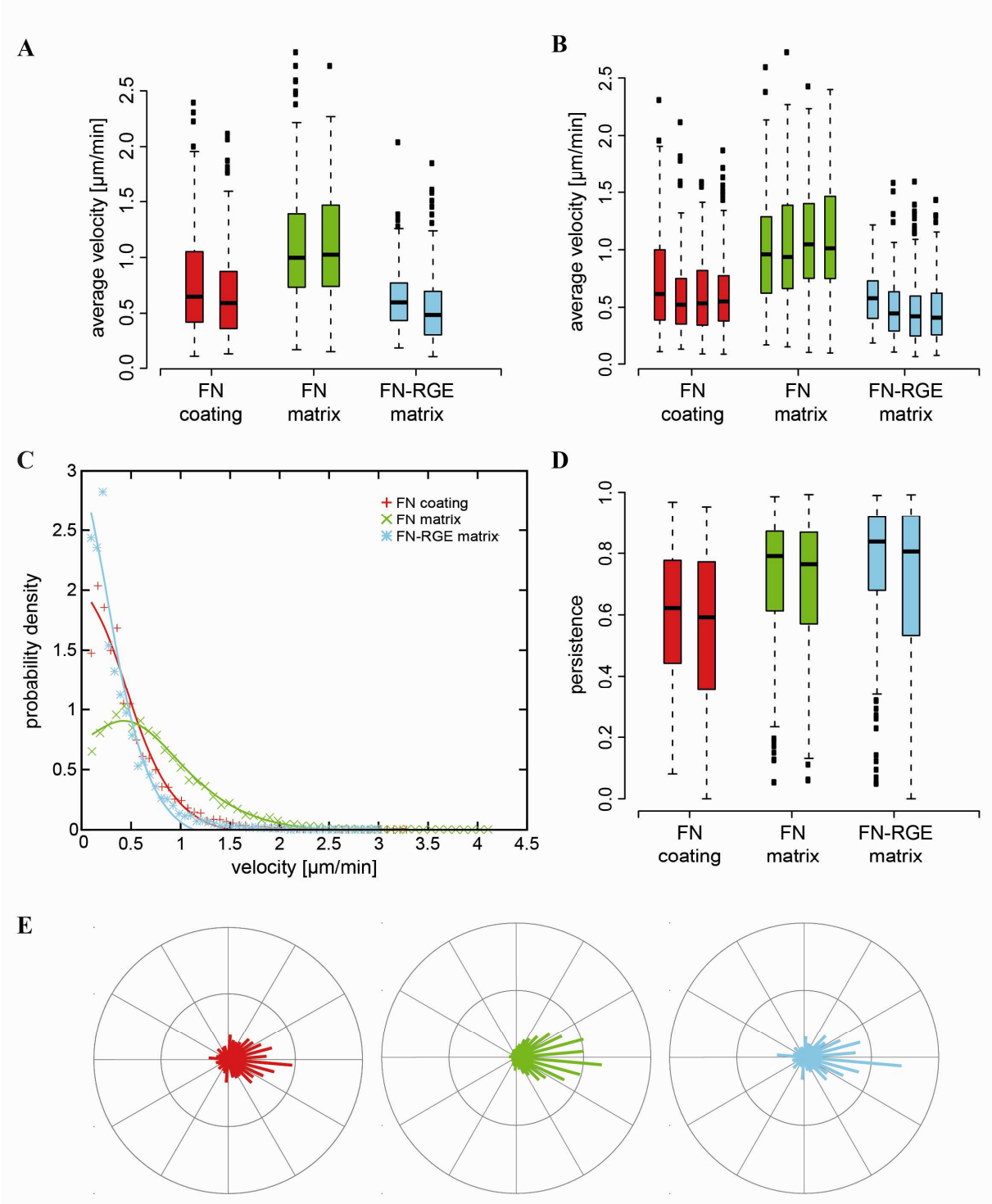

Figure 19: Analysis of migration speed and persistence of HT1080 cells in different FN environments

Different cell migration parameters were analyzed for HT1080 cells seeded on FN coating (in red), FN matrix (in green) and FN-RGE matrix (in cyan). **A**, The first box of each colored group shows average migration speed for the observation period of 0-2 h, the second box for 2-4 h. The boxes are defined by the first and third quartile and the median indicated by the line. Data points outside the whiskers are outliers. **B**, Same as in A with additional time periods; the third box of each group shows the data for 4-6 h, the fourth box for 6-8 h. **C** The velocity histograms are plotted as scatter plots. Lines are fitted using a cubic spline interpolation. **D/E,** Analysis of directionality of migration, indicated as persistence for 0-2 h (first box of each group) and for 2-4 h (second box of each group) in the box-and-whisker plot (in D), and as persistence angle in the polar plots (in E).

6.3.4 3D FN matrices increase directionality of cell migration

For further analysis of cell migration behavior, directionality of cell migration was quantified. As shown in figure 19 D, HT1080 cells migrated with higher persistence on both fibrillar FN environments (FN matrix and FN-RGE matrix) than on FN coating. Polar plots (figure 19 E) give further information on the relative distance and direction of migrating cells. Here, the step angles of all cell tracks within the observation period of 4 h are plotted in 10° degree broad pockets with the horizontal line indicating no deviation (0° degree). Hence, the right side of the circle represents forward and the left side backward movement, whereby the bar length indicates the probability density at a certain angle. Directionality of migration was evident only for HT1080 cells on FN matrix (green) and on FN-RGE matrix (cyan). HT1080 cells migrating on FN coatings (red) showed a more randomized migration behavior.

An explanation for the enhanced persistence of migrating cells on fibrillar FN matrices can be found in the different organization of the two FN environments [129]. The fibrillar FN fibers provide a framework with an inherent directionality. Cells interacting with these fibers follow their direction and hence show a more directed movement implying contact guidance as potential mechanism for efficient cell movement. On FN coatings, FN molecules are randomly distributed with a high ligand density. Hence, migrating cells have numerous possibilities for choosing their migration pathway resulting in a less directed movement. These different migratory phenotypes can also explain the observed variation in cell morphology (figure 10). On fibrillar FN matrices, HT1080 cells are more elongated due to their alignment with the FN fibers, whereas on FN coatings they can bind to each FN molecule in their proximity and thereby assume a more round-shaped form. At the same time, cells migrating on FN-RGE matrices show a higher probability for moving backwards than on fibrillar FN with an intact RGD site (figure 19 E), suggesting cell adhesion to FN fibers via the RGD site is important for regulating persistence of cancer cells.

6.4 Evaluation of integrin receptor blocking on FN dependent cancer cell migration

So far, the results suggest that morphology and migration behavior of HT1080 cells is governed by the organization of FN. On 3D fibrillar FN matrices, cancer cells assume an elongated, spindle-shaped form, migrate with relatively high average speed and keep a certain direction over time. In contrast, on 2D FN coatings, HT1080 cells are round-shaped and show a less directed, slower movement. These findings suggest that cell migration on both types of FN environments may be based on different migration modes.

By using FN matrices with a mutated RGD-binding motif that inactivates this site for integrin binding [43], the involvement of the RGD site for cell migration on fibrillar FN was demonstrated (figure 19). There are at least eight integrin receptors that are able to interact with FN, namely $\alpha_3\beta_1$, $\alpha_4\beta_1$, $\alpha_5\beta_1$, $\alpha_8\beta_1$, $\alpha_9\beta_1$, $\alpha_v\beta_1$, $\alpha_v\beta_3$, $\alpha_v\beta_6$, and $\alpha_{IIb}\beta_3$ [39, 40]. Except for integrin $\alpha_3\beta_1$, $\alpha_4\beta_1$ and $\alpha_9\beta_1$, all integrins bind to the RGD site of FN [40, 41]. A promising candidate that could influence cell migration on fibrillar FN matrices is $\alpha_5\beta_1$ integrin. It is the main FN-binding receptor and the most important regulator of FN fibrillogenesis [36]. Since the α_v integrin subunit has the most similar structure to integrin α_5 [127] and this integrin can further replace the role of integrin α_5 in adhesion to FN as well as FN matrix assembly in α_5–null cells [39], the $\alpha_v\beta_3$ integrin was chosen as second candidate possibly involved in cancer cell migration on FN. Here, the influence of $\alpha_5\beta_1$ and $\alpha_v\beta_3$ integrin receptors on FN dependent cancer cell migration was evaluated by impairing the adhesion of those integrins to FN via function blocking antibodies.

6.4.1 Evaluation of integrin blocking antibodies

Initially, the effectiveness of $\alpha_5\beta_1$ and $\alpha_v\beta_3$ blocking antibodies was analyzed. It was demonstrated previously that adhesion of HT1080 cells on FN coatings [132] and fibrillar FN matrices [128] can be significantly decreased by functional blocking of $\alpha_5\beta_1$ integrin receptors. Blocking of $\alpha_v\beta_3$ integrin in HT1080 cells had no effect on FN dependent cell adhesion [128, 132], although this integrin receptor is able to bind FN in other cell lines [133]. Since a different anti- $\alpha_5\beta_1$ antibody was used in this thesis, the functionality of this clone (JBS5) was evaluated on FN coatings. Adhesion of preblocked and untreated HT1080 cells on FN coatings was quantified 1 h after cell seeding by phase contrast microscopy (figure 20 A). Preblocking of $\alpha_5\beta_1$ integrin receptors, alone or in combination with preblocked $\alpha_v\beta_3$ integrins, led to a significant decrease of adherent cells (figure 20 B). In

contrast, preblocking of $\alpha_v\beta_3$ integrin receptors did not influence adhesion of HT1080 cells on FN coatings. The adherent cell populations were then analyzed in respect to their spreading state (figure 20 C). Cells were characterized as non-spread based on their round shape and presence of only few protrusions. In the control sample, approximately 60 % of the cells were spread. Treatment of cells with $\alpha_5\beta_1$ integrin antibodies, alone or in combination with $\alpha_v\beta_3$ antibodies, led to a decreased fraction of spread cells (27 %).

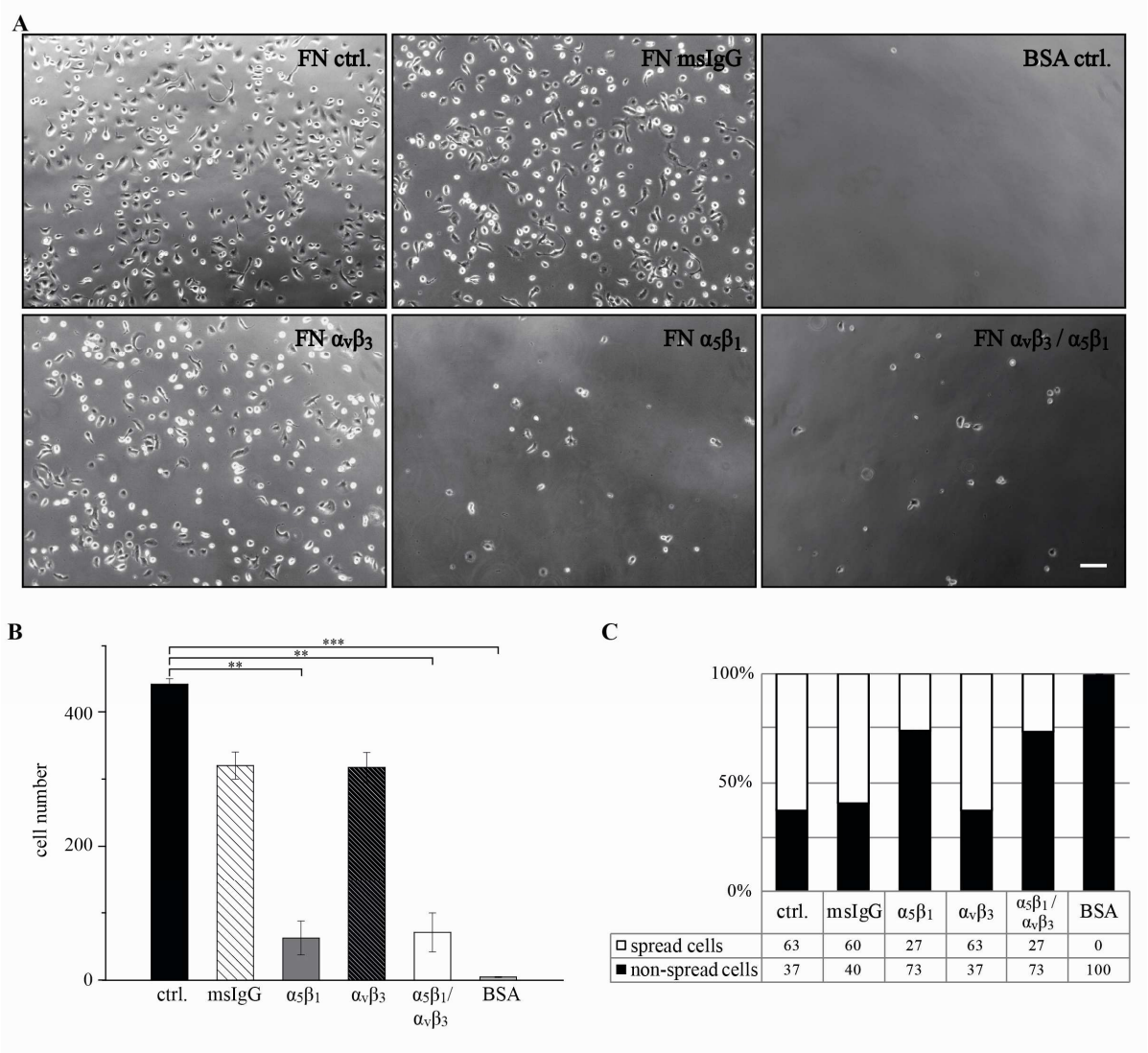

Figure 20: Blocking of cell adhesion on FN coatings

The blocking potential of antibodies directed against the integrin receptors $\alpha_v\beta_3$ and $\alpha_5\beta_1$ was tested on FN coatings. **A)** The coating, either FN or BSA (used as negative control) and the antibody treatment is indicated in each brightfield image (**control**: untreated cells, **msIgG:** isotype control, **$\alpha_v\beta_3$** and **$\alpha_5\beta_1$:** cells preblocked with the relevant antibodies). Scale bar, 50 µm. **B)**. The column chart shows mean of cell number and standard error of the mean (**SEM**) per treatment. Here, significant results are differentiated between highly significant (**) with $P < 0.005$ and extremely significant (***) with $P < 0.001$. **C)** The stacked column plot shows the proportion of spread and non-spread cells within a certain group.

These findings demonstrate that the JBS5 antibody efficiently blocks the binding of $\alpha_5\beta_1$ integrin receptors to FN.

Since blocking of integrin $\alpha_v\beta_3$ did not affect HT1080 cell adhesion on FN, the anti-$\alpha_v\beta_3$ integrin antibody blocking efficacy on VTN coatings, the main substrate for $\alpha_v\beta_3$ integrins [127] was evaluated. Surprisingly, HT1080 cells scarcely spread on VTN surfaces (figure 21 A). In addition, preblocking of cells with anti-$\alpha_v\beta_3$ integrin antibodies did not influence adhesion on VTN (figure 21 B). Nevertheless, the anti-$\alpha_v\beta_3$ integrin antibody clone LM609 used in this thesis was able to block the binding of $\alpha_v\beta_3$ integrin to VTN and FN in former studies [134, 135]. Taking these findings into consideration, along with the flow cytometry results (figure 11 A) that demonstrated only slightly elevated mean fluorescence intensity levels compared to unstained cells, it can be concluded that $\alpha_v\beta_3$ integrins must be expressed only in minor levels at the plasma membrane and do not play a major role in adhesion of HT1080 cells on FN or VTN. Although $\alpha_v\beta_3$ integrins are not required for attachment of cells on FN, it was demonstrated that they can still bind to fibrillar FN under certain circumstances [133]. Indeed, integrin $\alpha_v\beta_3$ can be chemically cross-linked to FN 60 min after plating HT1080 cells on FN coatings [132]. Overall, these results hint that $\alpha_v\beta_3$ integrins may still influence the migratory behavior of HT1080 cells on FN.

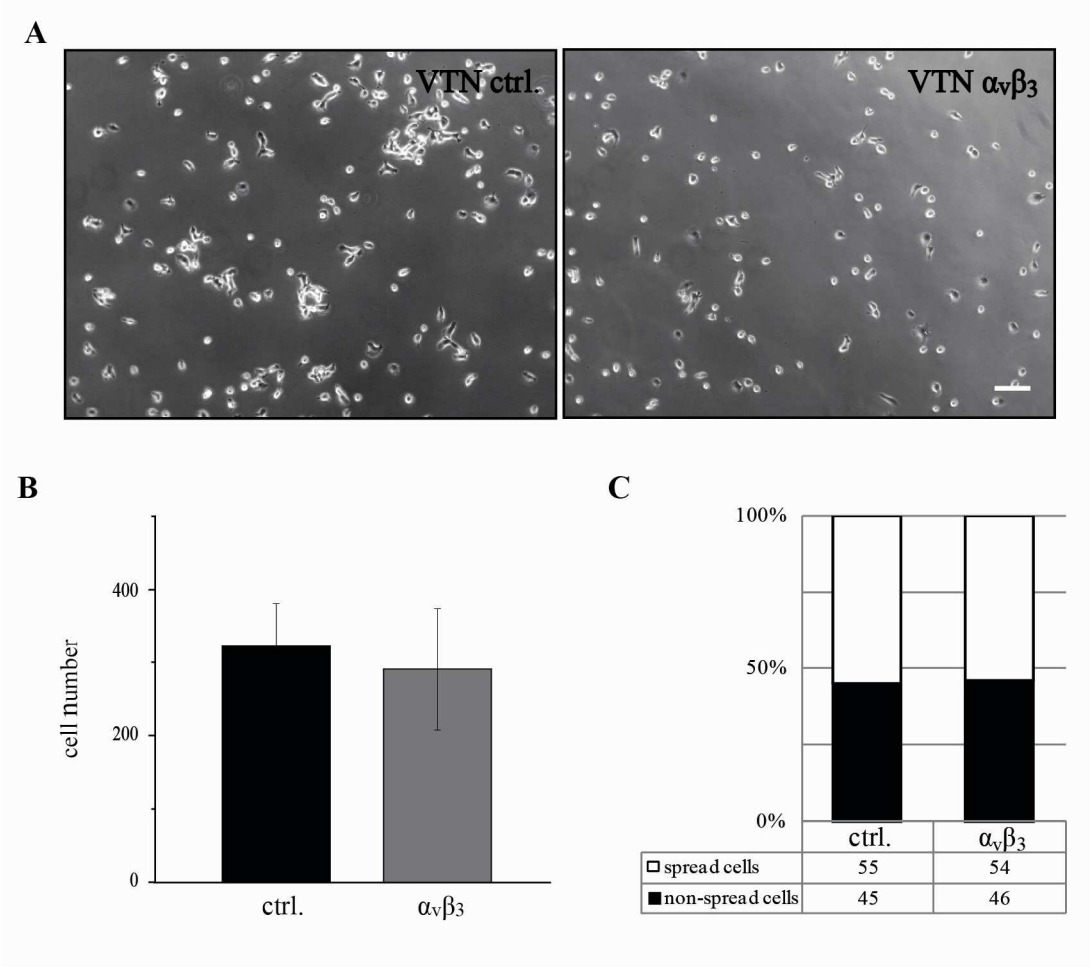

Figure 21: Blocking of cell adhesion on VTN

The blocking potential of the anti-$\alpha_v\beta_3$ antibody LM609 for cell adhesion on VTN was tested. **A)** Cells were either preblocked with antibodies directed against integrin $\alpha_v\beta_3$ or left untreated before plating on VTN coatings. **B)**. Cell number mean and SEM are plotted for each indicated condition. **C)** The proportion of spread and non-spread cells within a certain treatment group is depicted.

To summarize these findings, adhesion of HT1080 cells on FN coatings can be efficiently blocked with antibodies directed against $\alpha_5\beta_1$ integrins but not with antibodies directed against $\alpha_v\beta_3$ integrins. Furthermore, HT1080 cells show an impaired ability to adhere and spread on VTN coatings. Blocking of $\alpha_v\beta_3$ integrins has no effect on cell adhesion to VTN.

6.4.2 Preblocking of $\alpha_5\beta_1$ integrin affects cell morphology but not FN fiber breakage

Next, the effect of preblocking $\alpha_5\beta_1$ and $\alpha_v\beta_3$ integrins on cell morphology and interaction between cells and FN fibers was examined. As shown in fluorescence images, HT1080 cells with preblocked $\alpha_5\beta_1$ integrins, alone or in combination with $\alpha_v\beta_3$ integrins, were small and round-shaped in contrast to untreated cells or cells with preblocked $\alpha_v\beta_3$ integrins only (figure 22). Preblocking of integrins did not seem to impair the ability of HT1080 cells to rearrange the FN network. These findings suggest that $\alpha_5\beta_1$ integrins are important for adhesion of HT1080 cells to FN, while the migratory behavior of $\alpha_5\beta_1$ integrin-blocked cells remains unchanged. In contrast, $\alpha_v\beta_3$ integrins seem not to be involved in any of these processes.

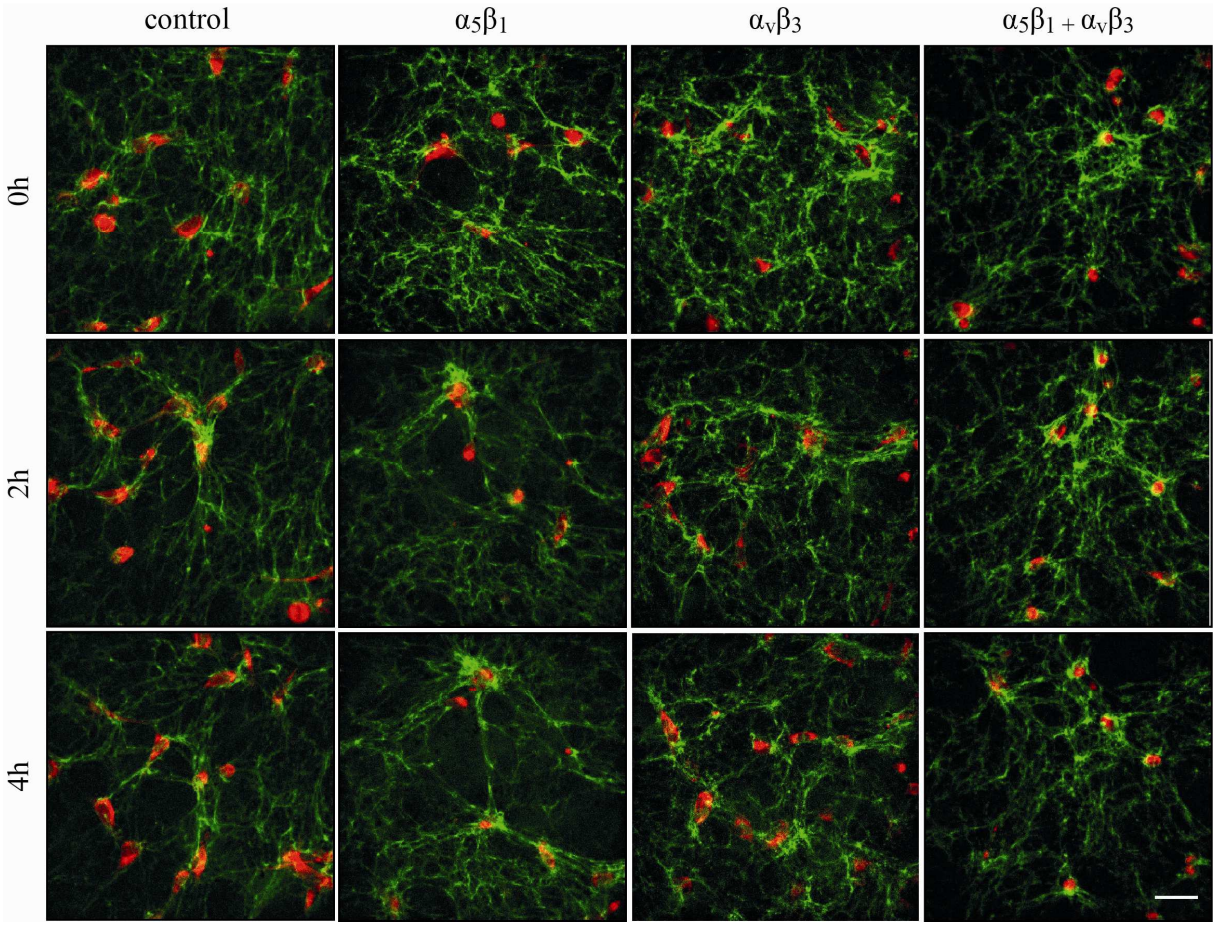

Figure 22: Fluorescence images of HT1080 cells with preblocked integrin receptors on FN matrices

HT1080 cells (red) were and plated on FN matrices (green). Fluorescence images are shown for time point 0 h, 2 h and 4 h. (**control**: untreated cells, **$\alpha_5\beta_1$**: preblocked $\alpha_5\beta_1$ integrin receptors, **$\alpha_v\beta_3$**: preblocked $\alpha_v\beta_3$ integrin receptors and **$\alpha_5\beta_1$ + $\alpha_v\beta_3$**: preblocked $\alpha_5\beta_1$ and $\alpha_v\beta_3$ integrin receptors). Scale bar, 50 µm.

6.4.3 Integrin $\alpha_5\beta_1$ promotes cell migration on 2D FN coatings but not on 3D fibrillar matrices

As shown in paragraph 6.4.1, preblocking of $\alpha_5\beta_1$ integrins but not of $\alpha_v\beta_3$ integrins significantly reduced initial adhesion of HT1080 cells on FN coatings. Here, the influence of integrin blocking on cancer cell migration behavior on both 2D and 3D FN environments was investigated. Therefore, $\alpha_5\beta_1$ and $\alpha_v\beta_3$ integrins were preblocked prior to seeding HT1080 cells on either FN coatings or FN matrices and average velocity and directionality of cell movement were calculated. Cells that did not move were not considered in this analysis.

As shown in figure 23 A, preblocking of $\alpha_5\beta_1$ integrin receptors reduced migration speed of HT1080 cells on FN coatings, while a slight increase in average velocity was observed for $\alpha_5\beta_1$ preblocked cells on fibrillar FN matrices. Blocking of $\alpha_v\beta_3$ integrins did not alter average velocity on both FN environments. According to the probability density plots (figure 23 B and C) the observed reduction in cell migration speed for $\alpha_5\beta_1$ preblocked cells on FN coating is statistically significant. These results suggest that $\alpha_5\beta_1$ promotes cell migration on 2D FN coatings, but not on 3D fibrillar matrices, which raises the question how migration on fibrillar FN is regulated.

The following two hypotheses might explain cancer cell migration on fibrillar FN. First, HT1080 cells change their mode of migration from the mesenchymal type, which involves FA and actin stress fiber formation, to an amoeboid migration, with no or only weak adhesive interactions [136]. On 2D FN coatings, HT1080 cells show characteristics of mesenchymal migration. In its globular conformation, FN primaryly interacts with $\alpha_5\beta_1$ integrins [137]. During FN fibrillogenesis, this interaction induces receptor clustering and the formation of FAs connecting the actin cytoskeleton with the substrate [41]. This connection allows the cell, after activation of downstream signaling cascades, to generate traction forces which lead to a forward movement of the cell body [138]. By blocking $\alpha_5\beta_1$ integrins on 2D FN coatings, HT1080 cells might fail to generate FAs and consequently traction forces [139], resulting in a reduced migration speed. In contrast, HT1080 cell migration within a 3D FN environment might be independent from FA formation in general because it is based on an amoeboid migration mechanism which is characterized by only weak adhesive interactions. As a consequence, $\alpha_5\beta_1$ and $\alpha_v\beta_3$ integrins are not necessary for cell migration on fibrillar FN (figure 23 A). In fact, preblocking of $\alpha_5\beta_1$ integrin did even increase average velocity of HT1080 cells on FN matrices to a minor extent. Amongst all FN-binding integrins, $\alpha_5\beta_1$ integrin has the highest affinity to bind FN and the highest FN-binding strength [36]. HT1080

cells might be held back in their movement by FN fibers because the adhesions of $\alpha_5\beta_1$ integrins to FN are not disassembled [128]. If $\alpha_5\beta_1$ integrins are blocked, HT1080 cells can move forward without hindrance.

A second explanation on how cell migration is regulated within fibrillar FN matrices is that other than $\alpha_5\beta_1$ or $\alpha_v\beta_3$ integrins might be involved. Due to its unfolded and stretched confirmation, fibrillar FN induces the binding of integrins other than $\alpha_5\beta_1$ or $\alpha_v\beta_3$ [39]. The FAs formed by these integrins might be less stable than the FAs formed between $\alpha_5\beta_1$ integrins and FN. FA stability has been shown to be a crucial regulator of cell migration velocity on 2D FN coatings, whereby less stable FA and subsequent higher FA turnover enabled fast cell migration [88]. Although $\alpha_5\beta_1$ integrin is necessary to promote cell migration on FN coatings, the high binding strength of $\alpha_5\beta_1$ might allow only slow FA turnover and thus relatively slow cell migration. In contrast, cells on fibrillar FN, which might form less stable FAs, could thus achieve higher speed. Since the RGD motif is necessary for promoting fast cell migration on 3D fibrillar FN matrices (figure 19 A and B) and the involvement of $\alpha_5\beta_1$ as well as $\alpha_v\beta_3$ integrins could be excluded (figure 23 A), one or more of the following RGD-binding integrin receptors might regulate migration on 3D fibrillar matrices, namely $\alpha_8\beta_1$, $\alpha_v\beta_1$, $\alpha_v\beta_6$, or $\alpha_{IIb}\beta_3$ integrin. This speculation is in agreement with the hypothesis raised in 6.3.3, according to which cells interact with FN coating and FN matrix through distinct integrins resulting in different migration behavior as an answer on variations in matrix stiffness.

6.4.4 Integrin $\alpha_5\beta_1$ regulates directionality of cell migration on 2D FN coatings but not on 3D fibrillar matrices

At last, the influence of integrins on directionality of HT1080 on FN-dependent cell migration was investigated. Concerning the persistence of cell migration on FN coatings (figure 23 D and E), blocking of $\alpha_5\beta_1$ integrin resulted in a more random cell migration, as cells showed increased probability of backwards movement. In contrast, $\alpha_v\beta_3$ integrin did not affect the directionality of cell movement. On fibrillar FN matrices (figure 23 D and F), blocking of integrin $\alpha_5\beta_1$ or $\alpha_v\beta_3$ had no effect on the directionality of HT1080 cell migration. These findings are in agreement with the results obtained for FN-RGE matrices (6.3.4) suggesting that both substrate topography and cell adhesion are main regulators for directed cell migration on FN environments.

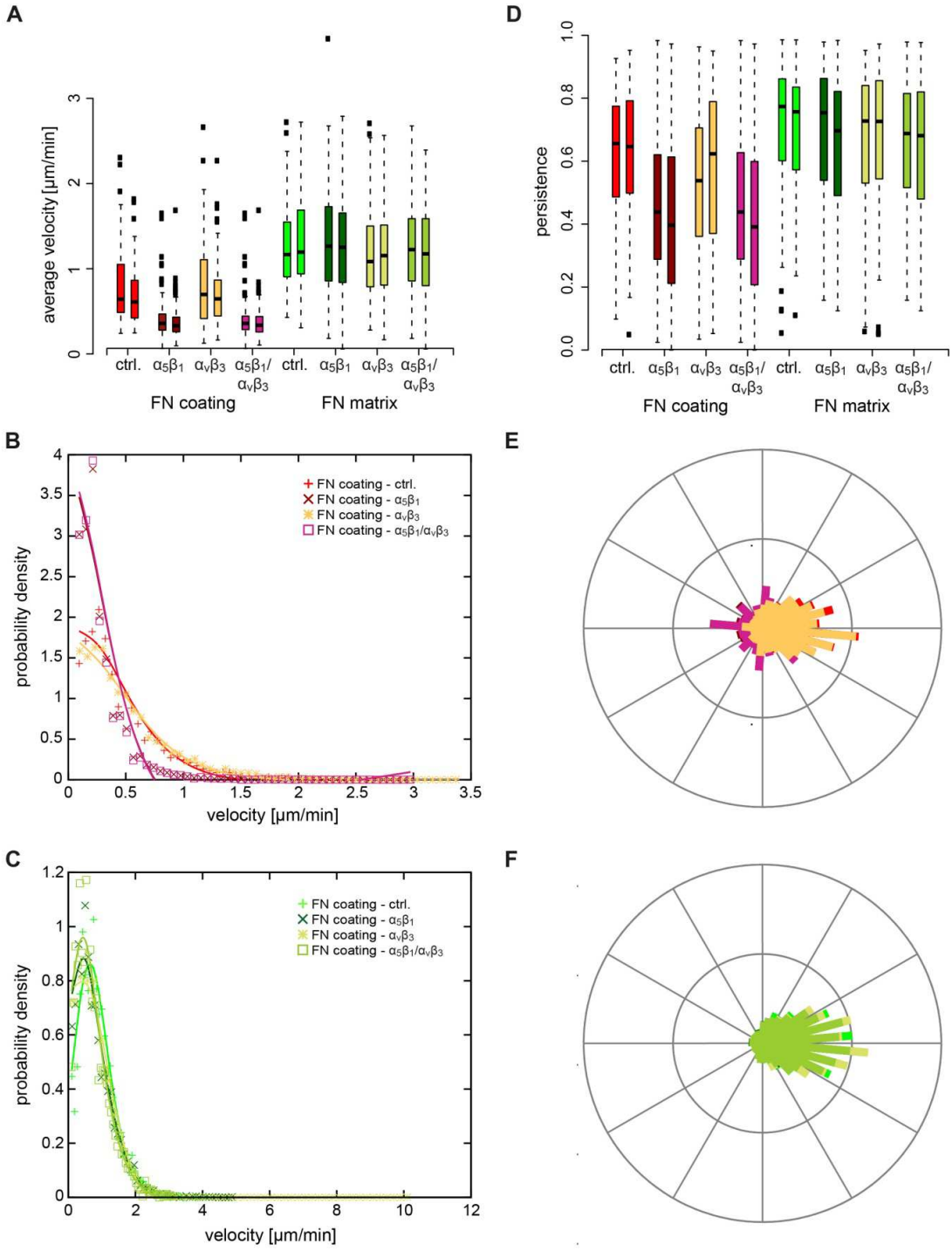

Figure 23: Effect of $\alpha_5\beta_1$ and $\alpha_v\beta_3$ integrin blocking on migration speed and persistence of HT1080 cells on different FN environments

HT1080 cells were either preblocked with antibodies directed against integrin $\alpha_5\beta_1$ (dark red/dark green), integrin $\alpha_v\beta_3$ (orange/light green), both integrins (pink/oliv) or left untreated (red/green), before seeding on FN coatings (red colors) or FN matrices (green colors). **A)** Migration speed of cells is plotted as a box-and-whisker plot comparing indicated groups and time periods (first box of each group: 0-2 h, second box of each group: 2-4 h). **B/C)** Probability density of average migration values for 4 h is plotted as a scatter plot for all indicated groups for B) FN coating and C) FN matrix. **D)** Box-and-whisker plot depicts directionality of cell migration on both FN environments. **E/F)** Polar plots show probability density of persistence angles for 4 h on FN coating (E) and on FN matrix (F).

6.5. Influence of MMP and myosin II inhibition on FN dependent cell migration

Beside the importance of integrins for cancer cell invasion, proteases, such as MMPs, are important regulators of tumor cell dissemination by degrading migration barriers as well as remodeling of the local tumor microenvironment [23]. In fact, there is a close relationship between cell adhesion, proteolysis and force generation [140, 141]. In this section, the influence of MMP activity on FN dependent cancer cell migration was examined. MMP activity was blocked with the broad-spectrum hydroxamate inhibitor GM6001 [142-144]. The hydroxamic acid group of GM6001 forms a complex with the zinc ion present at the catalytic active site [143], inhibiting enzyme activity of a broad range of MMPs. It has been observed that cancer cells are able to switch between protease dependent motility and contractility driven migration if MMPs are inhibited [90, 103, 145]. Consequently, the influence of myosin II inhibition on FN dependent cancer cell migration was further investigated.

6.5.1 Inhibition of myosin II influences morphology of HT1080 cells on 3D fibrillar FN matrices

Initially, effect of GM6001 and blebbistatin treatment on cell morphology was analyzed by fluorescence microscopy. Myosin II inhibition strongly influenced HT1080 cell morphology on FN matrices at both molar concentrations used (figure 24, left). Cells treated with blebbistatin assumed thin elongated shapes with multiple branching filopodia. On FN coatings, on the other hand, application of 25 µM myosin II inhibitor had no effect on cell morphology; while cell shape was altered to a small extent when 50 µM blebbistatin was applied (figure 24, right). In this case, some cells formed filopodia which was not observed for untreated cells (figure 17).

In contrast, MMP inhibition with GM6001 did not affect cell morphology of HT1080 cells cultured either on FN coatings or on fibrillar FN matrices (figure 25).

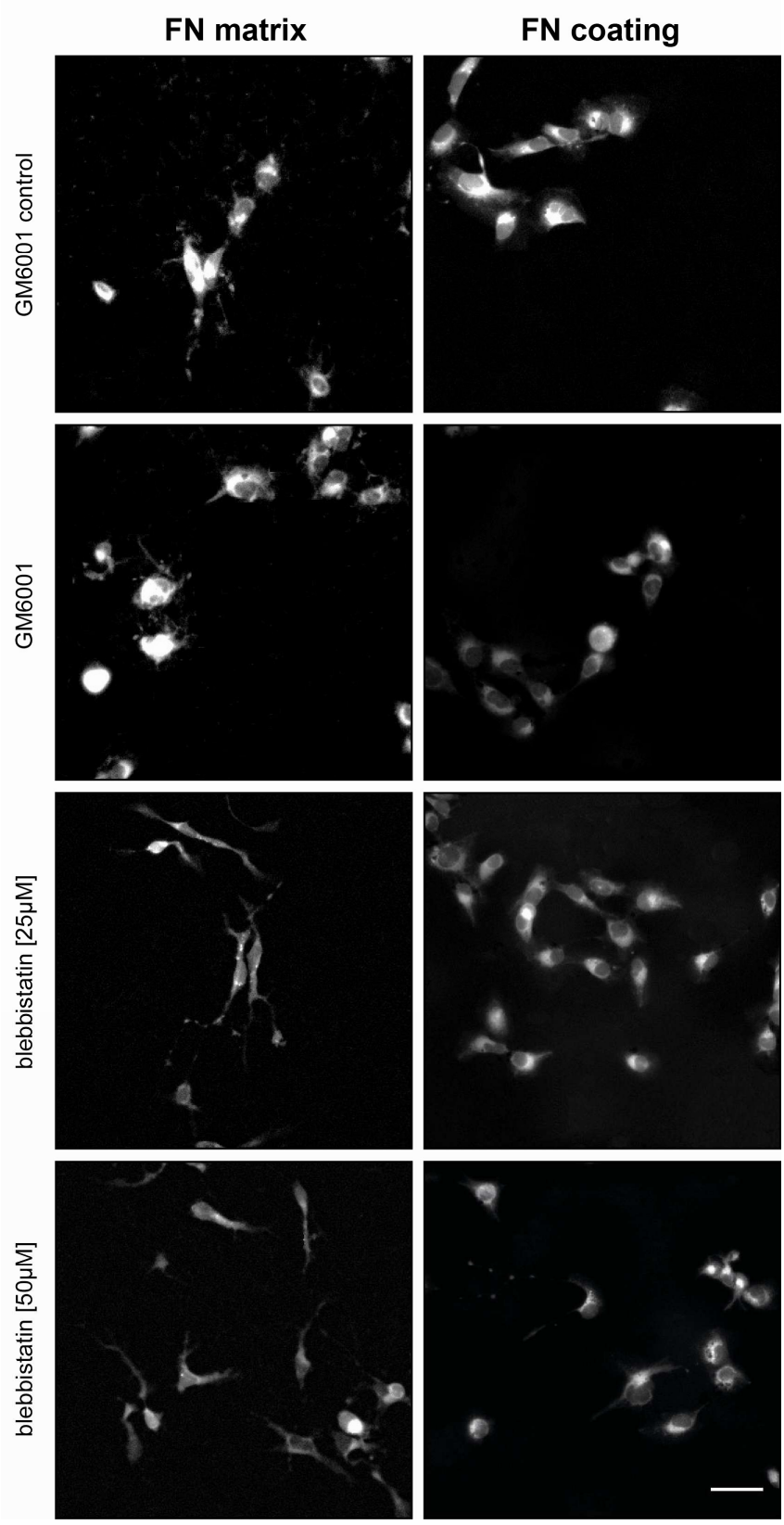

Figure 24: Fluorescence images of myosin II inhibited cells on different FN surfaces

HT1080 cells were plated on FN matrices or FN coatings and treated with 25 µM or 50 µM blebbistatin. Here, representative images are acquired 2 h after cell seeding. Scale bar, 50 µm.

6.5.2 Disruption of the fibrillar FN matrices is caused by contractile forces and not via proteolytic activity

Next, interactions between FN fibers and HT1080 cells treated with either GM6001 or blebbistatin were evaluated. The ability of HT1080 cells to remodel the fibrillar FN network (figure 18) was not impaired by MMP inhibition (figure 25). Accordingly, MMP activity seems not to be necessary for disruption of the FN matrix. In contrast, cells with myosin II-based contractility inhibited, leave the FN fibrillar matrices unaltered (figure 25). These results corroborate the hypothesis raised in paragraph 6.3.3, that the observed disruption of the fibrillar FN matrices is mainly caused mechanically through tearing FN fibers. In order to analyze if concentrated local proteolytic action might contribute to FN matrix disintegration by HT1080 cells, cell matrix interactions have to be studied at a higher resolution.

6.5.3 Evaluation of MMP and myosin II activity on average velocity

The influence of MMP and myosin II activity on migration speed within different FN environments was investigated by time-lapse microscopy. Inhibition of MMP activity by GM6001 did not alter migration speed of HT1080 cell migration on neither FN coatings nor FN matrices (figure 26), suggesting that proteolytic activity is not required for cell migration on FN. Similar results have been shown for breast cancer cells migrating in 3D collagen matrices [146]. Hereby, cancer cell migration was promoted through upregulation of ROCK1 activity, while MMP activity had only minor influence. In fact, tumor cells can escape MMP inhibition by switching their migration behavior from protease-driven locomotion to contractility dependent movement which requires upregulation of ROCK activity [147, 148]. To study this possibility, cell contractility was blocked by myosin II inhibition. Migration experiments demonstrated that addition of blebbistatin significantly reduces migration speed of HT1080 cells on FN matrices, but not on FN coatings (figure 26 A-C). These results are in agreement with previous studies on NIH3T3 cells [129, 149] and corroborate the hypothesis that HT1080 cell movement on FN coating is based on a mesenchymal mode of migration, while cell locomotion within 3D environments is mainly based on myosin II activity, as observed for amoeboid migration. Myosin contractility was demonstrated to increase the mechanical coupling between cell adhesions and acto-myosin resulting in larger cellular protrusions and fast cell movement [149]. This could further explain the increased migration speed of HT1080 on fibrillar FN matrices compared to FN coatings.

However, cell migration on FN coatings was neither effected by blebbistatin treatment nor by MMP inhibition. It has been shown previously that general MMP inhibition with GM6001 can increase expression of MT1-MMP in fibroblast cultured within collagen matrices [150, 151]. Accordingly, it might be possible that MT1-MMP activity compensate the inhibitory effect of GM6001 in HT1080 cells.

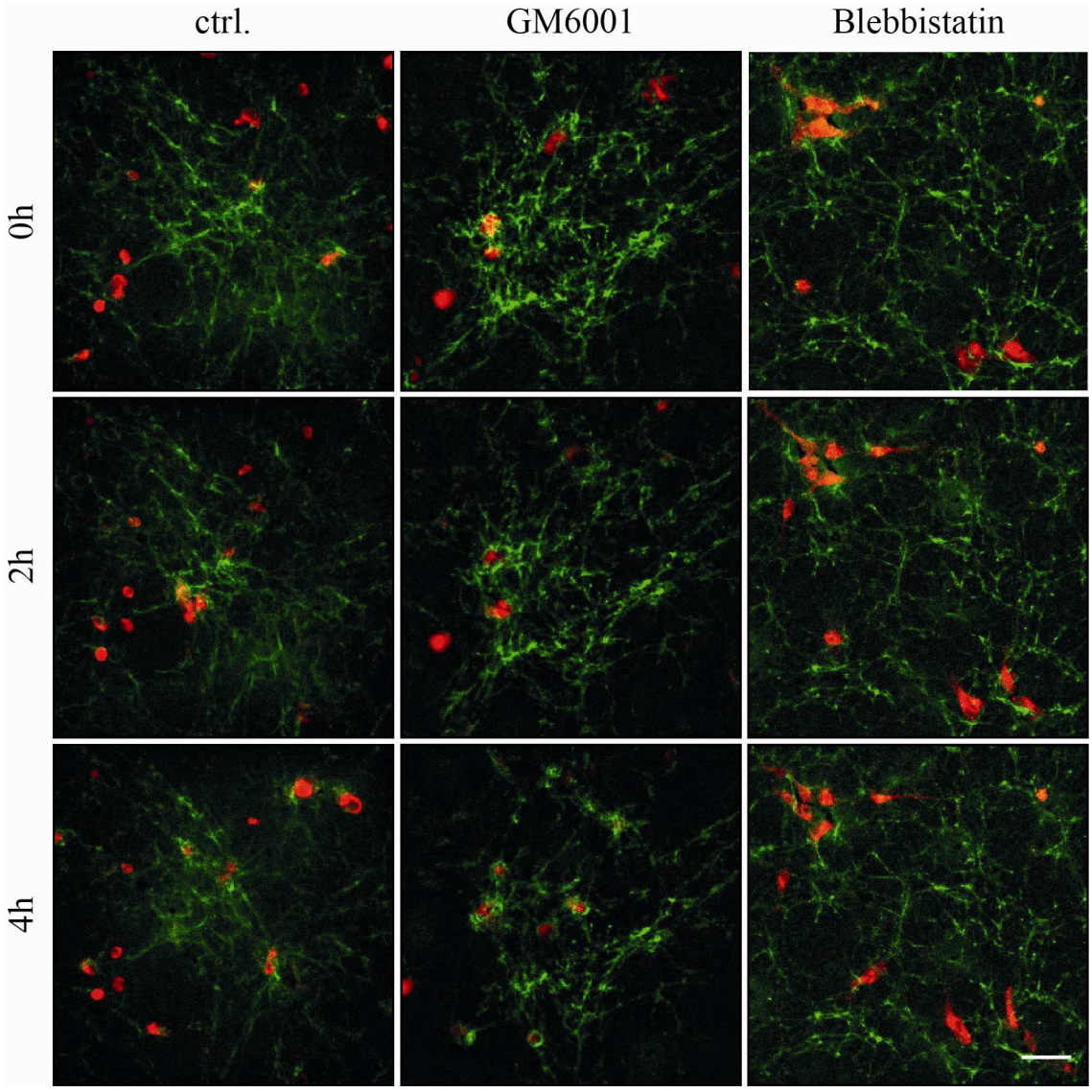

Figure 25: Fluorescence images of MMP and myosin II inhibited HT1080 cells on FN matrices

HT1080 cells (red) seeded on FN matrices (green) were treated with 10 µM of the GM6001 control (**ctrl**.) and the general MMP inhibitor (**GM6001**) or with 50 µm of the myosin II inhibitor (**blebbistatin**). Here, fluorescence images for 0 h, 2 h, and 4 h are depicted. Scale bar, 50 µm.

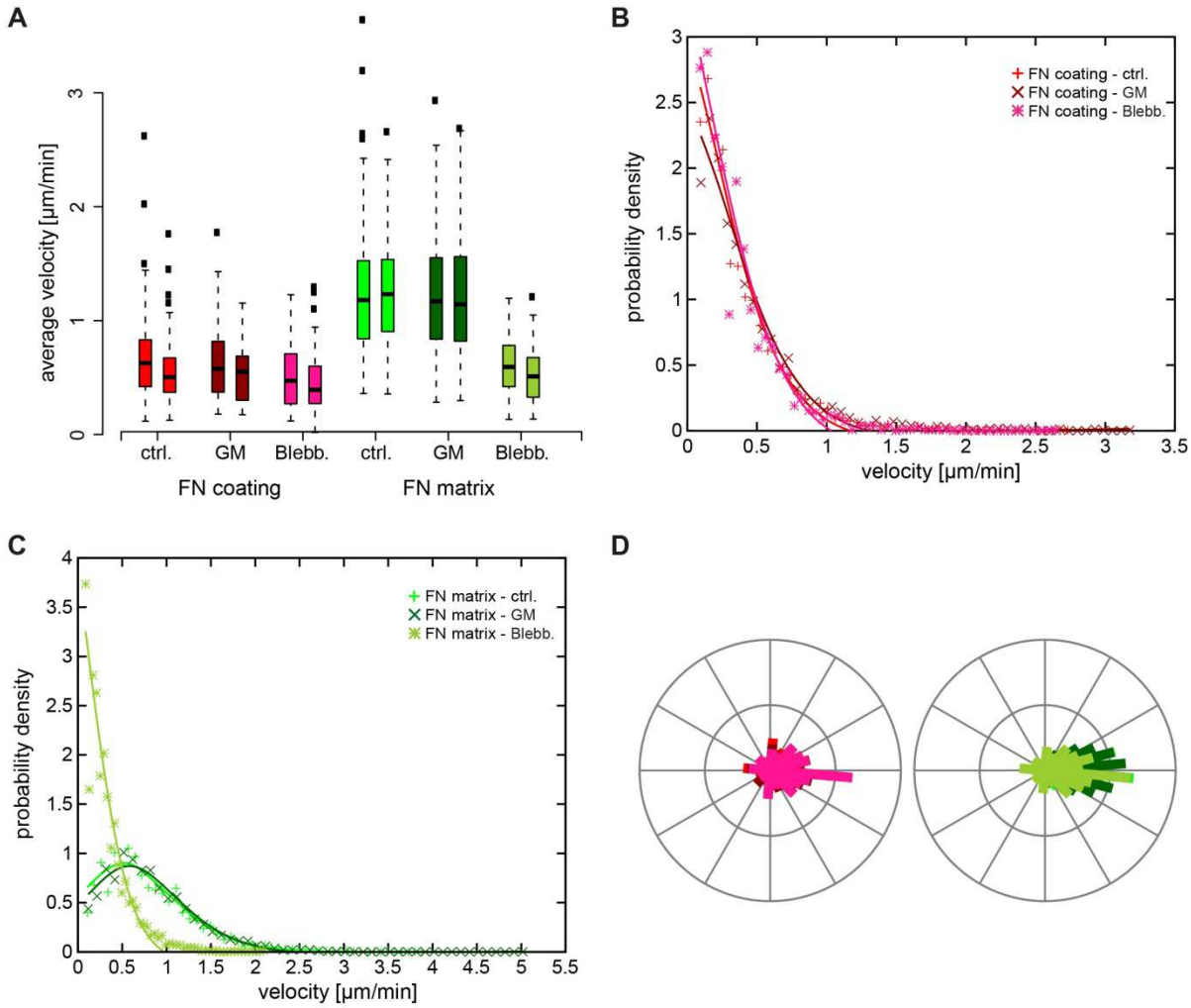

Figure 26: Analysis of migration speed and persistence of MMP inhibited cells on FN matrices

Migration of HT1080 cells, cultured in the presence of either 50 µM blebbistatin, 10 µM GM6001 or GM6001 control was monitored on FN coating (red colors) and FN matrix (green colors). **A)** Average velocity is plotted as a box-and-whisker plot comparing indicated groups for the time periods 0-2 h (left box of each group) and 2-4 h (right box of each group). **B/C)** Velocity is plotted as probability density for the first 4 h of the migration experiment. Cells were either plated on FN coatings (B) or on fibrillar FN matrices (C) Treatments are indicated on the upper right. **D)** Persistence angles for 4 h are plotted as polar plots. The left polar plot shows data on FN coatings with control (red), GM6001 (dark red) and blebbistatin (pink). On the right polar plot data for cells migrating on FN matrices is depicted with control (green), GM6001 (dark green) and blebbistatin (oliv).

6.5.4 Evaluation of MMP and myosin II activity on directionality of cell migration

Finally, the effect of GM6001 and blebbistatin treatment on the directionality of cell migration was quantified. As shown in figure 26 D general MMP inhibition did not affect persistence of HT1080 cells migration on both FN environments. Furthermore, directionality of cell movement was not influenced by myosin II inhibition on FN coatings. In contrast, cells on 3D fibrillar FN environments showed a more random cell migration when treated with blebbistatin in comparison to the control group, indicated by a higher probability for backward movement. These findings highlight the importance of myosin II-driven contractility for directed movement within fibrillar FN environments [149].

6.6 Influence of MT1-MMP on FN dependent cell migration

Within the MMP family one member, namely MT1-MMP, is of particular interest regarding its effect on FN dependent cell migration. It has previously been shown that MT1-MMP regulates cell migration through modulation of focal adhesion stability on FN coatings [88]. This is achieved by local lysis of FN at cell adhesions, facilitating FA turnover [152]. Furthermore. MT1-MMP activity might compensate GM6001 blocking effects on FN coatings. Here, the influence of MT1-MMP downregulation via RNA interference (RNAi) on cell migration was studied on FN coatings and fibrillar FN matrices.

6.6.1 Evaluation of MT1-MMP silencing efficiency

First, the conditions for MT1-MMP silencing were optimized in respect to the amount of transfection reagent, cell density and the point in time when cells were analyzed. In all cases, siRNA treatment led to a significant decrease in protein expression regardless of the altered parameter (figure 27 A). Consequently, the most convenient conditions were selected for all further experiments. Hence, 1.2×10^5 cells were seeded per well of a 24-well plate, transfection was performed with 1.5 µl of transfection reagent and cells were analyzed 48 h after transfection.

The effectiveness of MT1-MMP silencing under the selected conditions was assessed by flow cytometry (figure 27 B) and by western blot analysis (figure 27 C). Treatment of cells with siMT1-MMP decreases protein expression by 87 % compared to untreated cells (figure 27 A). The procedure for RNA silencing seems to have a minor influence on gene expression in general, as cell transfection with a non-targeting siRNA slightly reduces MT1-MMP expression levels. These results indicate that MT1-MMP protein expression can be successfully downregulated by transfection with siRNAs directed against MT1-MMP transcripts. Hence, it is possible to study the dependence of MT1-MMP on cell migration by comparing HT1080 cells with downregulated protease expression levels to control HT1080 cells.

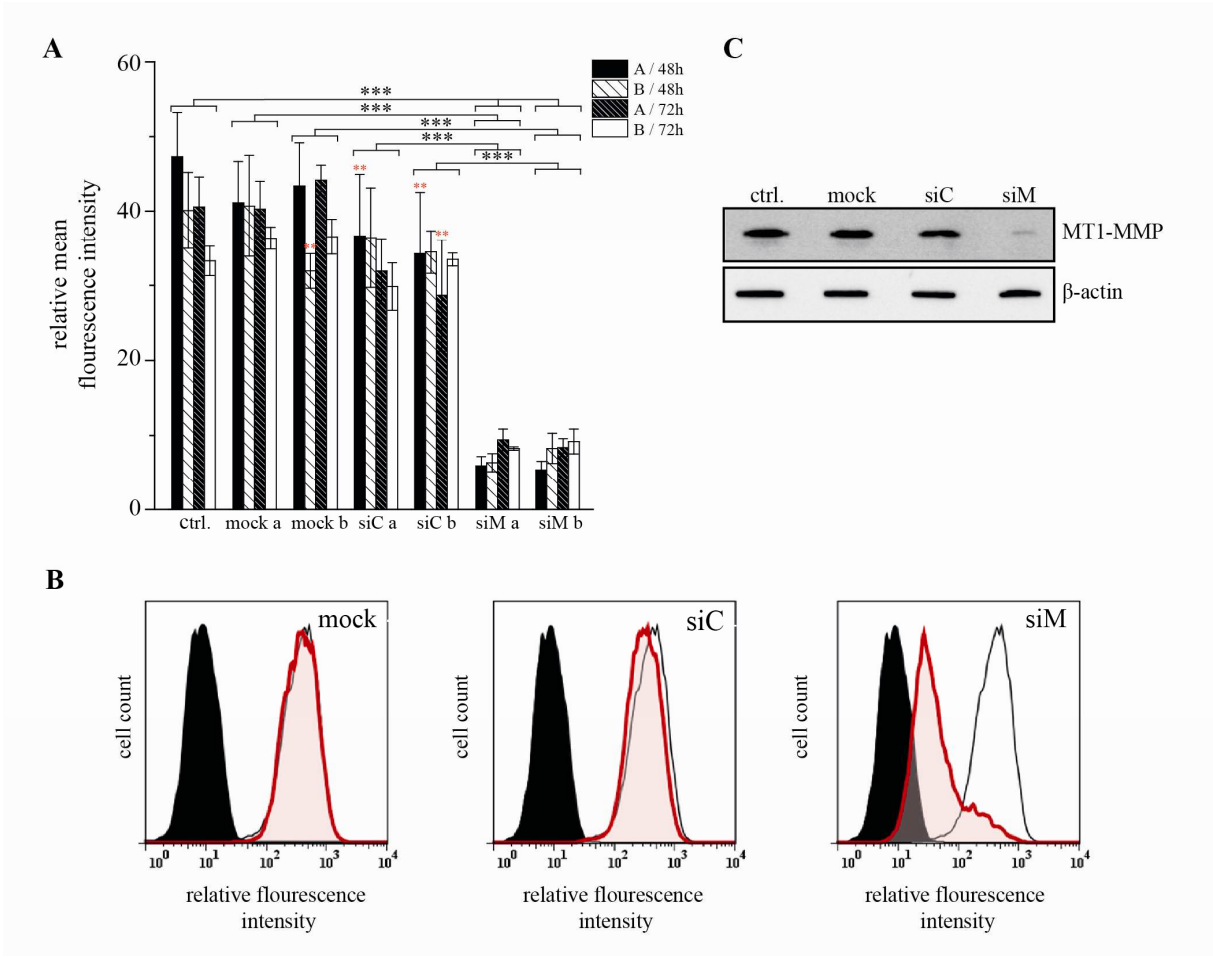

Figure 27: FACS and western blot analysis of MT1-MMP silencing in HT1080 cells

A) Different conditions to optimize MT1-MMP silencing are tested. Altered factors are the amount of transfection reagent (TR) used: **a:** 1.5 µl or **b:** 2 µl, cell density: **A:** 1.2 x 10^5 or **B:** 1.8 x 10^5 cells per well and the point in time when cells are analyzed: 48 h or 72 h after transfection. Cell surface expression of MT1-MMP is analyzed via FACS measurements. Here, the means of the respective relative fluorescence intensities and SEM are plotted. Here, significant results are differentiated between highly significant (**) with $P < 0.005$ and extremely significant (***) with $P < 0.001$. For simplifying the graphs, p-values are assigned to entire treatment groups. If within a group a p-value differs it is indicated above the respective column by red asterisks.
B) Representative FACS figures for the following conditions are chosen: 1.5 µl TR, 1.2 x 10^5 cells per well, 48 h after siRNA transfection. The histograms reflect the relative fluorescence intensities of differentially stained cell populations. Here, relative fluorescence intensity is plotted in a logarithmic scale on the x-axis and cell count is plotted on the y-axis. Black histograms represent the level of autofluorescence of cells stained with the secondary antibody only. The relative fluorescence intensities of MT1-MMP stained cell populations are indicated by black framed colorless histograms. Red histograms mark cell populations that are either **mock** (TR only), **siC** (non targeting siRNA) or **siM** transfected (siMT1-MMP) as indicated.
C) Western blot was with 5 µg total potein lysates from untreated cells **(ctrl.)**, cells treated with TR only **(mock)**, cells treated with non targeting siRNA **(siC)** and cells treated with siMT1-MMP **(siM)**. As loading control β-actin is detected.

6.6.2 MT1-MMP does not influence cell morphology on fibrillar FN

First, cell morphology and cell-FN fiber interactions upon MT1-MMP depletion were investigated. MT1-MMP silencing in HT1080 cells cultured on FN matrices had no effect on cell shape or on the ability of cells to disrupt the fibrillar FN network, if compared to cells transfected with a non-targeting siRNA (figure 28). This finding is in agreement with the results of general MMP inhibition presented in paragraph 6.5.1 and 6.5.2. Additional blocking of $\alpha_5\beta_1$ integrins in MT1-MMP silenced cells produced no supplementary outcome.

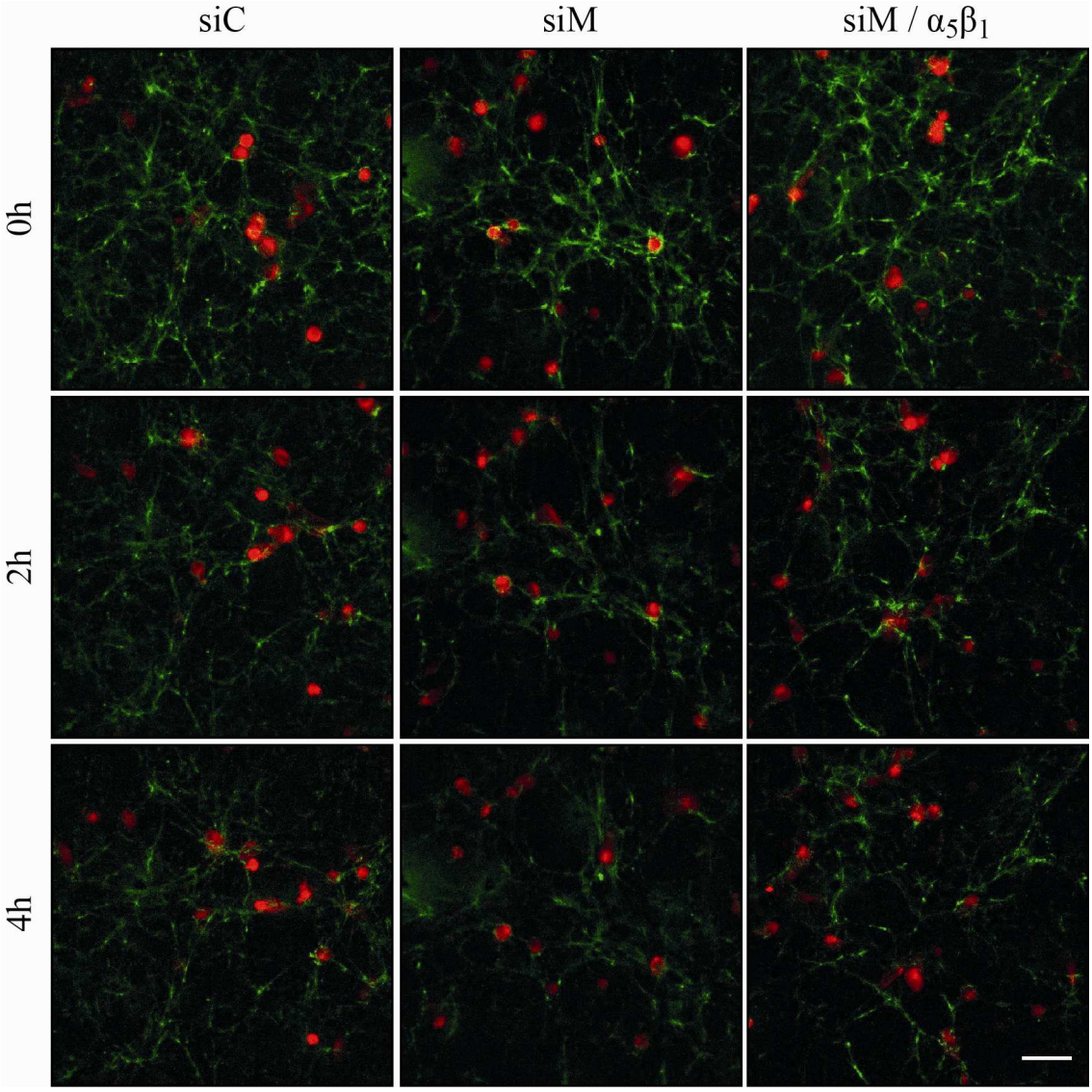

igure 28: Fluorescence images of siMT1-MMP silenced HT1080 cells on FN matrices

48 h after siRNA transfection, HT1080 cells (red) were seeded on FN matrices (green). Here, representative fluorescence images acquired at 0 h, 2 h and 4 h are depicted per condition (**siC:** cells transfected with siControl; **siM:** cells transfected with an siRNA targeting MT1-MMP transcripts; **siM/$\alpha_5\beta_1$:** same as siM with additional preblocking of $\alpha_5\beta_1$ integrins). Scale bar, 50 µm.

6.6.3 MT1-MMP promotes cell migration on 2D FN coatings, but not in 3D fibrillar FN matrices

MT1-MMP silenced HT1080 cells from the same batch were seeded on FN coatings or FN matrices and their MT1-MMP expression levels were analyzed after 1 h. Interestingly, MT1-MMP expression levels were higher on FN coatings compared to cells seeded on FN matrices (figure 29 A). The observed increase of MT1-MMP expression post seeding suggest that MT1-MMP-silenced cells on FN coatings try to compensate for MT1-MMP depletion, either by enhancing its expression or by stabilization the protein at the plasma membrane.

Next, the influence of MT1-MMP on HT1080 cell migration was evaluated. MT1-MMP silencing significantly decreased average velocity of HT1080 cells on FN coatings (figure 29 B and C), while on fibrillar FN matrices migration speed slightly increased (figure 29 B and D). Interestingly, MT1-MMP silencing resulted in a more randomized migration on both FN environments (figure 29 E). These results suggest that MT1-MMP is in general important for directed cell movement and promotes fast cell migration on FN coatings.

The aformentioned differences in migration behavior might be connected to the ability of MT1-MMP to cleave different integrin subunits [83]. Hence, the influence of MT1-MMP silencing on α_5 and β_1 integrin expression was determined by western blot analysis. It is shown in figure 29 A, that MT1-MMP silencing resulted in slightly elevated expression levels of α_5 (1.4-fold) and β_1 (1.3-fold) integrins on FN coatings. Accordingly, MT1-MMP might positively regulate migration speed by cleavage of $\alpha_5\beta_1$ integrins which enhances FA turnover. In contrast, integrin expression levels on fibrillar FN remained unaltered upon MT1-MMP silencing. On FN coatings, MT1-MMP-silenced cells additionally preblocked with $\alpha_5\beta_1$ integrin antibodies migrated with significantly reduced speed and showed a more randomized cell migration compared to the control and MT1-MMP-silenced groups (figure 29 B, C and E) In contrast, the combination of both treatments had no cooperative effect on average velocity or directionality of cell migration on fibrillar FN matrices (figure 29 B, D and E).

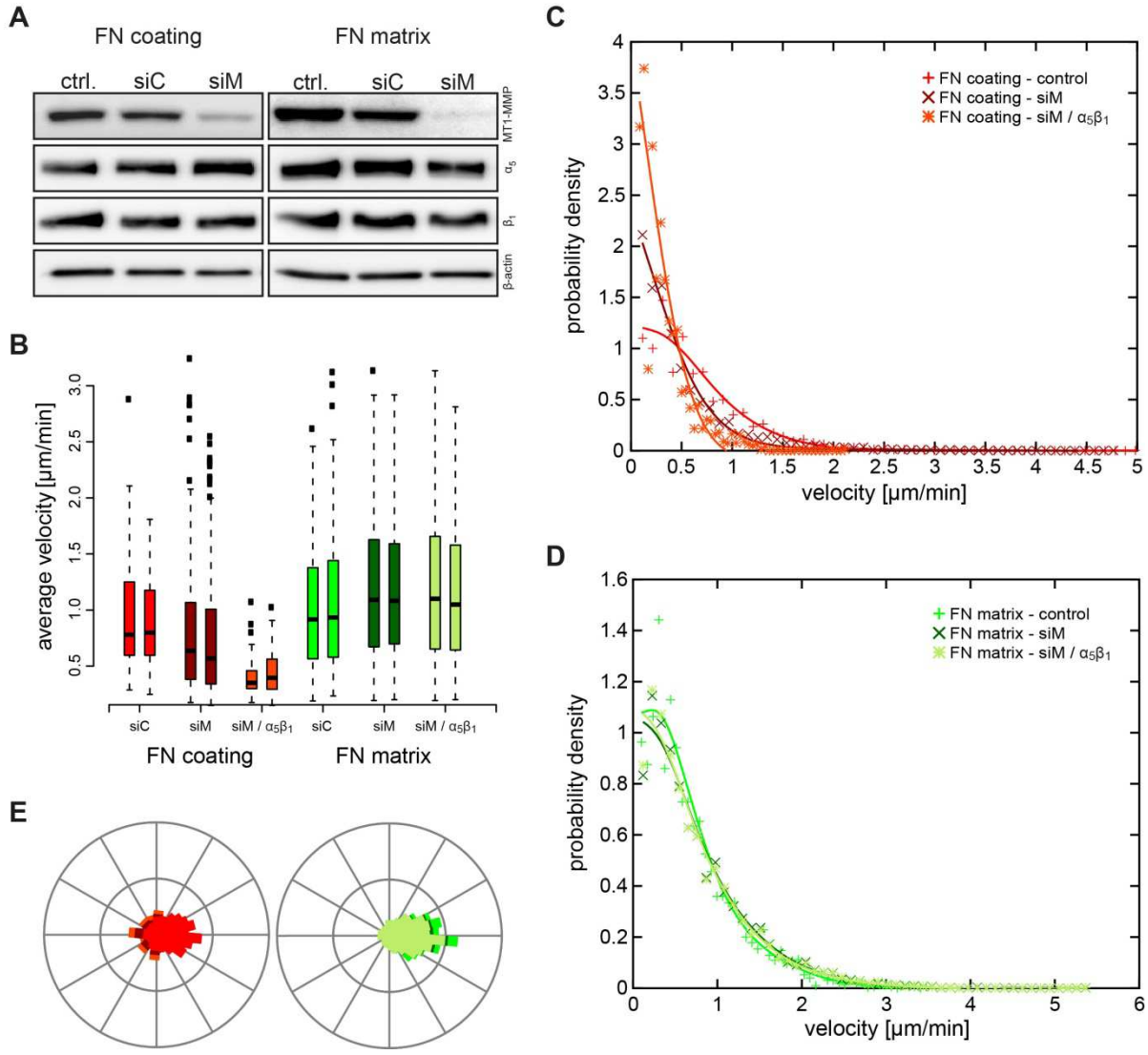

Figure 29: Analysis of migration speed and persistence of siMT1-MMP silenced cells on FN matrices

HT1080 cells were first transfected with siRNA directed against MT1-MMP transcripts (**siM**) or with a non-targeting siRNA (**siC**). 48 h after transfection cells were seeded on FN coatings or FN matrices. In addition, some MT1-MMP silenced cells were further preblocked with $\alpha_5\beta_1$ specific antibodies to inhibit integrin receptor function. **A)** Western blot of integrin subunits α_5 and β_1 as well as MT1-MMP was conducted 1 h after seeding the cells on different FN substrates. As loading control β-actin was detected. **B)**. Average migration speed of cells is plotted as a box-and-whisker plot comparing indicated groups at 0-2 h (left box) and 2-4 h (right box). **C/D)** Distribution of velocity values are plotted as scatter plots for the time period of 4 h on either FN coating (**C**) or FN matrices (**D**). **E)** Persistence angles are depicted as polar plots for HT1080 cells plated on either FN coating (left) or FN matrix (right).

6.7 Influence of MT1-MMP on adhesion mediated signaling within different FN environment

As demonstrated in paragraph 6.6, MT1-MMP differentialy regulates cell migration on FN coatings and on FN matrices. While MT1-MMP promotes cell migration on 2D FN coatings, it is not required for cell locomotion in a fibrillar FN matrices, where it seems to have an inhibtory effect. It has been suggested, that MT1-MMP influences cell migration behavior on FN coatings by modulating adhesion mediated signaling pathways [88]. Accordingly, the involvement of MT1-MMP in phosphorylation of FAK, ERK1/2 and cofilin were investigated in HT1080 cells cultured either on FN coatings or on fibrillar FN matrices by western blot analysis (figure 30).

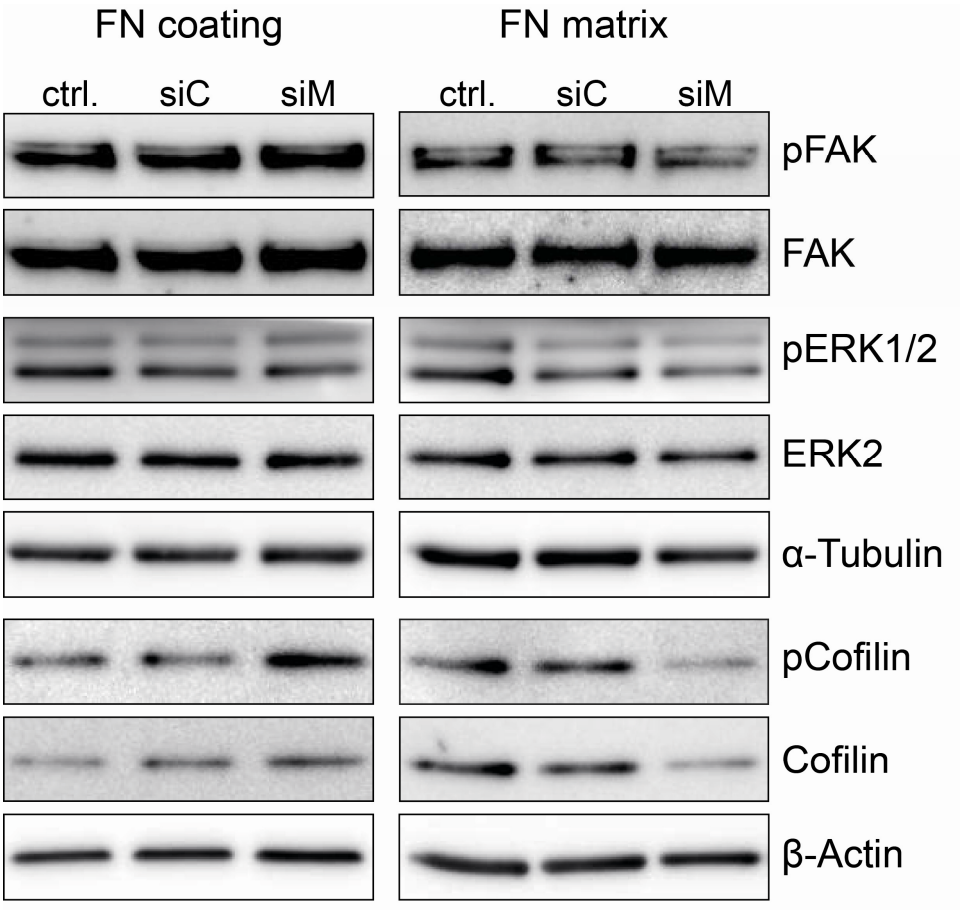

Figure 30: Western blot analysis of adhesion mediated signaling

48 h after siRNA transfection HT1080 cells were plated on either fibrillar FN matrices or on FN coatings. After 1 h, expression and phosphorylation of FAK (Tyr397), ERK1/2 (Tyr204/187) and cofilin (Ser3) were investigated by western blot analysis for the following treatment groups. **ctrl.**: untreated cells, **siC**: cells transfected with non-targeting siRNA and **siM**: cells transfected with siMT1-MMP. As loading control β-actin and α-tubulin were chosen.

MT1-MMP silencing has an opposite effect on protein expression and phosphorylation, if HT1080 cells are cultured on 2D FN coatings or 3D fibrillar FN matrices (figure 30):

On FN coatings, MT1-MMP depleted cells showed increased cofilin expression levels resulting in a 1.8-fold upregulation of cofilin phosphorylation, while expression and phosphorylation of FAK and ERK2 remain unaltered. In contrast, HT1080 cells cultured on FN matrices, showed a 2.9-fold downregulation of cofilin expression and subsequent phosphorylation as well as a 1.2-fold downregulation of FAK phosphorylation upon MT1-MMP silencing.

Integrin-mediated cell migration is dependent on FAK phosphorylation [153]. It was previously demonstrated on FN coatings, that MT1-MMP regulates FAs stability and turnover via FAK cleavage [88, 152]. In these experiments, any changes in FAK protein expression or phosphorylation were observed, when cells were seeded on FN coatings. A possible explanation might be that HT1080 cells need to be cultured for longer periods than 1 h on FN coatings in order to affect FAK phosphorylation. In contrast, on FN matrices, FAK phosphorylation was slightly reduced (-1.2-fold) upon MT1-MMP silencing suggesting that MT1-MMP positively regulates FAK phosphorylation at Tyr397. It has been shown previously that reduced FAK Tyr397phosphorylation is connected to higher turnover of FAs promoting cell migration on FN coatings [88]. Accordingly, upon MT1-MMP silencing HT1080 cells migrate faster on fibrillar FN matrices due to reduced FAK Tyr397 phosphorylation.

Here, MT1-MMP is presented as an additional regulator of cofilin activity. On FN coatings, cofilin shows lower phosphorylation levels and subsequently higher activity if MT1-MMP is present. It has been demonstrated previously that $\alpha_5\beta_1$ integrin-mediated adhesions on FN coatings lead to phosphorylation and subsequent inactivation of cofilin [154]. Consequently actin dynamics are reduced, resulting in more randomized cell migration. These findings support those results which showed reduced average speed and persistence of HT1080 cells migrating on 2D compared to 3D FN environments. Interestingly, MT1-MMP counteracts the $\alpha_5\beta_1$ integrin dependent phosphorylation of cofilin. If MT1-MMP is depleted, phosphorylation/inactivation of cofilin increases (1.8-fold), resulting in lower migration speed and less directed cell migration. Hence, this new function of MT1-MMP allows cells to differentially regulate cell migration behavior on FN coatings.

Within 3D fibrillar FN matrices, MT1-MMP activity is associated with phosphorylation/inactivation of cofilin, as MT1-MMP depleted cells show reduced cofilin

expression (2.8-fold) and subsequent phosphorylation. Accordingly, cells migrate faster on fibrillar FN matrices in case of MT1-MMP depletion since in this case cofilin activity and actin dynamics are enhanced.

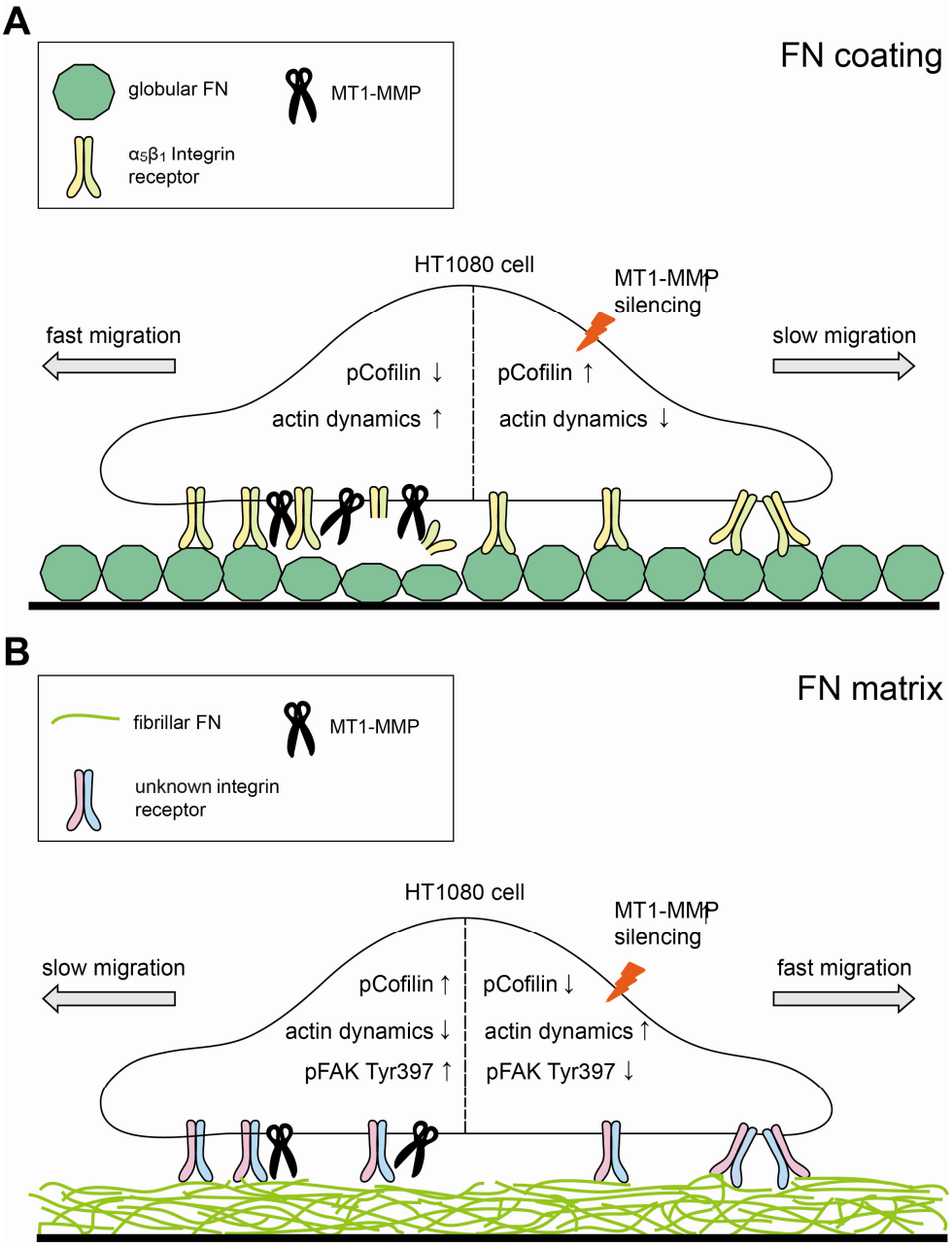

Figure 31: MT1-MMP differentially regulates cell migration on FN coatings and FN matrices

This scheme depicts molecular mechanisms that govern cell migration on A) FN coatings and B) FN matrices. The left side of the cell is showing integrin-mediated signaling events under control conditions, whereas the right site of the cell depicts the cellular response on MT1-MMP silencing. It is important to note that "slow" and "fast migration" are relative terms, describing the effect on MT1-MMP on average velocity in a specific FN environment.

6.8 Influence of MT1-MMP and fibrillar FN on cell motility gene expression

Up to now, the presented data validate MT1-MMP as an important regulator of cell migration behavior in FN environments. To determine if MT1-MMP further acts through changing the expression levels of genes relevant for cell migration, an mRNA expression screening on genes involved in cell migration was performed using a RT-PCR array[6].

As depicted in figure 32, MT1-MMP silencing only affected its own gene expression. Interestingly, siMT1-MMP transfected HT1080 cells cultured on ibiTreat dishes showed a more efficient downregulation of MT1-MMP gene expression (-14.5-fold; figure 32 B) than cells cultured on FN matrices (-5.3-fold, figure 32 A). As observed in western blot analysis (figure 29 A), MT1-MMP protein expression in MT1-MMP-silenced cells is higher on FN coatings than on FN matrices. Taken these findings into consideration, HT1080 cells might counteract MT1-MMP depletion upon adhesion to FN, whereby they are more efficient on FN coatings than on FN matrices.

It should be noted that this experiment was performed in two biological replicates. Hence, only major changes in gene expression could be detected. Since the software used for analyzing the array data requires three datasets for detecting small but significant changes in gene-expression, an additional experiment has to be conducted.

[6] A complete list of genes tested with the RT-PCR array Human Cell Motility can be found in the appendix

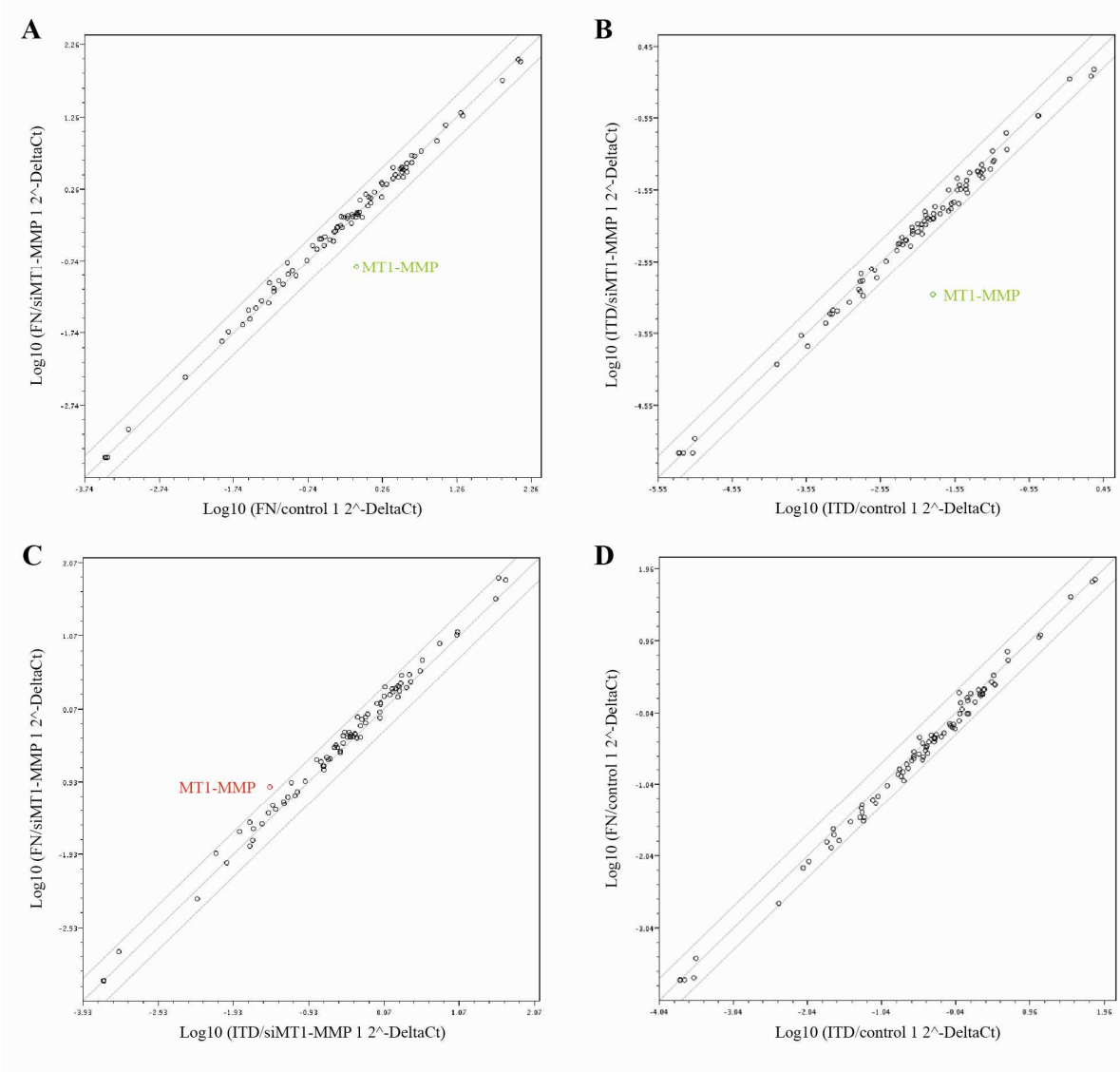

Figure 32: Scatter plots of results from the Cell Motility RT^2-PCR Array
Gene expression of HT1080 cells cultured on either FN matrix or ITDs for 16 h was analyzed using a RT^2-PCR array. The scatter plots compare the normalized expression of every analyzed gene between two groups indicated on the x- and y-axis: **FN/control:** cells cultured on FN matrices, **FN/siMT1-MMP:** MT1-MMP silenced cells cultured on FN matrices, **ITD/control:** cells cultured on ibiTreat dishes and **ITD/siMT1-MMP:** MT1-MMP silenced cells cultured on ibiTreat dishes. Unchanged gene expression is marked by the central line. All data points below that line indicate genes with downregulated expression, all data points above that line indicate genes with upregulated expression. The two boundaries next to the central line mark the threshold set at 2.0 which corresponds to a 2-fold change in gene expression. Genes outside this boundary are indicated by name and color (green for down- and red for up regulation of gene expression). **A)** Test group: FN/siMT1-MMP vs. control group: FN/control, **B)** Test group: ITD/siMT1-MMP vs. control group: IDT/control, **C)** Test group: FN/siMT1-MMP vs. control group: ITD/siMT1-MMP, **D)** Test group: FN/control vs. control group: IDT/control.

6.9 Analysis of adhesion structures within 3D fibrillar FN matrices

In order to investigate the hypothesis that cell migration on 3D fibrillar FN matrices is based on an amoeboid migration mode which is associated with weak adhesions, adhesive structures indicated by vinculin straining were monitored in HT1080 cells by fluorescence microscopy. The analysis of 3D adhesions has proven itself to be a challenging procedure which needs further optimization. As depicted in figure 33, the FN matrix is already strongly remodeled resulting in huge FN-free areas where cells can interact with the surface of the culture dish instead of the FN fibers. Accordingly, it is hard to judge which of the observed adhesions are truly cell-matrix adhesions and which are interactions of cells with the underlying culture dish surface. In future work, images should be taken at earlier time points, e. g. 2 h after cell seeding, to ensure a homogenous FN matrix coverage. In addition, the usage of a confocal microscopy combined with z-stack recording should improve the resolution of the images.

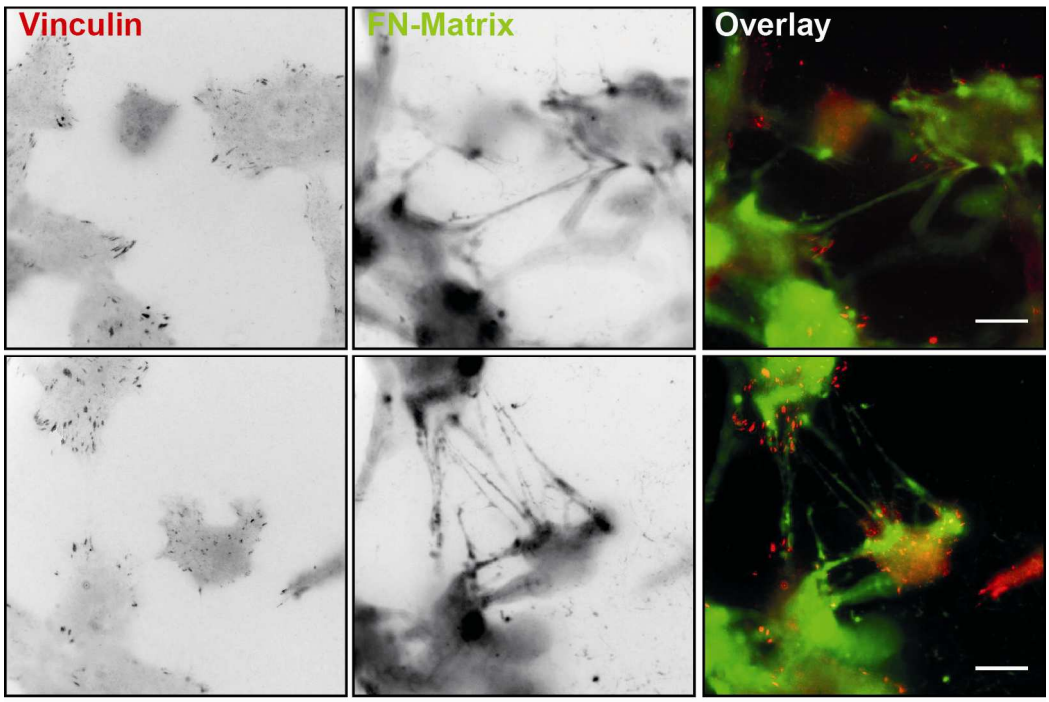

Figure 33: IIF images of FAs in HT1080 cells cultured on FN matrices
Vinculin was stained by IIF to indicate adhesions in HT1080 cell cultured on fibrillar FN matrices. Images were acquired with an inverted fluorescence microscope 6 h after cell seeding. Scale bar, 25 µm.

7. Conclusion and Outlook

In this thesis, the migration behavior of a human fibrosarcoma cell line (HT1080) on 2D FN coatings and 3D fibrillar matrices was investigated by analyzing different parameters such as the ability of cancer cells to rearrange the fibrillar FN network, cell morphology, average velocity and directionality of cell migration. The results of this thesis suggest that the topography of ECM structures is the main regulator of cell migration behavior.

In agreement with this hypothesis, it was demonstrated that HT1080 cells showed great differences in average velocity and directionality of migration depending on the type of FN environment presented (figure 34). The mechanical properties of both FN substrates are transmitted inside the cell via integrins, inducing the appropriate responses. 2D coatings constituted by globular FN show a random distribution and high density of $\alpha_5\beta_1$ integrin ligands. Accordingly, $\alpha_5\beta_1$ integrin binding of HT1080 cells induces flat and round-shaped cell morphology as well as a less directed and slower migration compared to 3D fibrillar FN matrices. In a fibrillar FN environment, HT1080 cells align along FN fibers due to adhesions that are mediated by an RGD-binding integrin other than $\alpha_5\beta_1$ or $\alpha_v\beta_3$. Since RGD sites are distributed in an inherent order (along the FN fibers) HT1080 cells assume elongated shapes, allowing fast and persistent cell movement based on contact guidance.

The observed differences in cell migration are based on distinct molecular mechanisms which are triggered by the biochemical and physical properties of both types of FN environments. On 2D coatings, cancer cell migration is dependent on adhesion, mediated by $\alpha_5\beta_1$ integrins and MT1-MMP activity. It is speculated that MT1-MMP facilitates FA turnover by cleavage of $\alpha_5\beta_1$ integrins, and actin polymerization through activation of cofilin, thus promoting cancer cell migration and persistence. The exact mechanism describing how cofilin is activated by MT1-MMP remains to be elucidated. It is further proposed that the relative slow and random cell movement on FN coatings observed in HT1080 cells is based on the mesenchymal migration mode.

In contrast, the experiments conducted in this thesis demonstrated that cell migration on 3D FN matrices is highly dependent on myosin II contractility, whereas proteolytic activity seems not to be involved. On the contrary, MT1-MMP silencing enhances migration speed in fibrillar FN matrices through reduction of FAK Tyr397 phosphorylation which in turn enhances turnover of adhesions, and through increase in cofilin activity, resulting in increased actin dynamics.

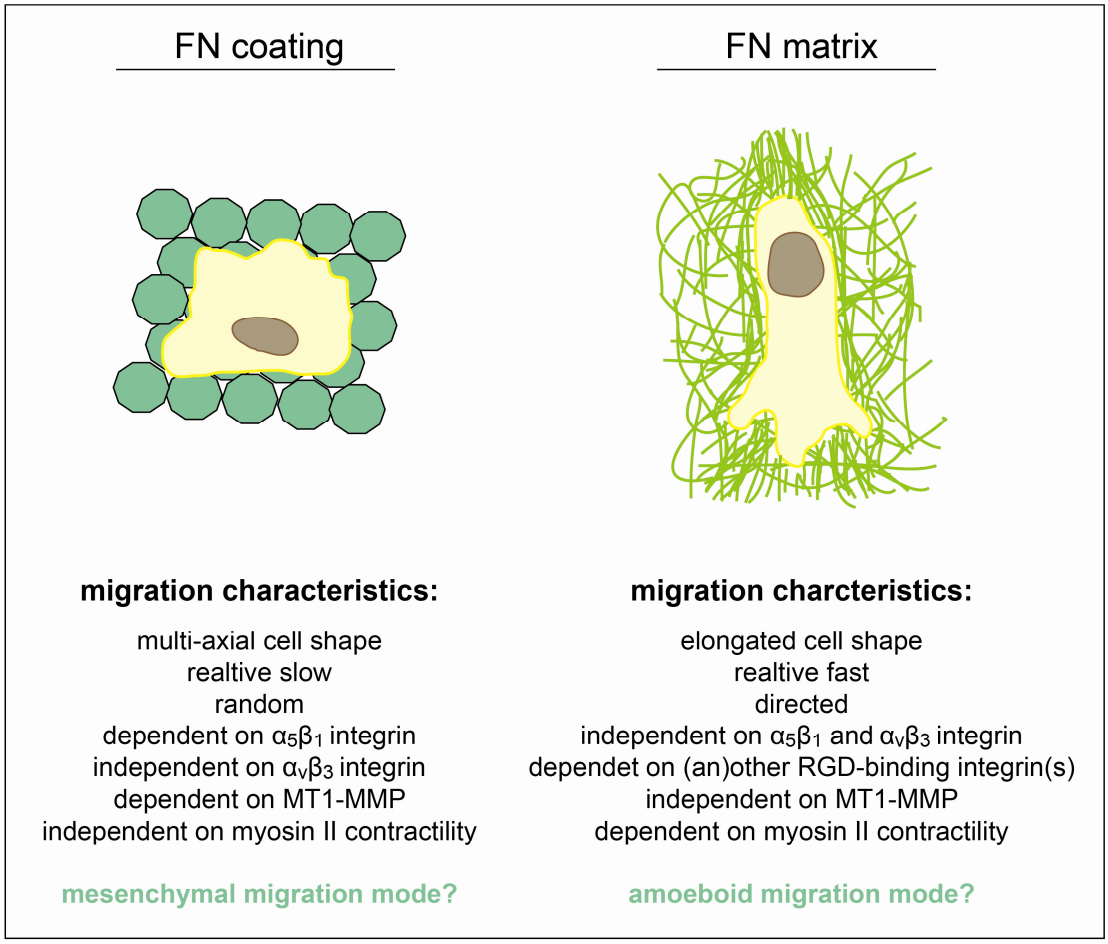

Figure 34: HT1080 cell migration is differentially regulated on FN coatings and on FN matrices
Scheme indicating how cell migration is regulated on FN coating and FN matrices

The exact nature of 3D adhesions and cell-matrix interactions that drive migration within this 3D fibrillar FN environment needs to be determined in future work. So far, it has been observed that cancer cells wrap themselves in FN and have furthermore the ability to rearrange the fibrillar network. The results presented here suggest that general MMP inhibition or MT1-MMP silencing is not involved in FN-matrix interactions. The disintegration of FN matrices seems to be mechanical in nature and might depend on myosin II contractility or cellular interaction with the RGD site in FN. It was further shown that these interactions do not require $\alpha_5\beta_1$ or $\alpha_v\beta_3$ integrins. A promising candidate for mediating cell adhesion to fibrillar FN might be $\alpha_v\beta_1$ integrin [39]. Revealing the nature of the adhesion structure and their dynamics would give further insight whether cell migration on fibrillar matrices is indeed based on the amoeboid mechanisms, as speculated.

To summarize, integrin-mediated adhesions and proteolytic activity are important determinants of cell migration. Interestingly, integrins and MT1-MMP differentially regulate FN-dependent cell migration as a response on structural properties of the extracellular environment. Targeting structural components of the tumor microenvironment should therefore be considered as promising strategy to hinder cancer cell dissemination and metastasis.

8. Appendix:

8.1 List of genes analyzed with the Human Cell Motility RT^2-PCR Array[7]

GeneBank	Description	Gene Name
NM_001102	Actinin, alpha 1	FLJ40884, FLJ54432
NM_001104	Actinin, alpha 3	MGC117002, MGC117005
NM_004924	Actinin, alpha 4	ACTININ-4, DKFZp686K23158, FSGS, FSGS1
NM_005722	ARP2 actin-related protein 2 homolog (yeast)	ARP2
NM_005721	ARP3 actin-related protein 3 homolog (yeast)	ARP3
NM_005163	V-akt murine thymoma viral oncogene homolog 1	AKT, MGC99656, PKB, PKB-ALPHA, PRKBA, RAC, RAC-ALPHA
NM_001663	ADP-ribosylation factor 6	DKFZp564M0264
NM_004309	Rho GDP dissociation inhibitor (GDI) alpha	GDIA1, MGC117248, RHOGDI, RHOGDI-1
NM_003899	Rho guanine nucleotide exchange factor (GEF) 7	BETA-PIX, COOL-1, COOL1, DKFZp686C12170, DKFZp761K1021, KIAA0142, KIAA0412, Nbla10314, P50, P50BP, P85, P85COOL1, P85SPR, PAK3, PIXB
NM_006340	BAI1-associated protein 2	BAP2, FLAF3, IRSP53
NM_014567	Breast cancer anti-estrogen resistance 1	CAS, CAS1, CASS1, CRKAS, FLJ12176, FLJ45059, P130Cas
NM_005186	Calpain 1, (mu/I) large subunit	CANP, CANP1, CANPL1, muCANP, muCL
NM_001748	Calpain 2, (m/II) large subunit	CANP2, CANPL2, CANPml, FLJ39928, mCANP
NM_001753	Caveolin 1, caveolae protein, 22kDa	BSCL3, CGL3, MSTP085, VIP21
NM_001791	Cell division cycle 42 (GTP binding protein, 25kDa)	CDC42Hs, G25K
NM_005507	Cofilin 1 (non-muscle)	CFL
NM_016823	V-crk sarcoma virus CT10 oncogene homolog (avian)	CRKII
NM_000757	Colony stimulating factor 1 (macrophage)	MCSF, MGC31930
NM_005231	Cortactin	EMS1, FLJ34459
NM_005219	Diaphanous homolog 1 (Drosophila)	DFNA1, DIA1, DRF1, FLJ25265, LFHL1, hDIA1
NM_001935	Dipeptidyl-peptidase 4	ADABP, ADCP2, CD26, DPPIV, TP103
NM_001963	Epidermal growth factor	HOMG4, URG
NM_005228	Epidermal growth factor receptor	ERBB, ERBB1, HER1, PIG61, mENA
NM_001008493	Enabled homolog (Drosophila)	ENA, MENA, NDPP1
NM_003379	Ezrin	CVIL, CVL, DKFZp762H157, FLJ26216, MGC1584, VIL2
NM_004460	Fibroblast activation protein, alpha	DKFZp686G13158, DPPIV, FAPA
NM_002006	Fibroblast growth factor 2 (basic)	BFGF, FGFB, HBGF-2
NM_000601	Hepatocyte growth factor (hepapoietin A; scatter factor)	DFNB39, F-TCF, HGFB, HPTA, SF
NM_000618	Insulin-like growth factor 1 (somatomedin C)	IGF-I, IGF1A, IGFI
NM_000875	Insulin-like growth factor 1 receptor	CD221, IGFIR, IGFR, JTK13, MGC142170, MGC142172, MGC18216
NM_004517	Integrin-linked kinase	DKFZp686F1765, ILK-2, P59
NM_000885	Integrin, alpha 4 (antigen CD49D, alpha 4 subunit of VLA-4 receptor)	CD49D, IA4, MGC90518
NM_002211	Integrin, beta 1 (fibronectin receptor, beta polypeptide, antigen CD29 includes MDF2, MSK12)	CD29, FNRB, GPIIA, MDF2, MSK12, VLA-BETA, VLAB
NM_000211	Integrin, beta 2 (complement component 3 receptor 3 and 4 subunit)	CD18, LAD, LCAMB, LFA-1, MAC-1, MF17, MFI7
NM_000212	Integrin, beta 3 (platelet glycoprotein IIIa, antigen CD61)	CD61, GP3A, GPIIIa
NM_002314	LIM domain kinase 1	LIMK, LIMK-1
NM_002745	Mitogen-activated protein kinase 1	ERK, ERK2, ERT1, MAPK2, P42MAPK, PRKM1, PRKM2, p38, p40, p41, p41mapk
NM_000245	Met proto-oncogene (hepatocyte growth factor receptor)	AUTS9, HGFR, RCCP2, c-Met
NM_004995	Matrix metallopeptidase 14 (membrane-inserted)	1, MMP-14, MMP-X1, MT-MMP, MT-MMP 1, MT1-MMP, MT1MMP, MTMMP1
NM_004530	Matrix metallopeptidase 2 (gelatinase A, 72kDa gelatinase, 72kDa type IV collagenase)	CLG4, CLG4A, MMP-II, MONA, TBE-1
NM_004994	Matrix metallopeptidase 9 (gelatinase B, 92kDa gelatinase, 92kDa type IV collagenase)	CLG4B, GELB, MANDP2, MMP-9
NM_002444	Moesin	-
NM_005964	Myosin, heavy chain 10, non-muscle	MGC134913, MGC134914, NMMHCB
NM_002473	Myosin, heavy chain 9, non-muscle	DFNA17, EPSTS, FTNS, MGC104539, MHA, NMHC-II-A,

[7] The table was adapted from http://www.sabiosciences.com/genetable.php?pcatn=PAHS-128Z

		NMMHCA
NM_006097	Myosin, light chain 9, regulatory	LC20, MGC3505, MLC2, MRLC1, MYRL2
NM_053025	Myosin light chain kinase	DKFZp686I10125, FLJ12216, KRP, MLCK, MLCK1, MLCK108, MLCK210, MSTP083, MYLK1, smMLCK
NM_002576	P21 protein (Cdc42/Rac)-activated kinase 1	MGC130000, MGC130001, PAKalpha
NM_005884	P21 protein (Cdc42/Rac)-activated kinase 4	-
NM_005022	Profilin 1	-
NM_006218	Phosphoinositide-3-kinase, catalytic, alpha polypeptide	MGC142161, MGC142163, PI3K, p110-alpha
NM_002659	Plasminogen activator, urokinase receptor	CD87, U-PAR, UPAR, URKR
NM_002660	Phospholipase C, gamma 1	NCKAP3, PLC-II, PLC1, PLC148, PLCgamma1
NM_002662	Phospholipase D1, phosphatidylcholine-specific	-
NM_002737	Protein kinase C, alpha	AAG6, MGC129900, MGC129901, PKC-alpha, PKCA, PRKACA
NM_000314	Phosphatase and tensin homolog	10q23del, BZS, DEC, GLM2, MGC11227, MHAM, MMAC1, PTEN1, TEP1
NM_005607	PTK2 protein tyrosine kinase 2	FADK, FAK, FAK1, FRNK, pp125FAK
NM_004103	PTK2B protein tyrosine kinase 2 beta	CADTK, CAKB, FADK2, FAK2, PKB, PTK, PYK2, RAFTK
NM_002827	Protein tyrosine phosphatase, non-receptor type 1	PTP1B
NM_002859	Paxillin	FLJ16691
NM_006908	Ras-related C3 botulinum toxin substrate 1 (rho family, small GTP binding protein Rac1)	MGC111543, Rac-1, TC-25, p21-Rac1
NM_002872	Ras-related C3 botulinum toxin substrate 2 (rho family, small GTP binding protein Rac2)	EN-7, Gx, HSPC022
NM_002890	RAS p21 protein activator (GTPase activating protein) 1	CM-AVM, CMAVM, DKFZp434N071, GAP, PKWS, RASA, RASGAP, p120GAP, p120RASGAP
NM_002906	Radixin	DFNB24
NM_000539	Rhodopsin	CSNBAD1, MGC138309, MGC138311, OPN2, RP4
NM_001664	Ras homolog gene family, member A	ARH12, ARHA, RHO12, RHOH12
NM_004040	Ras homolog gene family, member B	ARH6, ARHB, MST081, MSTP081, RHOH6
NM_175744	Ras homolog gene family, member C	ARH9, ARHC, H9, MGC1448, MGC61427, RHOH9
NM_005168	Rho family GTPase 3	ARHE, Rho8, RhoE, memB
NM_005406	Rho-associated, coiled-coil containing protein kinase 1	MGC131603, MGC43611, P160ROCK, PRO0435
NM_014631	SH3 and PX domains 2A	FISH, SH3MD1, TSK5
NM_005417	V-src sarcoma (Schmidt-Ruppin A-2) viral oncogene homolog (avian)	ASV, SRC1, c-SRC, p60-Src
NM_003150	Signal transducer and activator of transcription 3 (acute-phase response factor)	APRF, FLJ20882, HIES, MGC16063
NM_003174	Supervillin	DKFZp686A17191
NM_000660	Transforming growth factor, beta 1	CED, DPD1, LAP, TGFB, TGFbeta
NM_003255	TIMP metallopeptidase inhibitor 2	CSC-21K
NM_006289	Talin 1	ILWEQ, KIAA1027, TLN
NM_003370	Vasodilator-stimulated phosphoprotein	-
NM_003373	Vinculin	CMD1W, CMH15, MVCL
NM_003376	Vascular endothelial growth factor A	MGC70609, MVCD1, VEGF, VPF
NM_003380	Vimentin	FLJ36605
NM_003931	WAS protein family, member 1	FLJ31482, KIAA0269, SCAR1, WAVE, WAVE1
NM_006990	WAS protein family, member 2	SCAR2, WAVE2, dJ393P12.2
NM_003941	Wiskott-Aldrich syndrome-like	DKFZp779G0847, MGC48327, N-WASP, NWASP
NM_003387	WAS/WASL interacting protein family, member 1	MGC111041, PRPL-2, WASPIP, WIP
NM_001101	Actin, beta	PS1TP5BP1
NM_004048	Beta-2-microglobulin	-
NM_002046	Glyceraldehyde-3-phosphate dehydrogenase	G3PD, GAPD, MGC88685
NM_000194	Hypoxanthine phosphoribosyltransferase 1	HGPRT, HPRT
NM_001002	Ribosomal protein, large, P0	L10E, LP0, MGC111226, MGC88175, P0, PRLP0, RPP0

8.2 List of abbreviations

2D	two-dimensional
3D	three-dimensional
ANOVA	one way analysis of variance
Arg	arginine
Asp	aspartic acid
CAF	cancer-associated fibroblast
cDNA	copyDNA
D	aspartic acid
DEPC	diethylpyrocarbonate
DIC	differential interference contrast
DMEM	Dulbecco´s Modified Eagle´s Medium
DNA	desoxyribonucleic acid
DPBS	Dulbecco´s phosphate buffered saline
E	glutamate
ECM	extracellular matrix
EDTA	ethylenediaminetetraacetic acid
ER	endoplasmatic reticulum
ERK2	extracellular-signal-regulated kinase-2
EtOH	ethanol
FA	focal adhesion
FACS	fluorescence activated cell sorting
FAK	focal adhesion kinase
FBS	fetal bovine serum
FN	fibronectin
G	glycine
GAG	glycosaminoglycan
gDNA	genomic desoxyribonucleic acid
GPI	glycosylophosphatidylinositol
Gly	glycine
IIF	indirect immunofluorescence
ITD	ibiTreat dishes
MAPK	mitogen-activated protein kinase
min	minute
MMP	matrix metalloproteinase
MT1-MMP	membrane-type 1 matrix metalloproteinase
NCS	newborn calf serum
ON	over night
PCR	polymerase chain reaction
PFA	paraformaldehyde
PVDF	polyvenylidene fluoride
R	arginine
RNA	ribonucleic acid
RNAi	RNA interference
RPMI	Roswell Park Memorial Institute (name of cell culture medium)
RT	room temperature
RT^2-PCR	realtime PCR

SDS-PAGE	sodium dodecylsulfate polyacrylamide gel electrophoresis
SEM	standard error of the mean
Ser	serine
siRNA	small interfering ribonucleid acid
TAE	Tris-acetate-EDTA
TIMP	tissue inhibitor of matrix metalloproteinases
Tyr	tyrosine
VASP	vasodilator-stimulated phosphoprotein
VTN	vitronectin
YPet	yellow fluorescent protein optimized for FRET

9. Bibliography:

1. Jemal, A., et al., *Cancer statistics, 2008.* CA Cancer J Clin, 2008. **58**(2): p. 71-96.
2. Niederlaender, *Causes of death.* 2006.
3. Kamb, A., *What's wrong with our cancer models?* Nat Rev Drug Discov, 2005. **4**(2): p. 161-5.
4. Ferlay, J., et al., *Estimates of the cancer incidence and mortality in Europe in 2006.* Ann Oncol, 2007. **18**(3): p. 581-92.
5. Kola, I. and J. Landis, *Can the pharmaceutical industry reduce attrition rates?* Nat Rev Drug Discov, 2004. **3**(8): p. 711-5.
6. Kamb, A., S. Wee, and C. Lengauer, *Why is cancer drug discovery so difficult?* Nat Rev Drug Discov, 2007. **6**(2): p. 115-20.
7. Hanahan, D. and R.A. Weinberg, *The hallmarks of cancer.* Cell, 2000. **100**(1): p. 57-70.
8. Sporn, M.B., *The war on cancer.* Lancet, 1996. **347**(9012): p. 1377-81.
9. Hanahan, D. and R.A. Weinberg, *Hallmarks of cancer: the next generation.* Cell, 2011. **144**(5): p. 646-74.
10. Grivennikov, S.I., F.R. Greten, and M. Karin, *Immunity, inflammation, and cancer.* Cell, 2010. **140**(6): p. 883-99.
11. Chambers, A.F., A.C. Groom, and I.C. MacDonald, *Dissemination and growth of cancer cells in metastatic sites.* Nat Rev Cancer, 2002. **2**(8): p. 563-72.
12. Bacac, M. and I. Stamenkovic, *Metastatic cancer cell.* Annu Rev Pathol, 2008. **3**: p. 221-47.
13. Cox, T.R. and J.T. Erler, *Remodeling and homeostasis of the extracellular matrix: implications for fibrotic diseases and cancer.* Dis Model Mech, 2011. **4**(2): p. 165-78.
14. Weiss, L., *Cancer cell traffic from the lungs to the liver: an example of metastatic inefficiency.* Int J Cancer, 1980. **25**(3): p. 385-92.
15. Weiss, L., *Metastatic inefficiency.* Adv Cancer Res, 1990. **54**: p. 159-211.
16. Psaila, B. and D. Lyden, *The metastatic niche: adapting the foreign soil.* Nat Rev Cancer, 2009. **9**(4): p. 285-93.
17. Cretu, A. and P.C. Brooks, *Impact of the non-cellular tumor microenvironment on metastasis: potential therapeutic and imaging opportunities.* J Cell Physiol, 2007. **213**(2): p. 391-402.
18. Lu, P., V.M. Weaver, and Z. Werb, *The extracellular matrix: a dynamic niche in cancer progression.* J Cell Biol, 2012. **196**(4): p. 395-406.
19. Hashizume, H., et al., *Openings between defective endothelial cells explain tumor vessel leakiness.* Am J Pathol, 2000. **156**(4): p. 1363-80.
20. Hynes, R.O., *The extracellular matrix: not just pretty fibrils.* Science, 2009. **326**(5957): p. 1216-9.
21. Page-McCaw, A., A.J. Ewald, and Z. Werb, *Matrix metalloproteinases and the regulation of tissue remodelling.* Nat Rev Mol Cell Biol, 2007. **8**(3): p. 221-33.
22. Egeblad, M. and Z. Werb, *New functions for the matrix metalloproteinases in cancer progression.* Nat Rev Cancer, 2002. **2**(3): p. 161-74.
23. Kessenbrock, K., V. Plaks, and Z. Werb, *Matrix metalloproteinases: regulators of the tumor microenvironment.* Cell, 2010. **141**(1): p. 52-67.
24. Kalluri, R. and M. Zeisberg, *Fibroblasts in cancer.* Nat Rev Cancer, 2006. **6**(5): p. 392-401.

25. Kass, L., et al., *Mammary epithelial cell: influence of extracellular matrix composition and organization during development and tumorigenesis.* Int J Biochem Cell Biol, 2007. **39**(11): p. 1987-94.
26. Butcher, D.T., T. Alliston, and V.M. Weaver, *A tense situation: forcing tumour progression.* Nat Rev Cancer, 2009. **9**(2): p. 108-22.
27. Levental, K.R., et al., *Matrix crosslinking forces tumor progression by enhancing integrin signaling.* Cell, 2009. **139**(5): p. 891-906.
28. Paszek, M.J., et al., *Tensional homeostasis and the malignant phenotype.* Cancer Cell, 2005. **8**(3): p. 241-54.
29. Hewitt, R.E., et al., *Laminin and collagen IV subunit distribution in normal and neoplastic tissues of colorectum and breast.* Br J Cancer, 1997. **75**(2): p. 221-9.
30. Kaplan, R.N., et al., *VEGFR1-positive haematopoietic bone marrow progenitors initiate the pre-metastatic niche.* Nature, 2005. **438**(7069): p. 820-7.
31. Erler, J.T., et al., *Hypoxia-induced lysyl oxidase is a critical mediator of bone marrow cell recruitment to form the premetastatic niche.* Cancer Cell, 2009. **15**(1): p. 35-44.
32. Bissell, M.J. and D. Radisky, *Putting tumours in context.* Nat Rev Cancer, 2001. **1**(1): p. 46-54.
33. Lodish, H.F., *Molecular cell biology*. 7th ed. 2013, New York: W.H. Freeman and Co. xxxiii, 1154, 58 p.
34. Alberts, B., *Molecular biology of the cell*. 5th ed. 2008, New York: Garland Science. 1 v. (various pagings).
35. Lu, P., et al., *Extracellular matrix degradation and remodeling in development and disease.* Cold Spring Harb Perspect Biol, 2011. **3**(12).
36. Singh, P., C. Carraher, and J.E. Schwarzbauer, *Assembly of fibronectin extracellular matrix.* Annu Rev Cell Dev Biol, 2010. **26**: p. 397-419.
37. To, W.S. and K.S. Midwood, *Plasma and cellular fibronectin: distinct and independent functions during tissue repair.* Fibrogenesis Tissue Repair, 2011. **4**: p. 21.
38. Johnson, K.J., et al., *The compact conformation of fibronectin is determined by intramolecular ionic interactions.* J Biol Chem, 1999. **274**(22): p. 15473-9.
39. Yang, J.T. and R.O. Hynes, *Fibronectin receptor functions in embryonic cells deficient in alpha 5 beta 1 integrin can be replaced by alpha V integrins.* Mol Biol Cell, 1996. **7**(11): p. 1737-48.
40. Liao, Y.F., et al., *The EIIIA segment of fibronectin is a ligand for integrins alpha 9beta 1 and alpha 4beta 1 providing a novel mechanism for regulating cell adhesion by alternative splicing.* J Biol Chem, 2002. **277**(17): p. 14467-74.
41. Hynes, R.O., *Integrins: bidirectional, allosteric signaling machines.* Cell, 2002. **110**(6): p. 673-87.
42. Leong, J.M., et al., *An aspartate residue of the Yersinia pseudotuberculosis invasin protein that is critical for integrin binding.* EMBO J, 1995. **14**(3): p. 422-31.
43. Takahashi, S., et al., *The RGD motif in fibronectin is essential for development but dispensable for fibril assembly.* J Cell Biol, 2007. **178**(1): p. 167-78.
44. Geiger, B., et al., *Transmembrane crosstalk between the extracellular matrix--cytoskeleton crosstalk.* Nat Rev Mol Cell Biol, 2001. **2**(11): p. 793-805.
45. Berrier, A.L. and K.M. Yamada, *Cell-matrix adhesion.* J Cell Physiol, 2007. **213**(3): p. 565-73.
46. Choi, C.K., et al., *Actin and alpha-actinin orchestrate the assembly and maturation of nascent adhesions in a myosin II motor-independent manner.* Nat Cell Biol, 2008. **10**(9): p. 1039-50.

47. Zaidel-Bar, R., et al., *Early molecular events in the assembly of matrix adhesions at the leading edge of migrating cells.* J Cell Sci, 2003. **116**(Pt 22): p. 4605-13.
48. Hotulainen, P. and P. Lappalainen, *Stress fibers are generated by two distinct actin assembly mechanisms in motile cells.* J Cell Biol, 2006. **173**(3): p. 383-94.
49. Zaidel-Bar, R., et al., *Functional atlas of the integrin adhesome.* Nat Cell Biol, 2007. **9**(8): p. 858-67.
50. Kanchanawong, P., et al., *Nanoscale architecture of integrin-based cell adhesions.* Nature, 2010. **468**(7323): p. 580-4.
51. Lawson, C., et al., *FAK promotes recruitment of talin to nascent adhesions to control cell motility.* J Cell Biol, 2012. **196**(2): p. 223-32.
52. Schlaepfer, D.D. and S.K. Mitra, *Multiple connections link FAK to cell motility and invasion.* Curr Opin Genet Dev, 2004. **14**(1): p. 92-101.
53. Gimona, M., *The microfilament system in the formation of invasive adhesions.* Semin Cancer Biol, 2008. **18**(1): p. 23-34.
54. Gimona, M., et al., *Assembly and biological role of podosomes and invadopodia.* Curr Opin Cell Biol, 2008. **20**(2): p. 235-41.
55. Deryugina, E.I., et al., *MT1-MMP initiates activation of pro-MMP-2 and integrin alphavbeta3 promotes maturation of MMP-2 in breast carcinoma cells.* Exp Cell Res, 2001. **263**(2): p. 209-23.
56. Mueller, S.C., et al., *A novel protease-docking function of integrin at invadopodia.* J Biol Chem, 1999. **274**(35): p. 24947-52.
57. Desgrosellier, J.S. and D.A. Cheresh, *Integrins in cancer: biological implications and therapeutic opportunities.* Nat Rev Cancer, 2010. **10**(1): p. 9-22.
58. Guo, W. and F.G. Giancotti, *Integrin signalling during tumour progression.* Nat Rev Mol Cell Biol, 2004. **5**(10): p. 816-26.
59. Mitra, S.K. and D.D. Schlaepfer, *Integrin-regulated FAK-Src signaling in normal and cancer cells.* Curr Opin Cell Biol, 2006. **18**(5): p. 516-23.
60. Ilic, D., et al., *Reduced cell motility and enhanced focal adhesion contact formation in cells from FAK-deficient mice.* Nature, 1995. **377**(6549): p. 539-44.
61. Sternlicht, M.D. and Z. Werb, *How matrix metalloproteinases regulate cell behavior.* Annu Rev Cell Dev Biol, 2001. **17**: p. 463-516.
62. Brooks, P.C., et al., *Localization of matrix metalloproteinase MMP-2 to the surface of invasive cells by interaction with integrin alpha v beta 3.* Cell, 1996. **85**(5): p. 683-93.
63. Ludwig, T., *Local proteolytic activity in tumor cell invasion and metastasis.* Bioessays, 2005. **27**(11): p. 1181-91.
64. Gross, J. and C.M. Lapiere, *Collagenolytic activity in amphibian tissues: a tissue culture assay.* Proc Natl Acad Sci U S A, 1962. **48**: p. 1014-22.
65. Verma, R.P. and C. Hansch, *Matrix metalloproteinases (MMPs): chemical-biological functions and (Q)SARs.* Bioorg Med Chem, 2007. **15**(6): p. 2223-68.
66. Lehti, K., et al., *Proteolytic processing of membrane-type-1 matrix metalloproteinase is associated with gelatinase A activation at the cell surface.* Biochem J, 1998. **334 (Pt 2)**: p. 345-53.
67. Stanton, H., et al., *The activation of ProMMP-2 (gelatinase A) by HT1080 fibrosarcoma cells is promoted by culture on a fibronectin substrate and is concomitant with an increase in processing of MT1-MMP (MMP-14) to a 45 kDa form.* J Cell Sci, 1998. **111 (Pt 18)**: p. 2789-98.
68. Holmbeck, K., et al., *MT1-MMP-deficient mice develop dwarfism, osteopenia, arthritis, and connective tissue disease due to inadequate collagen turnover.* Cell, 1999. **99**(1): p. 81-92.

69. Zhou, Z., et al., *Impaired endochondral ossification and angiogenesis in mice deficient in membrane-type matrix metalloproteinase I.* Proc Natl Acad Sci U S A, 2000. **97**(8): p. 4052-7.
70. Holmbeck, K., et al., *MT1-MMP: a tethered collagenase.* J Cell Physiol, 2004. **200**(1): p. 11-9.
71. Sato, H., et al., *A matrix metalloproteinase expressed on the surface of invasive tumour cells.* Nature, 1994. **370**(6484): p. 61-5.
72. Seiki, M., *Membrane-type 1 matrix metalloproteinase: a key enzyme for tumor invasion.* Cancer Lett, 2003. **194**(1): p. 1-11.
73. Hotary, K.B., et al., *Membrane type I matrix metalloproteinase usurps tumor growth control imposed by the three-dimensional extracellular matrix.* Cell, 2003. **114**(1): p. 33-45.
74. Bergers, G., et al., *Effects of angiogenesis inhibitors on multistage carcinogenesis in mice.* Science, 1999. **284**(5415): p. 808-12.
75. Coussens, L.M., B. Fingleton, and L.M. Matrisian, *Matrix metalloproteinase inhibitors and cancer: trials and tribulations.* Science, 2002. **295**(5564): p. 2387-92.
76. Knauper, V., et al., *Cellular mechanisms for human procollagenase-3 (MMP-13) activation. Evidence that MT1-MMP (MMP-14) and gelatinase a (MMP-2) are able to generate active enzyme.* J Biol Chem, 1996. **271**(29): p. 17124-31.
77. Ohuchi, E., et al., *Membrane type 1 matrix metalloproteinase digests interstitial collagens and other extracellular matrix macromolecules.* J Biol Chem, 1997. **272**(4): p. 2446-51.
78. Itoh, Y. and M. Seiki, *MT1-MMP: an enzyme with multidimensional regulation.* Trends Biochem Sci, 2004. **29**(6): p. 285-9.
79. Poincloux, R., F. Lizarraga, and P. Chavrier, *Matrix invasion by tumour cells: a focus on MT1-MMP trafficking to invadopodia.* J Cell Sci, 2009. **122**(Pt 17): p. 3015-24.
80. Wang, Y. and M.A. McNiven, *Invasive matrix degradation at focal adhesions occurs via protease recruitment by a FAK-p130Cas complex.* J Cell Biol, 2012. **196**(3): p. 375-85.
81. Genis, L., et al., *Functional interplay between endothelial nitric oxide synthase and membrane type 1 matrix metalloproteinase in migrating endothelial cells.* Blood, 2007. **110**(8): p. 2916-23.
82. van Hinsbergh, V.W. and P. Koolwijk, *Endothelial sprouting and angiogenesis: matrix metalloproteinases in the lead.* Cardiovasc Res, 2008. **78**(2): p. 203-12.
83. Ratnikov, B.I., et al., *An alternative processing of integrin alpha(v) subunit in tumor cells by membrane type-1 matrix metalloproteinase.* J Biol Chem, 2002. **277**(9): p. 7377-85.
84. Deryugina, E.I., et al., *Processing of integrin alpha(v) subunit by membrane type 1 matrix metalloproteinase stimulates migration of breast carcinoma cells on vitronectin and enhances tyrosine phosphorylation of focal adhesion kinase.* J Biol Chem, 2002. **277**(12): p. 9749-56.
85. Galvez, B.G., et al., *ECM regulates MT1-MMP localization with beta1 or alphavbeta3 integrins at distinct cell compartments modulating its internalization and activity on human endothelial cells.* J Cell Biol, 2002. **159**(3): p. 509-21.
86. Wolf, K., et al., *Multi-step pericellular proteolysis controls the transition from individual to collective cancer cell invasion.* Nat Cell Biol, 2007. **9**(8): p. 893-904.
87. Gonzalo, P., et al., *MT1-MMP and integrins: Hand-to-hand in cell communication.* Biofactors, 2010. **36**(4): p. 248-54.

88. Takino, T., et al., *Membrane-type 1 matrix metalloproteinase modulates focal adhesion stability and cell migration.* Exp Cell Res, 2006. **312**(8): p. 1381-9.
89. Friedl, P. and K. Wolf, *Plasticity of cell migration: a multiscale tuning model.* J Cell Biol, 2010. **188**(1): p. 11-9.
90. Friedl, P. and K. Wolf, *Tumour-cell invasion and migration: diversity and escape mechanisms.* Nat Rev Cancer, 2003. **3**(5): p. 362-74.
91. Katoh, K., et al., *Rho-kinase--mediated contraction of isolated stress fibers.* J Cell Biol, 2001. **153**(3): p. 569-84.
92. Chew, T.L., et al., *A fluorescent resonant energy transfer-based biosensor reveals transient and regional myosin light chain kinase activation in lamella and cleavage furrows.* J Cell Biol, 2002. **156**(3): p. 543-53.
93. Lauffenburger, D.A. and A.F. Horwitz, *Cell migration: a physically integrated molecular process.* Cell, 1996. **84**(3): p. 359-69.
94. Palecek, S.P., et al., *Integrin-ligand binding properties govern cell migration speed through cell-substratum adhesiveness.* Nature, 1997. **385**(6616): p. 537-40.
95. Nagata-Ohashi, K., et al., *A pathway of neuregulin-induced activation of cofilin-phosphatase Slingshot and cofilin in lamellipodia.* J Cell Biol, 2004. **165**(4): p. 465-71.
96. Sidani, M., et al., *Cofilin determines the migration behavior and turning frequency of metastatic cancer cells.* J Cell Biol, 2007. **179**(4): p. 777-91.
97. Sun, C.X., M.A. Magalhaes, and M. Glogauer, *Rac1 and Rac2 differentially regulate actin free barbed end formation downstream of the fMLP receptor.* J Cell Biol, 2007. **179**(2): p. 239-45.
98. Oser, M. and J. Condeelis, *The cofilin activity cycle in lamellipodia and invadopodia.* J Cell Biochem, 2009. **108**(6): p. 1252-62.
99. Wang, W., R. Eddy, and J. Condeelis, *The cofilin pathway in breast cancer invasion and metastasis.* Nat Rev Cancer, 2007. **7**(6): p. 429-40.
100. Carlier, M.F., et al., *Actin depolymerizing factor (ADF/cofilin) enhances the rate of filament turnover: implication in actin-based motility.* J Cell Biol, 1997. **136**(6): p. 1307-22.
101. Ichetovkin, I., W. Grant, and J. Condeelis, *Cofilin produces newly polymerized actin filaments that are preferred for dendritic nucleation by the Arp2/3 complex.* Curr Biol, 2002. **12**(1): p. 79-84.
102. Arber, S., et al., *Regulation of actin dynamics through phosphorylation of cofilin by LIM-kinase.* Nature, 1998. **393**(6687): p. 805-9.
103. Wolf, K., et al., *Compensation mechanism in tumor cell migration: mesenchymal-amoeboid transition after blocking of pericellular proteolysis.* J Cell Biol, 2003. **160**(2): p. 267-77.
104. Friedl, P., K.S. Zanker, and E.B. Brocker, *Cell migration strategies in 3-D extracellular matrix: differences in morphology, cell matrix interactions, and integrin function.* Microsc Res Tech, 1998. **43**(5): p. 369-78.
105. Green, J.A. and K.M. Yamada, *Three-dimensional microenvironments modulate fibroblast signaling responses.* Adv Drug Deliv Rev, 2007. **59**(13): p. 1293-8.
106. Rasheed, S., et al., *Characterization of a newly derived human sarcoma cell line (HT-1080).* Cancer, 1974. **33**(4): p. 1027-33.
107. Soule, H.D., et al., *A human cell line from a pleural effusion derived from a breast carcinoma.* J Natl Cancer Inst, 1973. **51**(5): p. 1409-16.

108. van Muijen, G.N., et al., *Establishment and characterization of a human melanoma cell line (MV3) which is highly metastatic in nude mice.* Int J Cancer, 1991. **48**(1): p. 85-91.
109. Jensen, F.C., et al., *Infection of Human and Simian Tissue Cultures with Rous Sarcoma Virus.* Proc Natl Acad Sci U S A, 1964. **52**: p. 53-9.
110. Gluzman, Y., *SV40-transformed simian cells support the replication of early SV40 mutants.* Cell, 1981. **23**(1): p. 175-82.
111. Ohashi, T. and H.P. Erickson, *Revisiting the mystery of fibronectin multimers: the fibronectin matrix is composed of fibronectin dimers cross-linked by non-covalent bonds.* Matrix Biol, 2009. **28**(3): p. 170-5.
112. Mao, Y. and J.E. Schwarzbauer, *Stimulatory effects of a three-dimensional microenvironment on cell-mediated fibronectin fibrillogenesis.* J Cell Sci, 2005. **118**(Pt 19): p. 4427-36.
113. Schneider, C.A., W.S. Rasband, and K.W. Eliceiri, *NIH Image to ImageJ: 25 years of image analysis.* Nature Methods | Historical Commentary, 2012. **9**(7): p. 671-675.
114. Haraguchi, M., et al., *Snail regulates cell-matrix adhesion by regulation of the expression of integrins and basement membrane proteins.* J Biol Chem, 2008. **283**(35): p. 23514-23.
115. Lambrechts, A. and C. Ampe, eds. *The Motile Actin System in Health and Disease*. 2008, Transworld Reseacrh Network. 123-156.
116. Simon, K.O., et al., *The alphavbeta3 integrin regulates alpha5beta1-mediated cell migration toward fibronectin.* J Biol Chem, 1997. **272**(46): p. 29380-9.
117. Hotary, K., et al., *A cancer cell metalloprotease triad regulates the basement membrane transmigration program.* Genes Dev, 2006. **20**(19): p. 2673-86.
118. Xue, W., et al., *Urokinase-type plasminogen activator receptors associate with beta1 and beta3 integrins of fibrosarcoma cells: dependence on extracellular matrix components.* Cancer Res, 1997. **57**(9): p. 1682-9.
119. Birkenmeier, T.M., et al., *The alpha 5 beta 1 fibronectin receptor. Characterization of the alpha 5 gene promoter*. J Biol Chem, 1991. **266**(30): p. 20544-9.
120. Lohi, J., et al., *Regulation of membrane-type matrix metalloproteinase-1 expression by growth factors and phorbol 12-myristate 13-acetate.* Eur J Biochem, 1996. **239**(2): p. 239-47.
121. Sato, T., et al., *Identification of the membrane-type matrix metalloproteinase MT1-MMP in osteoclasts.* J Cell Sci, 1997. **110 (Pt 5)**: p. 589-96.
122. Galvez, B.G., et al., *Membrane type 1-matrix metalloproteinase is activated during migration of human endothelial cells and modulates endothelial motility and matrix remodeling.* J Biol Chem, 2001. **276**(40): p. 37491-500.
123. Itoh, Y. and M. Seiki, *MT1-MMP: a potent modifier of pericellular microenvironment.* J Cell Physiol, 2006. **206**(1): p. 1-8.
124. Remacle, A., G. Murphy, and C. Roghi, *Membrane type I-matrix metalloproteinase (MT1-MMP) is internalised by two different pathways and is recycled to the cell surface.* J Cell Sci, 2003. **116**(Pt 19): p. 3905-16.
125. Zucker, S., et al., *Rapid trafficking of membrane type 1-matrix metalloproteinase to the cell surface regulates progelatinase a activation.* Lab Invest, 2002. **82**(12): p. 1673-84.
126. Clark, E.S. and A.M. Weaver, *A new role for cortactin in invadopodia: regulation of protease secretion.* Eur J Cell Biol, 2008. **87**(8-9): p. 581-90.
127. Hynes, R.O., *Integrins: versatility, modulation, and signaling in cell adhesion.* Cell, 1992. **69**(1): p. 11-25.

128. Engler, A.J., et al., *A novel mode of cell detachment from fibrillar fibronectin matrix under shear.* J Cell Sci, 2009. **122**(Pt 10): p. 1647-53.
129. Doyle, A.D., et al., *One-dimensional topography underlies three-dimensional fibrillar cell migration.* J Cell Biol, 2009. **184**(4): p. 481-90.
130. Zaman, M.H., et al., *Migration of tumor cells in 3D matrices is governed by matrix stiffness along with cell-matrix adhesion and proteolysis.* Proc Natl Acad Sci U S A, 2006. **103**(29): p. 10889-94.
131. Baker, E.L., R.T. Bonnecaze, and M.H. Zaman, *Extracellular matrix stiffness and architecture govern intracellular rheology in cancer.* Biophys J, 2009. **97**(4): p. 1013-21.
132. Shi, Q. and D. Boettiger, *A novel mode for integrin-mediated signaling: tethering is required for phosphorylation of FAK Y397.* Mol Biol Cell, 2003. **14**(10): p. 4306-15.
133. Mao, Y. and J.E. Schwarzbauer, *Accessibility to the fibronectin synergy site in a 3D matrix regulates engagement of alpha5beta1 versus alphavbeta3 integrin receptors.* Cell Commun Adhes, 2006. **13**(5-6): p. 267-77.
134. Cheresh, D.A. and R.C. Spiro, *Biosynthetic and functional properties of an Arg-Gly-Asp-directed receptor involved in human melanoma cell attachment to vitronectin, fibrinogen, and von Willebrand factor.* J Biol Chem, 1987. **262**(36): p. 17703-11.
135. Charo, I.F., et al., *The vitronectin receptor alpha v beta 3 binds fibronectin and acts in concert with alpha 5 beta 1 in promoting cellular attachment and spreading on fibronectin.* J Cell Biol, 1990. **111**(6 Pt 1): p. 2795-800.
136. Wolf, K. and P. Friedl, *Extracellular matrix determinants of proteolytic and non-proteolytic cell migration.* Trends Cell Biol, 2011. **21**(12): p. 736-44.
137. Huveneers, S., et al., *Binding of soluble fibronectin to integrin alpha5 beta1 - link to focal adhesion redistribution and contractile shape.* J Cell Sci, 2008. **121**(Pt 15): p. 2452-62.
138. Zhong, C., et al., *Rho-mediated contractility exposes a cryptic site in fibronectin and induces fibronectin matrix assembly.* J Cell Biol, 1998. **141**(2): p. 539-51.
139. Schiller, H.B., et al., *beta1- and alphav-class integrins cooperate to regulate myosin II during rigidity sensing of fibronectin-based microenvironments.* Nat Cell Biol, 2013. **15**(6): p. 625-36.
140. Kirmse, R., H. Otto, and T. Ludwig, *Interdependency of cell adhesion, force generation and extracellular proteolysis in matrix remodeling.* J Cell Sci, 2011. **124**(Pt 11): p. 1857-66.
141. Kirmse, R., H. Otto, and T. Ludwig, *The extracellular matrix remodeled: Interdependency of matrix proteolysis, cell adhesion, and force sensing.* Commun Integr Biol, 2012. **5**(1): p. 71-3.
142. Grobelny, D., L. Poncz, and R.E. Galardy, *Inhibition of human skin fibroblast collagenase, thermolysin, and Pseudomonas aeruginosa elastase by peptide hydroxamic acids.* Biochemistry, 1992. **31**(31): p. 7152-4.
143. Nishino, N. and J.C. Powers, *Peptide hydroxamic acids as inhibitors of thermolysin.* Biochemistry, 1978. **17**(14): p. 2846-50.
144. Galardy, R.E., et al., *Inhibition of human skin fibroblast collagenase by phosphorus-containing peptides.* Matrix Suppl, 1992. **1**: p. 259-62.
145. Friedl, P., *Prespecification and plasticity: shifting mechanisms of cell migration.* Curr Opin Cell Biol, 2004. **16**(1): p. 14-23.
146. Raviraj, V., et al., *Regulation of ROCK1 via Notch1 during breast cancer cell migration into dense matrices.* BMC Cell Biol, 2012. **13**: p. 12.

147. Sahai, E. and C.J. Marshall, *Differing modes of tumour cell invasion have distinct requirements for Rho/ROCK signalling and extracellular proteolysis.* Nat Cell Biol, 2003. **5**(8): p. 711-9.
148. Friedl, P. and K. Wolf, *Proteolytic and non-proteolytic migration of tumour cells and leucocytes.* Biochem Soc Symp, 2003(70): p. 277-85.
149. Doyle, A.D., et al., *Micro-environmental control of cell migration--myosin IIA is required for efficient migration in fibrillar environments through control of cell adhesion dynamics.* J Cell Sci, 2012. **125**(Pt 9): p. 2244-56.
150. Townley, W.A., et al., *Matrix metalloproteinase inhibition reduces contraction by dupuytren fibroblasts.* J Hand Surg Am, 2008. **33**(9): p. 1608-16.
151. Martin-Martin, B., et al., *The effect of MMP inhibitor GM6001 on early fibroblast-mediated collagen matrix contraction is correlated to a decrease in cell protrusive activity.* Eur J Cell Biol, 2011. **90**(1): p. 26-36.
152. Takino, T., et al., *Inhibition of membrane-type 1 matrix metalloproteinase at cell-matrix adhesions.* Cancer Res, 2007. **67**(24): p. 11621-9.
153. Sieg, D.J., C.R. Hauck, and D.D. Schlaepfer, *Required role of focal adhesion kinase (FAK) for integrin-stimulated cell migration.* J Cell Sci, 1999. **112 (Pt 16)**: p. 2677-91.
154. Danen, E.H., et al., *Integrins control motile strategy through a Rho-cofilin pathway.* J Cell Biol, 2005. **169**(3): p. 515-26.

10. Acknowledgement:

This work would not have been possible without the support of many wonderful people. First, I want to thank my former supervisor Thomas Ludwig, who introduced me to the exciting world of the tumor microenvironment and matrix metalloproteinases. Throughout my thesis, I could rely on his advice. I am also very thankful to Joachim Spatz for the opportunity to finish my thesis in his group, for granting me the freedom to work independently and his absolute support. In addition. I want to thank my examining committee: Joachim Spatz, Peter Angel, for being my first supervisor, Suat Özbeck who kindly agreed on being the chair person during my oral examination and Jan Lohmann for accepting my invitation. I further want to thank my advisory committee Peter Angel, Thomas Korff and Ada Cavalcanti-Adam, who guided me throughout my entire thesis, for their advice and helpful comments on my work. Essential for finishing this thesis and submitting my publication was Ada. I learned so much from you during these last years, words cannot express my gratitude!

I am very glad that I had the opportunity to participate in different courses and seminars organized by the DKFZ International graduate school and HBIGS. Thereby a special thanks to Rolf Lutz, Sandra Martini, Lindsay Murrels and all other members of the graduate schools who supported me during the last years. In this context, I also want to thank Michael Boutros who made it possible for me to finish the DKFZ graduate program, albeit I had left the DKFZ.

I had a wonderful time in the Spatz group and want to thank all of you for creating a supportive and motivating working atmosphere. A special thanks to Dimitris, Ada, Rebecca, Thomas, Katharina, Theresa und Elli who took the time to read my thesis and gave me great feedback and further input. For fruitful discussions on statistical problems, I want to thank Annette Kopp-Schneider, Günther Sawitzki and in particular Tamás Haraszti, who did the statistical analysis of the migration experiments and generated those lovely plots. Thank you also to Katharina Wolf and Hannes Schröder for their helpful comments and suggestions on my experimental work. A special thanks to Matthias Schick from the Genomics and Proteomics core Facility of the DKFZ, for giving me the opportunity to use their RT-PCR light cycler machines. Thank you also to Maren Claus for her support on flow cytometry and the Institute of Immunology for allowing me to use their FACS-facility. I further want to thank the Nikon imaging center for their microscopy support. Apart from that, I also want to thank all those friendly people who helped me with administrative concerns, in particular our secretary in Heidelberg Renate Ulshöfer, Jutta Hess and Elisabeth Pfeilmeier from the MPI in Stuttgart, Sybille Schurin from CellNetworks and Claudia Roos from HBIGS.

Finally, I want to thank my entire family, especially my beloved parents for believing in me and for their encouragement. A special thanks to the man I love with all my heart, Niklas.